

Institute of Pharmacology and Toxicology

Director: Prof. Dr. rer. nat. Burkhard Hinz

# **Effect of cannabidiol on disease-associated functions of human vascular smooth muscle cells**

Role of the anti-oxidative enzyme heme oxygenase-1

---

Inaugural Dissertation

submitted in partial fulfilment

of the requirements for the academic degree

doctor rerum humanarum (Dr. rer. hum.)

of Rostock University Medical Center

Submitted by

Margit Schwartz, born March 30<sup>th</sup>, 1986 in Erfurt

Rostock, 06.11.2018



Dieses Werk ist lizenziert unter einer  
Creative Commons Namensnennung - Nicht kommerziell - Keine Bearbeitungen 4.0  
International Lizenz.

First Reviewer: Prof. Dr. rer. nat. Burkhard Hinz  
Universitätsmedizin Rostock  
Institut für Pharmakologie und Toxikologie

Second Reviewer: Prof. Dr. med. Bernhard Rauch  
Universitätsmedizin Greifswald  
Körperschaft des öffentlichen Rechts  
Institut für Pharmakologie  
Abteilung Allgemeine Pharmakologie

Third Reviewer: Prof. Dr. med. Karin Kraft  
Universitätsmedizin Rostock  
Zentrum für Innere Medizin  
Lehrstuhl für Naturheilkunde

Date of the defense: 24.07.2019







Parts of this work were published under the title “Up-regulation of heme oxygenase-1 expression and inhibition of disease-associated features by cannabidiol in vascular smooth muscle cells” (Oncotarget. 2018; 9:34595-34616).



# Table of Contents

<b>ABSTRACT .....</b>	<b>1</b>
<b>KURZZUSAMMENFASSUNG .....</b>	<b>2</b>
<b>1 INTRODUCTION .....</b>	<b>3</b>
<b>1.1 Vascular smooth muscle cells .....</b>	<b>3</b>
1.1.1 Characteristics .....	3
1.1.2 The physiological importance of the VSMC phenotype transition .....	5
1.1.3 Pathophysiology of dysregulated VSMC transition .....	5
<b>1.2 The heme oxygenase system .....</b>	<b>7</b>
1.2.1 Physiological function and degradation of heme .....	7
1.2.2 The HO isoenzymes and their characteristics .....	8
1.2.3 Mechanism and inducers of HO-1 induction .....	9
1.2.4 The physiological importance of HO-1 .....	11
<b>1.3 Cannabinoids .....</b>	<b>12</b>
1.3.1 Historical and biological background of <i>Cannabis</i> .....	12
1.3.2 The endocannabinoid system .....	13
1.3.3 Synthetic cannabinoid receptor agonists .....	15
1.3.4 Synthetic cannabinoid receptor antagonists .....	16
1.3.5 Other cannabinoid targets .....	16
1.3.6 CBD and THC in research and conventional medicine .....	17
1.3.7 CBD in cardiovascular disease and cancer .....	19
<b>2 AIM OF THE THESIS .....</b>	<b>21</b>
<b>3 MATERIALS AND METHODS .....</b>	<b>23</b>
<b>3.1 Materials .....</b>	<b>23</b>
<b>3.2 Methods .....</b>	<b>23</b>
3.2.1 Cultivation of adherent cells .....	23
3.2.2 Knockdown experiments using RNA interference .....	25
3.2.3 Analysis of mRNA expression via qRT-PCR .....	27
3.2.4 Analysis of cell migration .....	29
3.2.5 Analysis of cell proliferation .....	30
3.2.6 Protein expression analysis .....	31
3.2.7 Flow cytometry analyses .....	34
3.2.8 Statistics .....	36

---

4	RESULTS .....	37
4.1	Effects of cannabinoids on HO protein expression in HUASMC .....	37
4.2	Characteristics of CBD-mediated HO-1 induction.....	38
4.3	Involvement of cannabinoid-receptor signaling in CBD-mediated induction of HO-1.....	39
4.4	Involvement of ROS in CBD-mediated induction of HO-1 .....	41
4.5	Investigation of HUASMC phenotype in experimental conditions .....	43
4.6	Effect of CBD on proliferation and viability of HUASMC .....	44
4.7	Involvement of receptor-signaling in CBD-mediated anti-proliferative effects .....	46
4.8	Involvement of HO-1 in CBD-mediated anti-proliferative effects and viability in HUASMC: The SnPPIX approach.....	47
4.9	Involvement of HO-1 in CBD-mediated anti-proliferative effects and viability in HUASMC: The siRNA approach.....	49
4.10	Role of HO-1 in CBD-mediated anti-migratory effects.....	51
4.11	Role of CBD-mediated ROS in anti-proliferative effects and cell death of HUASMC.....	53
5	DISCUSSION .....	55
6	SUMMARY .....	65
7	ZUSAMMENFASSUNG .....	67
8	REFERENCES .....	69
9	LIST OF FIGURES.....	95
10	LIST OF TABLES.....	97
11	LIST OF ABBREVIATIONS.....	99
12	ATTACHMENT .....	103
12.1	Materials.....	103
12.2	Supplementary information .....	111
13	STATUTORY DECLARATION .....	117
14	ACKNOWLEDGEMENTS / DANKSAGUNGEN .....	119
15	CURRICULUM VITAE.....	121

## Abstract

Excessive proliferation and migration of vascular smooth muscle cells (VSMC) are closely linked to the development and progression of cardiovascular diseases and cancer. The cytoprotective enzyme heme oxygenase-1 (HO-1) has been shown to be involved in anti-proliferative and anti-migratory effects in VSMC. Cannabidiol (CBD), the major non-psychoactive constituent of *Cannabis*, has been shown to mediate numerous beneficial effects in several pathologic conditions.

Therefore, this thesis investigates the effect of CBD on the disease-associated functions of human umbilical artery smooth muscle cells (HUASMC) and the expression of HO-1. Both protein and mRNA expression of HO-1 were significantly increased by CBD in a time- and concentration-dependent manner. Although the expression of several cannabinoid-activated receptors (CB<sub>1</sub>R, CB<sub>2</sub>R, G protein-coupled receptor 55, transient receptor potential vanilloid 1) was demonstrated in HUASMC, an involvement of these receptors in the CBD-mediated HO-1 induction was excluded. Instead, the CBD-mediated increase of HO-1 protein was reduced by the glutathione precursor *N*-acetylcysteine (NAC), indicating the involvement of reactive oxygen species (ROS), which was confirmed by flow cytometric ROS detection. In addition to the CBD-induced increase of HO-1 expression, inhibition of growth factor-mediated proliferation and migration of HUASMC was observed. Neither the inhibition of HO-1 activity nor the knockdown of HO-1 protein reduced the CBD-mediated anti-proliferative and anti-migratory effects. In fact, inhibition or knockdown of HO-1 induced apoptosis and amplified the CBD-mediated anti-proliferative and anti-migratory effects. Overall, this work provides the first evidence of a CBD-mediated induction of HO-1 in VSMC and potential protective effects against excessive proliferation and migration of VSMC. While these data negate HO-1's involvement in the CBD-mediated inhibition of proliferation and migration, they also support HO-1's anti-apoptotic function in oxidative stress-induced cell fate.

## Kurzzusammenfassung

Ein exzessives Proliferations- und Migrationsverhalten von vaskulären glatten Muskelzellen (VSMC, engl.: vascular smooth muscle cells) ist eng mit der Entwicklung und dem Fortschreiten von Herz-Kreislauf-Erkrankungen und Krebs verknüpft. Das zytoprotektive Enzym Hämoxxygenase-1 (HO-1) ist nachweislich an anti-proliferativen und anti-migrativen Effekten in VSMC beteiligt. Für das wichtigste nicht-psychoaktive Cannabinoid des *Cannabis*, Cannabidiol (CBD), wurden zahlreiche potentiell therapeutisch relevante Effekte hinsichtlich verschiedener Erkrankungen nachgewiesen.

Die vorliegende Arbeit untersucht daher die Wirkung von CBD auf die krankheitsassoziierten Funktionen humaner glatter Muskelzellen der Nabelschnurarterie (HUASMC) sowie auf die Expression der HO-1. Die Expressionen von HO-1 Protein und mRNA wurden durch CBD zeit- und konzentrationsabhängig signifikant erhöht. Obwohl die Expression mehrerer Cannabinoid-aktivierter Rezeptoren (CB<sub>1</sub>R, CB<sub>2</sub>R, G-Protein-gekoppelter Rezeptor 55, Transient Rezeptorpotential Vanilloid 1) in HUASMC nachgewiesen wurde, konnte eine Beteiligung dieser Rezeptoren an der CBD-vermittelten Induktion der HO-1 ausgeschlossen werden. Stattdessen wurde der CBD-vermittelte Anstieg des HO-1 Proteins durch den Glutathion-Vorläufer N-Acetylcystein (NAC) vermindert, was auf die Beteiligung reaktiver Sauerstoffspezies (ROS) hindeutete und durch einen durchflusszytometrischen ROS-Nachweis bestätigt wurde. Begleitend zur CBD-induzierten Steigerung der HO-1 Expression wurde eine Hemmung der Wachstumsfaktor-vermittelten Proliferation und Migration von HUASMC beobachtet. Weder eine Hemmung der HO-1 Aktivität noch der Knockdown des HO-1 Proteins verminderten die CBD-vermittelten anti-proliferativen und anti-migrativen Effekte. Tatsächlich führten beide Ansätze zur Induktion von Apoptose und einer Verstärkung der CBD-vermittelten anti-proliferativen und anti-migrativen Effekte. Insgesamt liefert diese Arbeit den ersten Hinweis auf eine CBD-vermittelte Induktion der HO-1 und mögliche Schutzwirkungen gegen eine übermäßige Proliferation und Migration von VSMC. Wenngleich diese Daten eine Beteiligung der HO-1 an der CBD-vermittelten Hemmung von Proliferation und Migration widerlegen, untermauern sie gleichzeitig die anti-apoptotische Funktion der HO-1 unter oxidativen Stressbedingungen.

# 1 Introduction

## 1.1 Vascular smooth muscle cells

### 1.1.1 Characteristics

Vascular smooth muscle cells (VSMC) are an essential part of the blood vessel system. Arteries, veins and small arterioles consist of three morphologically different layers: tunica<sup>a</sup> intima, tunica media and tunica externa (Figure 1-1) [1]. The tunica intima consists of an extracellular matrix tissue, which is mainly composed of collagen and proteoglycans [1]. A single-layered endothelium on the luminal side and the inner elastic membrane on the peripheral side surround the tunica intima [1]. The tunica externa consists of connective tissue and fibroblasts and enables anchoring in the tissue and neuronal innervation of the blood vessel [1]. Smooth muscle cells (SMC) are mainly localized in the tunica media and regulate the blood vessel physics [1]. By coordinating contraction and dilatation, VSMC control the vascular tone and blood pressure of the entire organism [1]. VSMC are not terminally differentiated and have the ability to change from a contractile/quiescent phenotype to a synthetic/proliferative phenotype in a complex regulated process [2, 3].

Representing the two endpoints of a spectrum of intermediate VSMC phenotypes in vessels, these two phenotypes can be distinguished by morphological parameters and protein expression patterns (Figure 1-2) [2, 3]. Contractile VSMC are elongated, spindle-shaped cells containing large amounts of contractile filaments [2].

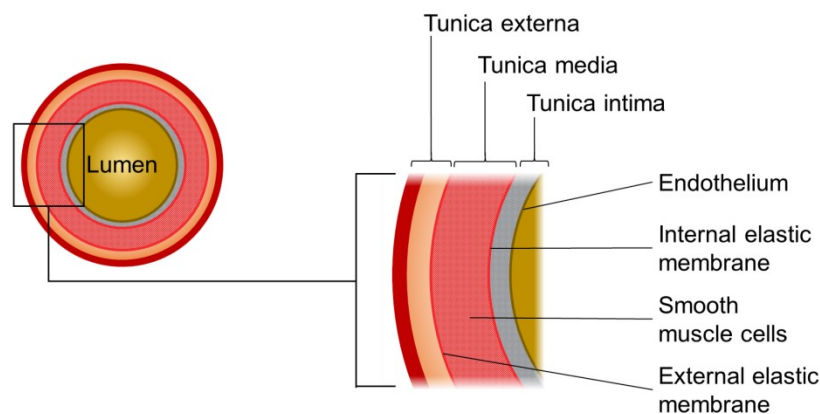


**Figure 1-1: Schematic cross-section of an arterial blood vessel structure.** From the outside to the inside (luminal side) the vessel consists of the following layers: tunica externa, tunica media and tunica intima. The tunica media is limited luminal and peripheral by the internal and external elastic membranes. At the luminal side, the vascular wall is limited by a single-layered endothelium. SMC are preferentially found in the tunica media. (Illustration created according to [1])

---

<sup>a</sup> from the Latin: tunica - robe, garb

The proteins used to identify the contractile/quiescent phenotype include especially  $\alpha$ -smooth muscle actin ( $\alpha$ -SMA), smooth muscle-myosin heavy chains (SM-MHC) and smoothelin, with the latter two being highly specific for this phenotype [2].

During the transition towards the synthetic/proliferative phenotype, the expression level of contractile marker proteins gradually decreases while expression levels of proteins such as collagen I and SMemb (embryonic form of myosin heavy chain) increases [2]. VSMC displaying a more synthetic/proliferative phenotype are therefore characterized by an enhanced proliferative and migrative capacity, synthesis of extracellular matrix proteins and a pronounced localization in the tunica intima [2]. The synthetic/proliferative phenotype can be identified by changes in the ratio of specific contractile markers (e.g. h-caldesmon and meta-vinculin) [2]. In terms of morphology, VSMC of the synthetic/proliferative phenotype are less elongated and show a cobblestone morphology in culture, which is also referred to as epithelioid or rhomboid [2]. Ultrastructural investigations on synthetic/proliferative VSMC showed an increased amount of cell organelles (e.g. endoplasmic reticulum [ER], Golgi complex and ribosomes), all of which are involved in protein synthesis [4].

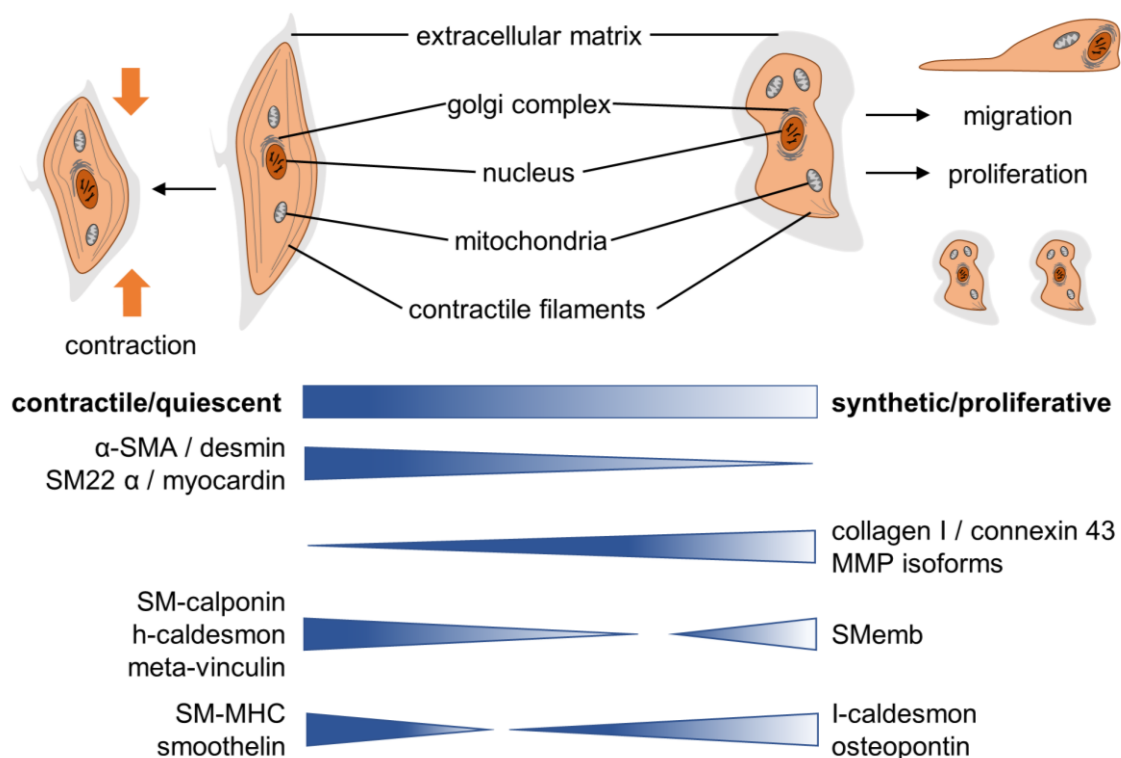


**Figure 1-2: Phenotype-dependent characteristics and marker proteins of VSMC.** Schematic illustration of morphologic and phenotype-dependent functional properties of contractile (left) and synthetic (right) VSMC. The changes of some marker proteins during phenotype transition are indicated by triangles.  $\alpha$ -SMA:  $\alpha$ -smooth muscle actin; SM22  $\alpha$ : smooth muscle protein 22  $\alpha$ ; SM-calponin: smooth muscle-calponin; SM-MHC: smooth muscle-myosin heavy chain; MMP: matrix metalloproteinase; SMemb: embryonic smooth muscle-myosin heavy chain (Illustration created according to [2, 3])



### 1.1.2 The physiological importance of the VSMC phenotype transition

The VSMC within a particular vessel exhibit variations in morphological and functional characteristics as well as differences in the expression of marker proteins, reflecting the presence of several different phenotypes [5–8]. This array of possible phenotypes forms a heterogeneous arrangement with (epi)genetically [9] controlled limitations for each SMC subpopulation [2]. The phenotype transition of VSMC is particularly important for the establishment of a vascular network in embryogenesis [2]. Nevertheless, vascular remodeling and repairs are also required to adapt to changes in physiological stress such as pregnancy, movement, or vascular injuries [2]. Endothelium-modulated, long-lasting, or chronic mechanical forces, such as hydrodynamic shear and tensile stresses, which are intensified by blood flow or blood pressure [10], stimulate the remodeling of the vessel wall. In addition, VSMC react directly to mechanical stretching mediated by certain transmembrane receptors [10]. Besides these physical factors, a number of biochemical factors are involved in the transition of the VSMC phenotype. These include extracellular matrix proteins [8, 11–13], cytokines [14, 15] and several growth factors such as platelet-derived growth factor (PDGF) [16–24] and fibroblast growth factor (FGF) [2, 3].

### 1.1.3 Pathophysiology of dysregulated VSMC transition

Despite its physiological role, the dysregulation of phenotype transition, together with the abnormal proliferation and migration of VSMC, is closely associated with the development and progression of cardiovascular diseases and cancer.

#### *VSMC in cardiovascular disease*

The World Health Organization (WHO) has once again declared ischemic heart diseases and strokes, both acute complications of atherosclerotic vessel reconstruction, as leading causes of death worldwide [25]. Atherosclerosis, formerly considered a response to endothelial injury, is an inflammatory disease [26]. While multifactorial endothelial dysfunction is the underlying cause of this disease, VSMC are of great importance for the progression of this process [27, 28]. Well-established risk factors include elevated serum cholesterol levels (especially low-density lipoprotein [LDL]), reactive oxygen species (ROS, caused e. g. by cigarette smoking), hypertension, and diabetes mellitus [27]. The restoration of the endothelial function requires compensatory mechanisms that alter its normal properties. Consequently, endothelial adhesion and permeability increases, thus changing the endothelium from being anti-coagulant to being pro-coagulant [27]. A prolonged inflammatory reaction additionally stimulates the proliferation and migration of VSMC and thus promotes

the development of an intermediate lesion and the thickening of the vascular wall [27, 29]. This process is called intimal hyperplasia [27, 29]. Immigration, proliferation and activation of immune cells results in a release of hydrolytic enzymes, cytokines, chemokines and growth factors in the inflamed region which leads to further damages and potential tissue necrosis [27]. The cyclic repetition of immune cell accumulation, proliferation, and migration of VSMC and the formation of fibrous tissue leads to further expansion and reorganization of the lesion [27]. The result is an advanced complex lesion, a so-called plaque, which is a core of lipid and necrotic tissue that is covered by a fibrous cap [27]. When exceeding a certain point, the luminal diameter will no longer be maintained by compensatory dilatation of the vessel [27]. The lesion then invades the vessel lumen and impairs the blood flow (i. e. stenosis of the vessel) [27]. The erosion or acute rupture of an unstable plaque causes occlusion of the vessel lumen and thus the acute clinical complications ischemic heart disease and stroke [28]. VSMC have an ambivalent role in the process of atherogenesis. Although VSMC proliferation and migration initially support the plaque formation, the plaque stability is enhanced by VSMC located in the fibrous cap [28]. In addition, therapeutic interventions intending to restore the blood flow in stenotic vessels are affected by abnormal VSMC proliferation and migration, contributing to the recurrence of vessel narrowing, called (in-stent) restenosis [30, 31]. It is noteworthy that apoptosis of VSMC correlates with plaque rupture and inflammation in atherosclerosis [28].

#### *VSMC in angiogenesis and cancer progression*

The formation of blood and lymph vessels, angiogenesis and lymphangiogenesis, are well-balanced and important processes during both embryogenesis and wound healing [32]. An imbalance to the benefit of the factors supporting (lymph)angiogenesis promotes the malignancy and metastasis of solid tumors through nutrient and oxygen supply and the provision of pathways for tumor cell metastasis [32]. The "angiogenetic switch" is activated by a variety of factors. Metabolic stress, inflammatory reactions and genetic mutations lead to the production and release of numerous pro-angiogenic molecules, including the vascular endothelial growth factor (VEGF), which is a major factor in the initiation of angiogenesis [33]. In the highly complex process of cancer angiogenesis, VSMC and pericytes recruited by PDGF contribute to the stabilization and maturation of the emerging tumor vessels [33]. The abnormal proliferation of VSMC thus correlates with (blood)vessel formation in cancer and other non-neoplastic diseases [31, 33]. In order to inhibit the tumor growth and the formation of metastases, anti-angiogenic strategies are used as (neo-)adjuvant treatments to regular cancer therapies (e. g. surgical removal of primary tumors, chemotherapy and irradiation) [34, 35]. These anti-angiogenic approaches

mainly interfere with VEGF signaling [34, 35]. However, the efficacy of these therapies is limited by cancer-specific reactivity, resistance development, and toxicity [34, 35]. Consequently, influencing the predominant disease-associated features of VSMC, proliferation and migration, could positively affect the success of clinical treatment of cardiovascular disease and cancer.

## 1.2 The heme oxygenase system

The heme oxygenase (HO) system is the key player in cellular heme metabolism and homeostasis [36] and has attracted considerable attention in past years in the context of vascular diseases [37, 38] and cancer [39].

### 1.2.1 Physiological function and degradation of heme

Heme is a ubiquitous, iron-containing molecule and acts as a prosthetic group<sup>b</sup> of metalloproteins, so-called hemoproteins [40, 41]. For example, heme is part of the red blood pigment hemoglobin, the iron and oxygen binding protein myoglobin in muscle tissue, and various other enzymes such as cytochromes and catalase. The most common type of heme is heme b, also known as iron-(Fe-)protoporphyrin IX (FePPIX). Although the HO substrate heme is an essential molecule for aerobic organisms, it produces some unfavorable, even toxic effects when unbound [40, 42]. The release of free heme occurs in severe pathological hemolysis (e. g. in sickle cell anemia, malaria and after ischemia/reperfusion [I/R]), tissue damage or in conditions with increased hemoprotein degradation (e. g. oxidative stress) [40]. In 1968, Tenhunen et al. investigated the process of heme degradation and thereby identified its underlying enzymatic nature and HO as the rate-limiting enzyme of this reaction (Figure 1-3) [36]. The HO activity catalyzes the oxidative conversion of FePPIX into biliverdin IX $\alpha$ , carbon monoxide (CO) and divalent iron ions (Fe<sup>2+</sup>) [43]. The HO activity depends on the presence of both molecular oxygen (O<sub>2</sub>) and the phosphorylated form of the reduced coenzyme nicotinamide adenine dinucleotide (NADH), NADPH/H<sup>+</sup><sup>c</sup> [36]. In contrast, the reaction product CO inhibits the HO activity [36]. Consequently, HO enzymes belong to the class of mixed function oxygenases<sup>d</sup> and involve the cytochrome P450 (CYP450) enzymes in the mechanism

---

<sup>b</sup> A prosthetic group (also known as cofactor) is covalently linked to an enzyme (or protein) and is necessary for its function.

<sup>c</sup> Donor of electrons and protons. Used as a reducing agent in reductive biosynthesis.

<sup>d</sup> Enzymes that perform reduction-oxidation reactions in which one oxygen atom of molecular oxygen is incorporated into the organic substrate, while the other oxygen atom is reduced and combined with hydrogen ions to form water.

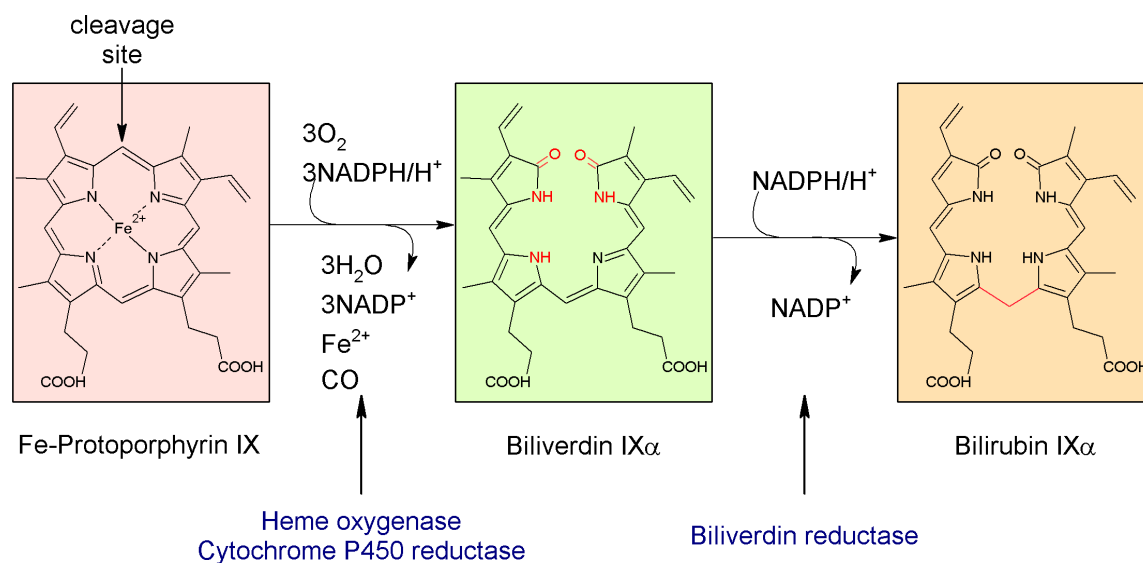


**Figure 1-3: Reaction of the enzyme-coupled heme degradation.** The heme oxygenase catalyzes the oxidative cleavage of the pyrrole rings of the heme molecule (Fe-protoporphyrin IX) at the methine bridge (marked as the cleavage site) whereby carbon monoxide (CO) and iron ( $\text{Fe}^{2+}$ ) are released. NADPH/ $\text{H}^+$  is required as a reducing agent for the formation of water. The resulting biliverdin IX $\alpha$  is characterized by its greenish color. Under catalysis by cytosolic biliverdin reductase, the middle methine group is reduced into a methylene group. The reducing agent used here again is NADPH/ $\text{H}^+$ . The resulting red-orange product is bilirubin IX $\alpha$ .

of heme degradation [36, 43, 44]. Subsequently after its production biliverdin IX $\alpha$  is converted to the bile pigment bilirubin<sup>e</sup> IX $\alpha$  by biliverdin reductase, which was identified in 1965 [45]. While CO is eliminated by lung exhalation,  $\text{Fe}^{2+}$  is bound directly to the iron transport molecule ferritin, a ubiquitously expressed protein that ensures the storage and controlled release of iron [46].

### 1.2.2 The HO isoenzymes and their characteristics

So far, two isoenzymes of the HO protein have been identified. In 1986, Maines et al. were the first to isolate two constitutive isoforms of HO from microsomal fractions of rat liver, which were subsequently designated HO-1 and HO-2 [47]. In 1997, a rat brain-derived complementary DNA (cDNA) indicated the presence of a third isoform, designated HO-3. This cDNA coded for a hemoprotein that shared 90% similarity with HO-2 but exhibited lower enzyme activity [48]. However, further analyses failed to amplify HO-3 messenger RNA (mRNA) and to detect HO-3 related proteins in Western blot [49]. It was thus assumed that HO-3 related genes in rat were processed pseudogenes derived from HO-2 transcripts [49]. Until today, the existence of putative HO-3-proteins is not yet completely proven. Investigations regarding the isoenzymes HO-1 and HO-2 revealed fundamental differences in the characteristics

<sup>e</sup> From the Latin: ruber - red

of both proteins, especially with respect to their activities [47]. In contrast to HO-2, the basal activity of HO-1 is 2–3-fold lower, but can be increased in response to various chemicals such as cobalt, cadmium, and heme<sup>f</sup> [47]. Differences in protein sequence and molecular structure were first indicated by experiments analyzing thermolability and antigenic specificity [47] and were later confirmed by sequence analysis of the isolated proteins [50] (see suppl. Figure 12-1, page 111). While the human HO-1 was identified as a 32 kDa protein [51] consisting of 288 amino acids, HO-2 is a 36 kDa protein consisting of 316 amino acids [50, 52]. The amino acid sequences of HO-1 and HO-2 share 43% identity and contain a conserved catalytic nuclear domain [50], known as the “HO signature” (GenBank<sup>TM</sup>). This HO signature is a 24 amino acid long peptide region with 100% similarity in predicted secondary structures of HO-1 and HO-2 of different species [53]. Further analyses confirmed that HO-1 could not be a post-transcriptional product of HO-2 [50] and showed that both proteins are encoded by different genes [50, 54, 55]. *HMOX1*, the gene encoding HO-1, was localized on chromosome 22q12.3 [54, 55], while the HO-2-encoding gene, *HMOX2*, was mapped to the chromosomal location 16p13.3 [54]. Additionally, HO-1 and HO-2 differ in their number of heme regulatory motifs (HRMs), identified as a cysteine proline (CP) motif [56]. While human HO-1 lacks CP motifs [50], human HO-2 contains two conserved HRMs involving the cysteines Cys265 and Cys282 and an additional CP motif at Cys127 [57]. Although important for heme binding, these HRMs are not involved in the HO-catalyzed heme degradation [57, 58]. These differences also indicate for different physiological roles of HO-1 and HO-2 [59]. In fact, a regulatory role of HO-2 with respect to the expression of HO-1 was verified by the knockdown of HO-2 [60]. This approach led to activation of the HO-1 gene promoter, extended half-life of HO-1 mRNA and increased HO-1 protein levels [60]. It was therefore assumed that HO-2 can down-regulate the expression of HO-1 and thereby regulates the coordinated expression of HO-1 and HO-2 [60, 61].

### 1.2.3 Mechanism and inducers of HO-1 induction

Since the discovery of HO-1 inducibility [47], the underlying mechanisms and potential inducers of HO-1 expression were subject of several investigations and were reviewed in detail in [37, 62, 63]. The expression of HO-1 protein is induced by endogenous and exogenous substances that all cause cellular damage and oxidative stress. These include for example metalloporphyrins (e. g. heme), heavy metals, lipid metabolites, inflammatory cytokines, growth factors, reactive oxygen species (ROS) as well as UVA radiation, and hypoxia. Transcription of *HMOX1* is regulated by several stress responsive transcription factors (TFs) such as members of the heat shock

---

<sup>f</sup> Hydroxide of heme.

factors (HSFs), nuclear factor  $\kappa$ B (NF- $\kappa$ B), nuclear factor erythroid 2 (NF-E2) and activator protein 1 (AP 1) families [62]. A well-known evolutionary conserved mechanism regulating *HMOX1* transcription involves the TF nuclear factor (erythroid-derived 2)-like 2 (Nrf2, Figure 1-4) [63]. Under conditions of stress, Nrf2 is released from its inhibitor protein Kelch-like ECH-associated protein 1 (Keap1), which is responsible for the cytosolic sequestration and degradation of Nrf2 under normal conditions [63]. In addition, the nuclear heme binding protein BACH1 negatively regulates the expression of HO-1. BACH1 suppresses the transcription of *HMOX1* under physiological conditions [61, 64, 65], but is decoupled from the *HMOX1* promoter under conditions of intracellular stress or increased heme content [64]. The transcriptional activity of the HO-1 promoter is additionally regulated by a GT-repeat length polymorphism, suggesting a genetically programmed strength in the HO-1 response [66].

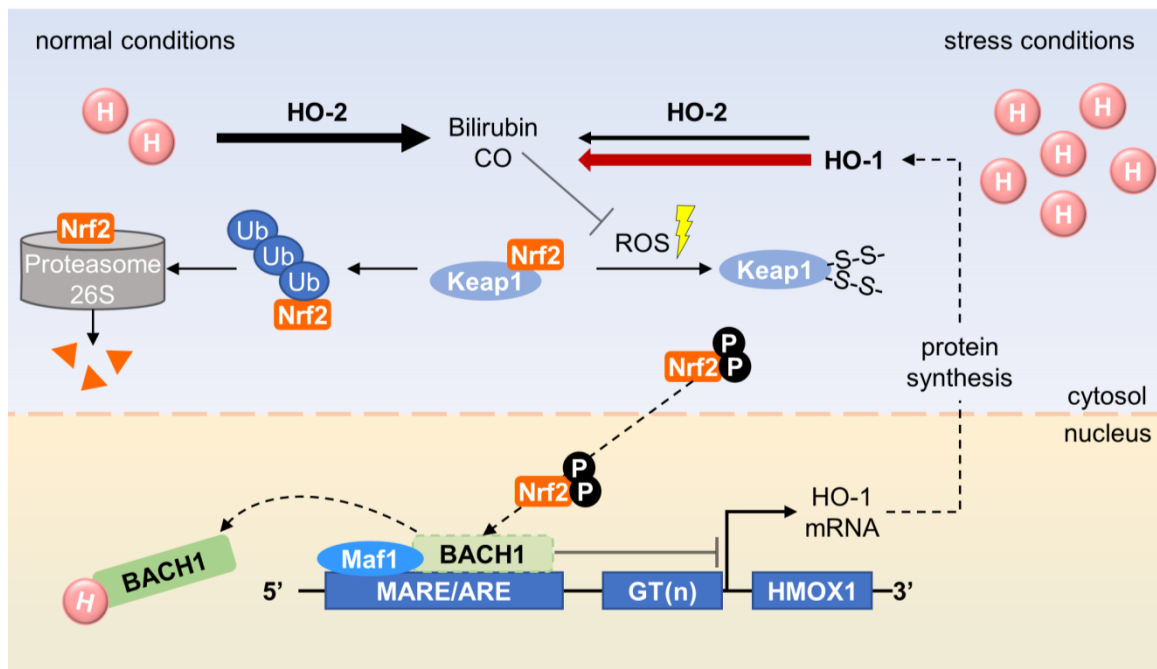


**Figure 1-4: Nrf2-dependent mechanism of *HMOX1* transcription under normal and stress conditions.** Under normal conditions, the level of released heme (H) is regulated and constantly kept low by heme oxygenase-2 (HO-2). Keap1 mediates cytoplasmic ejection of Nrf2. Keap1-bound Nrf2 is marked for proteasomal degradation by poly-ubiquitination (Ub). BACH1, together with the Maf protein, is bound to the MARE/ARE. This blocks the promoter of heme oxygenase-1 (HO-1) and thus also transcription of *HMOX1*. Stress conditions lead to an increased release and accumulation of heme molecules or to the formation of reactive oxygen species (ROS). *HMOX1* transcription is initiated by a combinatory mechanism. First, heme enters the nucleus and displaces the heme-binding protein BACH1. Second, ROS disrupt the Nrf2-binding disulfide bridge of Keap1. As a result, Nrf2 enters the nucleus. After binding to the Maf protein, Nrf2 activates the MARE/ARE and thus increases the transcription of Nrf2-regulated genes (e.g. *HMOX1*). Following translation of the HO-1 mRNA, active HO-1 protein in the cytosol contributes to the degradation of the accumulated heme. The heme oxygenase products bilirubin and carbon monoxide (CO) lead to an additional anti-oxidative effect and attenuate the influence of ROS. ARE: anti-oxidative response element; Keap1: Kelch-like ECH-associated protein 1; MARE: Maf-recognition element; Nrf2: nuclear factor (erythroid-derived 2)-like 2; P: indicates phosphorylation; (Illustration created according to [61, 63–65])

Additionally, various protein kinases, including mitogen-activated protein kinases (MAPKs), have been shown to be involved in the regulation of HO-1 [67–69]. Due to its classification as an apparently constitutive enzyme, there have been only few studies regarding possible pharmacological manipulations and potential functions of HO-2 (for review see [70]). Indeed, a few reports suggest a selective induction of HO-2 by some substances such as calmodulin, menadione, and glutamate [71–73].

#### 1.2.4 The physiological importance of HO-1

As mentioned above, various stimuli either originating from or causing cellular stress can induce the induction of HO-1. This is considered an evolutionarily conserved mechanism of cell protection [63]. The essential importance of HO-1 was emphasized by a few reports on human HO-1 deficiency. The very young patients presented herein suffered from persistent hemolytic anemia, growth retardation, chronic inflammation and iron deposition in organs [74, 75]. The high value of the anti-oxidative properties of HO-1 for the vascular and endothelial system was clearly demonstrated by the glomerular endothelial detachment following severe endothelial cell injury and the presence of atherosclerotic modifications in the aorta of HO-1-deficient patients [74, 76]. Transgenic knockout mice with a HO-1 deficiency also exhibited a reduced stress resistance, endothelial damage and liver and renal cytotoxicity [77].

The HO substrate heme has been shown to mediate LDL oxidation and endothelial injury, both of which are closely associated with atherosclerosis [42, 78, 79]. In contrast, HO-1 induction or administration of the HO products CO and bilirubin led to anti-oxidative effects in numerous studies on various pathological conditions [80–90]. For example, CO restored graft function after transplantation-associated cold I/R of the rat heart [91] and protected against hemorrhagic shock and reanimation-induced organ injury and systemic inflammation in mice [92]. Likewise, HO-1-derived bilirubin mediated protection of endothelial cells against oxidative stress in an *in vitro* model of hyperglycemia/diabetes [93]. The specific regulation of HO-1 by different pharmacological approaches is therefore considered a promising strategy to protect against a variety of diseases characterized by oxidative stress and inflammation, such as atherosclerosis [38, 94].

Regarding the progression of cardiovascular diseases, overexpression of HO-1, which was achieved by administration of plant-derived [14, 15, 17, 21, 23, 95–100] or other [19, 24, 101] substances, or via retroviral transfection [18, 95], showed many positive effects. Although HO-1 was investigated in numerous studies, there is still a lack of information about a possible manipulation of the HO system by cannabinoids, especially in VSMC.

## 1.3 Cannabinoids

### 1.3.1 Historical and biological background of *Cannabis*

*Cannabis sativa* L.<sup>§</sup> (hemp) is an annual herbaceous plant belonging to the family of *Cannabaceae* [102]. *Cannabis* has been traditionally used for thousands of years for ordinary (e. g. production of textiles and ropes) and medicinal purposes, but also as a recreational drug [103–106]. The geographical origin of *Cannabis* is probably located in Central Asia with the first known records of its medicinal uses dating back to about 2800 B.C. [106]. According to legends, the Chinese “Red Emperor” Shen Nung<sup>h</sup> recommended the medicinal use of *Ma* (ancient Chinese word for *Cannabis*) for the treatment of gouty arthritis, rheumatism, and malaria in his pharmacological essays. He is therefore considered the "Father of Chinese herbal medicine". Artefacts from ancient times prove the medicinal and non-medicinal use of *Cannabis* also in Indian and Islamic countries [104, 106]. In 1843, the British physician O’Shaughnessy observed positive effects of *Cannabis* for the treatment of rheumatic complaints, spastic and convulsive disorders, tetanus, and cholera in traditional Indian medicine [107]. These observations were followed by the use of *Cannabis* extracts as sedatives, hypnotics, analgesics, and anticonvulsants in conventional medicine in the English-speaking world [104]. Due to the variability in composition and shelf life, opiates and synthetic drugs increasingly replaced *Cannabis* extracts in the early 20<sup>th</sup> century [104]. Finally, in 1961 the United Nations *Single Convention on Narcotic Drugs* prohibited the use of *Cannabis* except for scientific purposes.

The chemical composition of *Cannabis* is highly complex. To date, the number of known ingredients has increased to about 560 compounds of all chemical classes, including terpenes, modified sugars, hydrocarbons, steroids, quinones, flavonoids, nitrogenous substances and amino acids [105, 106, 108]. A mixture of about 120 mono- and sesquiterpenoids is responsible for the characteristic scent of the plant [106]. In the multitude of compounds, about 100 mono- to tetracyclic C<sub>21</sub>-(or C<sub>22</sub>-) terpenophenolic molecules form the best known and most specific group of substances present in *Cannabis sativa* [105, 108]. These so-called phytocannabinoids are also the most important secondary metabolites of *Cannabis* [109]. The direct precursor of most phytocannabinoids, cannabigerolic acid, is formed in an enzymatically driven condensation of a C<sub>12</sub> polyketide (olivetolic acid) and a monoterpene unit (geranyl pyrophosphate) [106]. The cannabinoid biosynthesis takes place in the glandular trichomes of the plant and serves as a potential self-defense mechanism, as phytocannabinoids induce apoptosis in plant and insect cells [110]. Among the

---

<sup>§</sup> Named after Carl von Linné, who first described *Cannabis sativa*.

<sup>h</sup> Also to be found as Chen Nung or Shennong.



phytocannabinoids,  $\Delta^9$ -tetrahydrocannabinol ( $\Delta^9$ -THC; in the following abbreviated as THC; see chap. 1.3.6, page 17) is the main psychoactive constituent of *Cannabis sativa*. In contrast, cannabidiol (CBD, see chap 1.3.6, page 17) is the most important non-psychoactive cannabinoid in the plant [106]. However, the presence of phytocannabinoids, cannabimimetic, or cannabinoid-like substances is not limited to *Cannabis* (reviewed in [111]).

### 1.3.2 The endocannabinoid system

The endocannabinoid system (ECS) consists of the cannabinoid receptors (CBRs), their endogenous ligands, so-called endocannabinoids, and the proteins that contribute to their biosynthesis and inactivation [112]. The ECS is involved in the regulation of several physiological functions such as movement, memory and learning, cognition, appetite, emesis, pain and immune system modulation [113]. Targeting the ECS represents therefore a promising therapeutic approach (reviewed in [114–117]).

#### *The cannabinoid receptors*

Investigations of the underlying mechanisms of THC's psychoactivity led to the discovery and characterization of the CB<sub>1</sub>R, which is predominantly present in the brain and testis [118–120]. A second receptor, CB<sub>2</sub>R, was identified and characterized in 1993 and shows more peripheral presence with high expressions in immune cells [121, 122]. However, further investigations extended these distributional limitations and showed that both receptors were expressed, albeit with low frequencies, in peripheral tissues such as adrenal glands, heart, lung, prostate, uterus, ovary, testicles, bone marrow, thymus and tonsils [122]. Additionally, CB<sub>2</sub>R was also found in cells of the central nervous system (CNS), e. g. in microglia cells [123] and neurons [124–126]. Both, CB<sub>1</sub>R and CB<sub>2</sub>R, are pertussis toxin-(PTX-)sensitive G<sub>i/o</sub> protein-coupled receptors whose signaling mediates inhibition of the adenylate cyclase [127–129]. Additionally, signaling of both CB<sub>1</sub>R and CB<sub>2</sub>R leads to activation of several MAPKs, such as p38 MAPK, c-Jun NH<sub>2</sub>-terminal kinase (JNK) and extracellular signal-regulated kinase (ERK) [130–136].

The activation of central CB<sub>1</sub>R influences the release of neurotransmitters, e. g.  $\gamma$ -aminobutyric acid (GABA), dopamine, noradrenaline, 5-hydroxytryptamine, glutamate and aspartate, thereby inducing the psychoactive effects of *Cannabis* [137–144]. In contrast to CB<sub>2</sub>R, CB<sub>1</sub>R signaling is associated with the modulation of several ion channels, including different types of voltage-gated calcium channels [137, 138, 141, 145, 146], G protein-coupled inward-rectifier potassium channels (K<sub>ir</sub>) [137, 146] and voltage-gated potassium channels [141, 147].

### Endocannabinoids and endocannabinoid-like compounds

Endocannabinoids (eCBs), lipophilic substances that are naturally produced in the body, act as ligands of cannabinoid receptors (Figure 1-5). The arachidonic acid derivative *N*-arachidonoyl-ethanolamide (AEA, anandamide<sup>i</sup>), first isolated from the porcine brain in 1992 [148], was identified as a competitive agonist with a THC-like affinity for the CB<sub>1</sub>R receptor [145, 149]. In contrast, AEA was shown to be almost inactive at CB<sub>2</sub>R [150, 151]. In 1995, another eCB, 2-arachidonoyl-glycerol (2-AG), was isolated from the peripheral tissue of the dog [152] and identified as the agonistic ligand of both receptors, the central CB<sub>1</sub>R and the peripheral CB<sub>2</sub>R [150, 153]. In 1993, the two brain-derived unsaturated fatty acid ethanolamides, *N*-homo- $\gamma$ -linolenyl-ethanolamide and *N*-7,10,13,16-docosatetraenyl-ethanolamide, were identified as CB<sub>1</sub>R ligands via a centrifugation-based ligand binding assay [154]. Since then, the substances *N*-arachidonoyl-dopamine (NADA) [155, 156], *O*-arachidonoyl-ethanolamine (virodhamine) [157] and 2-arachidonylglyceryl-ether (noladin ether, 2-AGE) [158] were additionally characterized as eCBs showing different affinities to CB<sub>1</sub>R and CB<sub>2</sub>R.

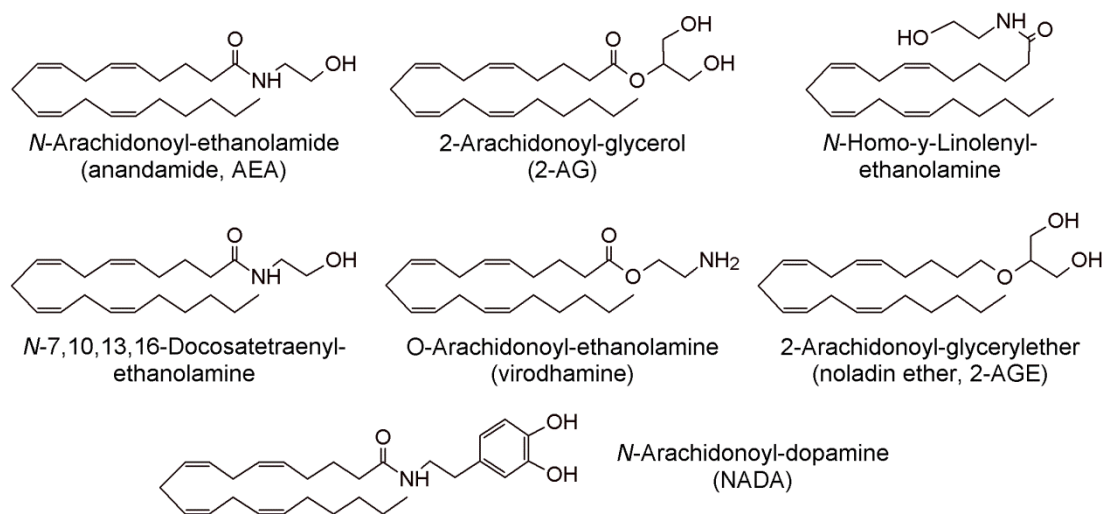


**Figure 1-5: Chemical structures of endocannabinoids.**

Endocannabinoid-like compounds (ELC, Figure 1-6) are saturated or mono-unsaturated fatty acids like *N*-acylethanol-amides (e. g. *N*-oleyl-ethanolamide [OEA] and *N*-palmitoyl-ethanolamide [PEA]) and 2-monoacylglycerols (e. g. 2-oleoyl-glycerol [2-OG], 2-linoleoyl-glycerol [2-LG] and 2-palmitoyl-glycerol [2-PG]). Although ELC do not bind to the cannabinoid receptors CB<sub>1</sub>R and CB<sub>2</sub>R, they partly use the same

<sup>i</sup> From the Sanskrit: ananda - bliss

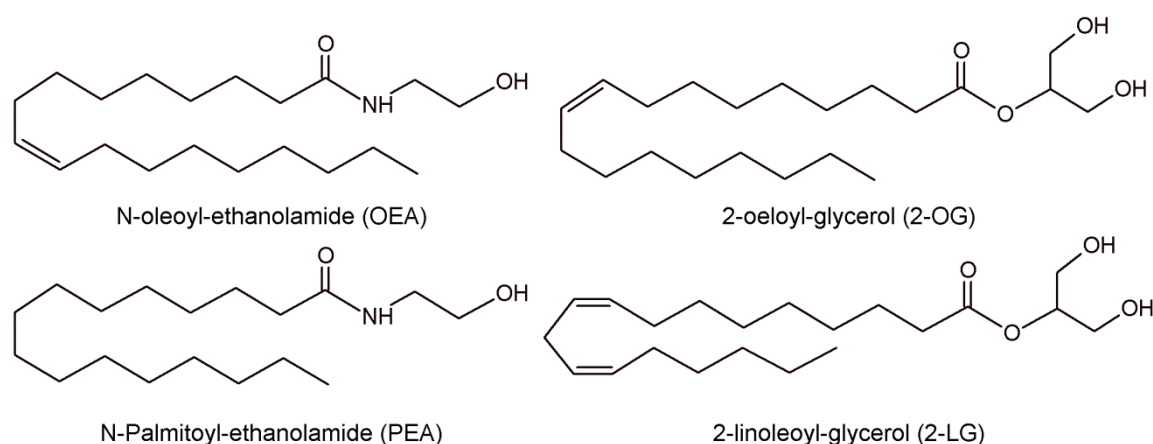


**Figure 1-6: Chemical structures of endocannabinoid-like compounds.**

enzymes for biosynthesis and degradation as the eCBs, mediate autonomous effects, and can amplify the eCB-mediated effects (reviewed in [159]). This ELC-mediated enhancement of eCB-mediated effects was named the “entourage effect”, which was first described in 1998 [160].

### 1.3.3 Synthetic cannabinoid receptor agonists

The intense research regarding the functionalities of the ECS-components required and enabled the production of diverse synthetic cannabinoid receptor ligands (Figure 1-7). The AEA analog R(+)-methanandamide (MA) exhibits metabolic stability against aminopeptidase hydrolysis and an approximately 4-fold higher affinity for CB<sub>1</sub>R than AEA [161].

In contrast, JWH-133 (1-deoxy-3-(1',1'-dimethylbutyl)- $\Delta^8$ -THC), which was synthesized and described in 1999 as one component of a series of 15 1-deoxy- $\Delta^8$ -THC analogues by John W. Huffman, shows a 200-fold selectivity for CB<sub>2</sub>R over CB<sub>1</sub>R [162]. Nowadays, the list of JWH-substances, including pyrrole-, indole-, and dibenzopyrane-derived compounds, comprises ligands of both, CB<sub>1</sub>R and CB<sub>2</sub>R, [162–164]. For example, JWH-015 is a CB<sub>2</sub>R-selective agonist [165].

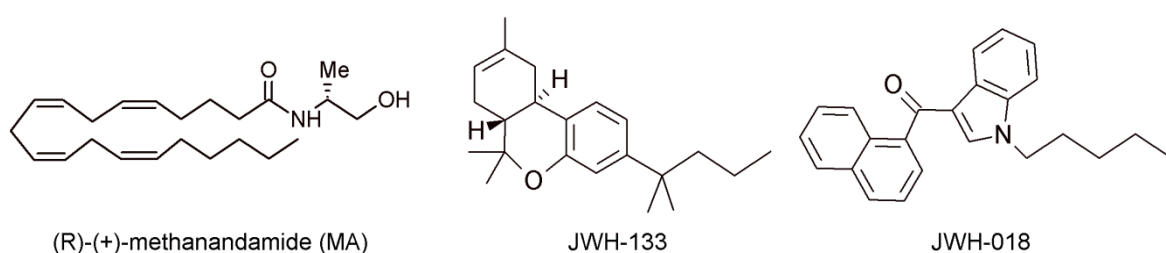


**Figure 1-7: Chemical structures of synthetic cannabinoid receptor agonists.**

In contrast, WIN-55,212-2, CP55,940, HU-210 and JWH-018 activate both, CB<sub>1</sub>R and CB<sub>2</sub>R, thereby showing partially higher potencies than THC [146, 165–167]. JWH-018 has recently aroused public and political interest, as it occurred in herbal mixtures that were smoked as a "high"-producing recreational drug and resulted in some reports of critical side effects [168–171].

#### 1.3.4 Synthetic cannabinoid receptor antagonists

In 1995, the characterization of the first highly selective CB<sub>1</sub>R-antagonist for studying the *in vivo* functions of the ECS, SR141716A (Rimonabant) [172], was followed by investigations regarding a series of CBR-targeting pyrazole compounds (Figure 1-8) [173]. Herein, the rimonabant analog AM251 was identified as potent CB<sub>1</sub>R antagonist [173], whereas AM630 (6-iodopravadoline) showed competitive antagonism at CB<sub>2</sub>R [174]. The strategies and therapeutic potential of targeting the ECS were reviewed in depth elsewhere [175–177].

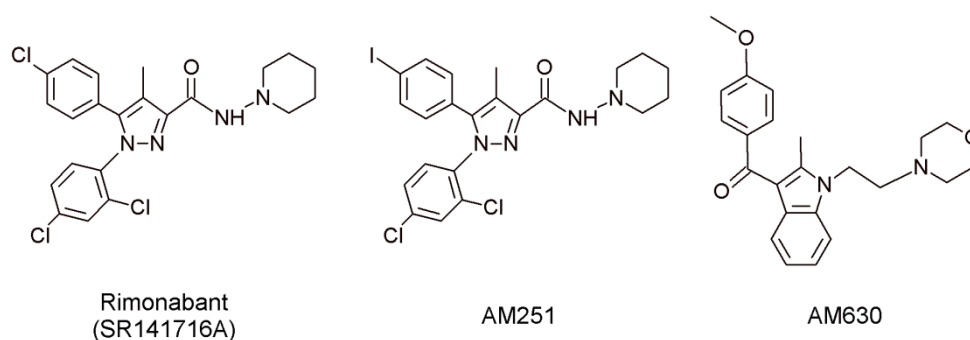


**Figure 1-8: Chemical structures of synthetic cannabinoid receptor antagonists.**

#### 1.3.5 Other cannabinoid targets

In addition to CB<sub>1</sub>R and CB<sub>2</sub>R, several other molecular targets for cannabinoids have been identified [176]. For example the transient receptor potential cation channel vanilloid 1 (TRPV1) was identified as a target of AEA [178] and NADA [156]. The TRPV1 is a non-selective, ligand-gated cation channel that regulates the influx of mono- and divalent cations, in particular Ca<sup>2+</sup> ions [179], and is widely distributed throughout the body [180]. The best known activators of TRPV1 are capsaicin, the irritant compound in hot chili peppers, temperatures above 43 °C and acidic conditions (pH < 6) [181]. The activation of TRPV1 leads to a painful, burning sensation caused by irritation of sensory neurons and the generation of action potentials [182]. Accordingly, TRPV1 has a crucial role in pain perception; its dysfunction is involved in various disease states, e. g. chronic pain and diabetes [181].

The G protein-coupled receptor 55 (GPR55), which was first characterized in 1999 [183], was identified as the target of various endogenous, plant and synthetic cannabinoids, including AEA, 2-AG, PEA, THC, CP55,940 and WIN55,212-2 [184]. The expression of GPR55 was verified in numerous organs, including the adrenal glands, the CNS, and the gastrointestinal tract [184]. Cannabinoids also interact with other molecular targets, including nuclear peroxisome proliferator-activated receptors/ (PPARs), serotonin (5-hydroxytryptamine; 5-HT) receptors, nicotinic acetylcholine and ionotropic glutamate receptors, as well as opioid receptors (for review see [176, 185, 186]).

### 1.3.6 CBD and THC in research and conventional medicine

#### *The differences between CBD and THC*

The first isolation and vague structural description of CBD already occurred in 1940 [187]. However, the structures of the two main phytocannabinoids, CBD and THC, were exactly clarified later by Mechoulam and his colleagues in the early 1960s (Figure 1-9) [188, 189]. The psychoactive effects of *Cannabis* and its components were investigated in several human and animal experiments [190–194] and, due to the progressive investigation of the ECS, they were attributed to the cannabinoid-mediated activation of central CB<sub>1</sub>R [119, 120]. Further analyses revealed that THC acts with high affinities at both receptors ( $K_i(\text{CB}_1\text{R}) \approx 40 \text{ nM}$ ;  $K_i(\text{CB}_2\text{R}) \approx 40 \text{ nM}$ ) while CBD, although possessing structural similarities to THC, showed only weak affinities ( $K_i(\text{CB}_1\text{R}) \approx 4,000 \text{ nM}$ ;  $K_i(\text{CB}_2\text{R}) \approx 2,900 \text{ nM}$ ) [128, 146, 165, 195]. This explains CBD's non-psychoactive nature. In contrast to THC, CBD stimulates the TRPV1 with a similar efficacy as the TRPV1 agonist capsaicin [196] and thus mediates an increase of the intracellular  $\text{Ca}^{2+}$  level, desensitization of TRPV1 against capsaicin and inhibition of AEA uptake and hydrolysis [195]. Regarding GPR55, both substances show different activities. While THC activates the receptor, CBD has been shown to have an antagonistic effect [184].

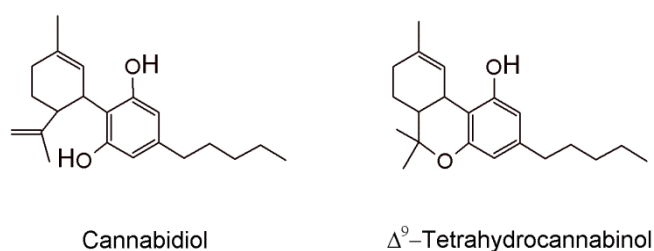


**Figure 1-9: Chemical structures of CBD and THC.**

<sup>i</sup> Transcription factor of target genes involved in e. g. metabolism and energy homeostasis.

### *Cannabinoid-based drugs in conventional medicine*

In 1981, a synthetic THC analog, Nabilone (international nonproprietary name [INN], Cesamet®) was approved for the suppression of chemotherapy-associated nausea and vomiting [176, 197]. Pure THC, marketed as Marinol® (INN: Dronabinol), was approved as an antiemetic in 1985 and as an appetite stimulant in 1992 for the treatment of AIDS-related body weight loss [176, 197]. In recent years, the interest of medical research in the ECS and cannabinoids as potential pharmacotherapeutic interventions for various indications has been emphasized [177, 198, 198–202]. The use of *Cannabis*-based drugs has been evaluated for Tourette's syndrome and recommended for the treatment of adult patients [203]. This is also supported by the findings of a study in which the administration of a combination of THC (10 mg/d) and CBD (20 mg/d) led to a rapid improvement of treatment-resistant symptoms in a patient with Tourette's syndrome [204]. Since 2017, a German legal reform permits the extraordinary medicinal prescription of *Cannabis* in the form of dried blossoms and extracts for patients with severe diseases (§ 31 paragraph 6 SGB V).

Since CBD lacks psychoactivity, it has emerged as the preferred candidate for preclinical research and has shown a favorable safety profile in a number of clinical studies [205]. CBD is part of the oro-mucosal spray Sativex® (INN: Nabiximols), which is approved for the therapy of treatment-resistant multiple sclerosis-(MS-)associated spasticity in 22 countries worldwide, including Germany since 2011 [206]. Sativex® contains roughly equal amounts of both, THC and CBD: each spray (100 µl) delivers a dose of 2.7 mg THC and 2.5 mg CBD (Sativex® package leaflet, 2015). The spray is additionally approved by Health Canada for the symptomatic relief of MS-associated neuropathic pain and as an adjuvant analgesic for opioid-resistant pain in cancer patients [176]. The benefits of Sativex® therapy for patients with MS have recently been confirmed in further clinical studies [207, 208]. According to its analgesic effect, a TRPV1-dependent anti-hyperalgesic effect of CBD has been demonstrated in acute inflammation [182, 209]. Positive anti-convulsing properties of CBD have been reported for decades [210–215]. This finally led to the approval of Epidiolex®, a THC-free CBD extract from *Cannabis*, by the U.S. Food & Drug Administration (FDA) in 2018. Epidiolex® is licensed for the treatment of rare seizure disorders (i. e. difficult-to-treat or rare forms of epilepsy such as Dravet syndrome, Lennox-Gastaut syndrome). In addition to anxiolytic [216–219] also neuroprotective effects [220–223] of CBD were reported. In these contexts, the participation of 5-HT receptors in these CBD-mediated effects was identified [222, 224]. Recently, several trials confirmed the neuroprotective effects of Sativex®-like combinations of phytocannabinoids in animal models and human patients with Huntington's disease [225–227]. CBD further induced the migration and

osteoblastic differentiation of mesenchymal stem cells, suggesting a potential role in wound healing and degenerative bone diseases [228]. Additionally, anti-oxidant properties of CBD have been demonstrated in several studies. For example, CBD reduced lipopolysaccharide-induced vasculitis in the mouse brain [229], protected against hepatic I/R injury [230] and acute alcohol-induced liver steatosis [231] in mouse models, and reduced ER stress in oligodendrocyte progenitor cells [232].

### 1.3.7 CBD in cardiovascular disease and cancer

Potential anti-cancer effects of CBD have been demonstrated by inhibition of cancer cell invasion [233–236] and endothelial cell angiogenesis [237], induction of cancer cell apoptosis [238], and immune cell-mediated cancer cell lysis [239]. The anti-tumor effects of cannabinoids and strategies targeting the ECS in terms of anti-cancer approaches have recently been intensely investigated [117, 240]. CBD has also indicated useful for mediating positive effects on cardiovascular pathologies, which have been investigated in detail elsewhere [241]. For example, CBD attenuated the high glucose-induced inflammatory response and barrier disruption in human coronary artery endothelial cells, indicating potential benefits against diabetic complications and atherosclerosis [242]. The cardioprotective effects of CBD were further substantiated *in vivo*. In a rat model of I/R [243] and a mouse model of diabetic cardiomyopathy, CBD attenuated myocardial dysfunction by reducing cardiac fibrosis, oxidative/nitrative stress, inflammation and cell death [242].





## 2 Aim of the thesis

The aim of this study was to investigate the potential benefit of CBD in terms of disease-associated characteristics of VSMC, namely the excessive proliferation and migration of these cells. In detail, the possible involvement of cannabinoid-activated receptors (CB<sub>1</sub>R, CB<sub>2</sub>R, TRPV1, and GPR55) and the role of HO-1 in CBD-mediated effects should be further evaluated. Human umbilical artery smooth muscle cells (HUASMC) were used as a suitable VSMC type.

To investigate a potential cannabinoid-mediated modulation of HO-1, analyses of protein and mRNA expression were performed. In further investigations, the underlying mechanism of the CBD effect on HO-1 should be further defined. Chemical inhibitors were used to investigate the involvement of cannabinoid-activated receptors at the protein level. The participation of reactive oxygen species (ROS) in HO-1 induction was analyzed at the protein level and by flow cytometry using the glutathione precursor *N*-acetylcysteine (NAC). In order to evaluate the influence of CBD on VSMC functions, proliferation, migration and viability analyses were performed.

The proliferation rate was quantified using the antibody-based BrdU incorporation assay. Additionally, photographic images of cell monolayers were taken to visualize these effects. The cell viability was determined by trypan blue exclusion staining and flow cytometry. Investigation of cellular migration was carried out using a modified Boyden chamber assay, which ended with staining and counting of the migrated cells. The role of HO-1 was investigated using both, a chemical inhibitor of HO-1 activity and knockdown of HO-1 protein expression via RNA interference.

The outcomes of these investigations provide the basis for further investigations of the effects of CBD and other cannabinoids on VSMC. Furthermore, the results of this work may complement the existing findings on the anti-tumor properties of cannabidiol, which may partly depend on VSMC functions. This study also contributes to further elucidation of the function of HO-1 in VSMC.



## 3 Materials and Methods

### 3.1 Materials

All materials, equipment, and software as well as the recipes of buffers and solutions used in the experimental and evaluating parts of this work were accurately listed in tabular form and included to the attachment of this thesis (see chap. 12.1, page 103).

### 3.2 Methods

#### 3.2.1 Cultivation of adherent cells

HUASMC are adherent cells which were maintained in antibiotic-free smooth muscle cell growth medium (SMCGM) supplemented with fetal calf serum (FCS; 5% [v/v]), epidermal growth factor (EGF; 0.5 ng/ml), basic fibroblast growth factor (bFGF; 2 ng/ml) and insulin (5 ng/ml). This medium composition is in the following referred to as complete SMCGM (cSMCGM). Cells were routinely cultured in cSMCGM in tissue culture flasks with a growth area of 75 cm<sup>2</sup> (TC75-flask) under standard culture conditions (5% CO<sub>2</sub>, 37 °C, humidified atmosphere). In some experiments, however, cells were cultured in a reduced SMCGM (rSMCGM) that contained 2% FCS [v/v] but lacked all other supplements.

#### *Expansion and subcultivation*

For expansion, one vial of cryopreserved HUASMC was quickly thawed in a pre-warmed water bath (37 °C) and the cell suspension was immediately transferred into a TC75-flask containing 12 ml of pre-warmed cSMCGM. After 24 h, the medium was exchanged by fresh, pre-warmed cSMCGM. Thereby, residues of the cryopreservation medium as well as non-adhering, dead cells were removed. Every second to third day the spent medium was aspirated and exchanged by fresh cSMCGM. Subconfluent monolayers were then harvested for subcultivation. Therefore, spent medium was aspirated and cells were carefully washed twice with 5 ml of pre-warmed Dulbecco's phosphate buffered saline (DPBS). Then, cells were enzymatically detached for 1–3 min with 3 ml of a pre-warmed 1X Trypsin-EDTA (TE) solution. The pancreatic enzyme trypsin is a serine protease, which specifically cuts proteins after defined amino acid sequences. Hereby, cellular adhesion proteins, which anchor cells to surfaces and enable cell-cell-interactions, are degraded and cells are released into the tissue culture medium. The progress of cell detachment was monitored by light microscopy and inactivated by addition of 7 ml Dulbecco's

modified Eagle's medium (DMEM) containing 10% FCS. Subsequently, cells were counted as described below. Viable cells were seeded in TC75-flasks at a density of 4,000–7,000 cells/cm<sup>2</sup>.

#### *Determination of cell number and viability*

The cell suspension was pelleted by centrifugation (210 x g, 5 min). Subsequently, the supernatant was aspirated and the cell pellet was resuspended in at least 1 ml of cSMCGM. The samples were analyzed for cell number and viability by trypan blue assay in a Luna-II™ automated cell counter. Trypan blue is an azo dye derived from *ortho*-tolidine that enters cells through defective cell membranes. Stained cells are thus considered dead. In contrast, viable cells will not stain positive for trypan blue. For this analysis, 10 µl of cell suspension were mixed with 10 µl of trypan blue solution. The mixture was injected into a counting slide. Cells with a size of 10–30 µm size were automatically counted and analyzed for cell viability.

#### *Cryopreservation*

Cryopreservation facilitates long-term storage of cells. For this purpose, subconfluent cell monolayers were detached from TC75-flasks and cell number was analyzed as described above. After an additional centrifugation (210 x g, 5 min) the cell pellet was resuspended in the cryopreservation medium cryo-SFM with a final density of 1,000,000 viable cells per ml. Subsequently, aliquots of 1 ml per cryopreservation vial were stored in a freezing container at -80 °C overnight. The special freezing container, which was filled with pre-cooled (-20 °C) isopropanol, allowed a controlled reduction of temperature by 1 °C per minute. On the next day, the vials were transferred into a liquid nitrogen tank for long term storage at -196 °C.

#### *Seeding and stimulation of adherent cells*

Cell culture experiments were performed in cell culture plates of different formats, such as 6-well, 12-well, 24-well, and 96-well. Proliferation analyses (see chap. Analysis of cell proliferation, page 30) were performed in 96-well format using 5,000 cells/well. For analysis of protein expressions (see chap. 3.2.6, page 31) and flow cytometry experiments (see chap. 3.2.7, page 34), experiments were conducted in 6-well or 12-well format using 150,000 cells/well or 60,000 cells/well, respectively. For analysis of mRNA expressions (see chap. 0, page 27), 33,000 cells were seeded in 24-well format. For seeding of cells into these plates, cells were enzymatically detached as described in *expansion and subcultivation* (page 23). Cell number and viability were

analyzed as described in *determination of cell number and viability* (page 24). The detached cells were resuspended in the appropriate volumes of the respective SMCGM, transferred to the desired wells and allowed to adhere for 24 h in a humidified atmosphere (37 °C, 5% CO<sub>2</sub>). On the next day, cells were examined for confluence and viability using light microscopy prior to stimulation with test substances. Then, supernatant medium was aspirated and exchanged by fresh, pre-warmed cell culture medium. A 1-h pre-incubation was performed in co-incubation experiments using *N*-acetylcysteine (NAC, glutathione precursor, see suppl. Figure 12-2, page 112), tin protoporphyrin IX (SnPPIX, inhibitor of HO-1 activity), or substances targeting CB<sub>1</sub>R (AM251), CB<sub>2</sub>R (AM630), TRPV1 (capsazepine) and GPR55 (O-1918, O-1602) respectively. The efficiency of SnPPIX in inhibiting HO-1 activity was explained by its competitive antagonism, resulting from a blockade of the heme binding site of HO-1 [244] and was further proven by bilirubin formation assays in several studies [244–246]. The receptor antagonists and O-1602 were used at 1 µM, a concentration that has been shown to sufficiently regulate the corresponding receptor activity [184, 228, 233, 247]. All incubations were performed in cSMCGM, with the exception of experiments using treatment with recombinant human PDGF-BB (hPDGF-BB, in the following abbreviated as PDGF). In these experiments, cells were seeded and stimulated in rSMCGM (without supplements, 2% FCS). Most test substances were dissolved in dimethyl sulfoxide (DMSO) or in ethanol and further diluted in cSMCGM or rSMCGM. Final concentrations in incubates were DMSO, 0.01% (v/v) (for AM251, AM630, capsazepine, O-1602 and O-1918); ethanol, 0.033% (v/v) (for CBD and THC) and 0.1% (v/v) (for JWH-133 and MA). Vehicle for SnPPIX in incubates was cSMCGM containing 0.04% (v/v) sodium hydroxide solution (NaOH, 1 M). For NAC, vehicle in incubates was cSMCGM containing 0.6% (v/v) DPBS. Vehicle for PDGF in incubates was rSMCGM containing 0.02% (v/v) 0.1 M acetic acid/0.1% bovine serum albumin.

### 3.2.2 Knockdown experiments using RNA interference

#### *Principle of RNA interference*

RNAs are polynucleotide chains bearing important roles in coding, decoding, regulation, and expression of genes. Protein expression is a result of gene transcription, in which the mRNAs produced are subsequently translated into proteins. RNA interference, mediated by small interfering RNAs (siRNAs), is a naturally occurring mechanism of eukaryotic cells leading to a specific switch-off of genes by disruption of the mRNA translation [248]. SiRNAs are double-stranded RNA molecules of 20–25 base pairs in length that interfere with the translation of the mRNA exposing the complementary nucleotide sequence. As a result, the targeted

mRNA is degraded, thus diminishing the translation of the respective protein. The mechanisms of RNA interference are illustrated and explained in more detail in Figure 3-1.

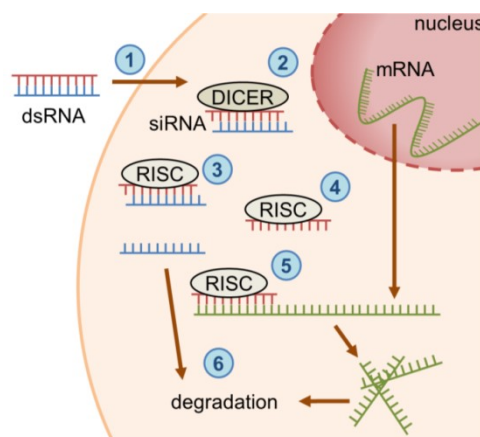


**Figure 3-1: Scheme of RNA interference.** After passing the cell membrane (1), the dsRNA molecules are truncated by Dicer (2). The siRNA molecules generated in this way, bind to the RNA-induced silencing complex (RISC, 3) which enzymatically separates sense (blue) and anti-sense strand (red, 4). The target mRNA is released from the nucleus and binds complementary to the anti-sense strand of the siRNA (5). The nuclease subunit of RISC splices the mRNA (5). Both, siRNA's sense strand and the spliced mRNA fragments are then degraded (6). (Illustration created according to [248]).

### *Transfection procedure*

Knockdown of HO-1 protein expression was performed using Lipofectamine™ RNAiMAX transfection reagent in a reversed procedure according to the manufacturer's instructions. In contrast to general transfection procedures, this method enables the enhancement of transfection efficiency and tolerability by transfecting cells in suspension. For one well of a 6-well plate, transfection complexes were generated by mixing 45 pmol siRNA with 5 µl Lipofectamine™ RNAiMAX in Opti-MEM to a final volume of 500 µl. The solutions were mixed thoroughly and incubated for 20–30 min at room temperature to form transfection complexes. Then, HUASMC at a density of 150,000 cells/2.5 ml SMCGM were seeded in 6-wells already containing the generated transfection complexes. Control cells were transfected with the same amount of a non-targeting siRNA (NON). Experimental settings were adapted for biochemical and flow cytometry assays, which were conducted in other well plate formats. The final concentration of siRNA was 15 nM. After 24 h, the transfection medium was replaced with fresh medium and cells were used for experiments.

### 3.2.3 Analysis of mRNA expression via qRT-PCR

#### *Historical and functional background of qRT-PCR method*

The combination of reverse transcription (RT), polymerase chain reaction (PCR), and quantification (q) is termed qRT-PCR. The PCR was developed by the biochemist Kary B. Mullis and his colleagues at the end of the 1980s [249, 250]. This method enables the *in vitro* amplification of DNA using a DNA polymerase (for detailed information please refer to Figure 3-2) [249, 250]. The method's name was derived from the chain reaction in which the products of the previous cycles are exponentially duplicated in the subsequent cycles. The investigation of gene expression patterns using RNA samples is enabled by the use of a RNA-dependent polymerase (RDP), also known as reverse transcriptase (RT). This enzyme naturally occurs in retroviruses (e. g. HIV) and DNA viruses (e. g. the hepatitis B virus) and transcribes RNA into DNA. The synthetic production of cDNA from natural RNA by use of a RDP from avian myeloblastosis virus (AMV) was first reported in 1971 [251]. One-step-RT-PCR, as used in the present study, was first described in 1990 [252]. The method utilizes the heat-stable Taq-polymerase, which derives from the bacterium *Thermus aquaticus*. Although being a DNA-polymerase, the Taq-polymerase exhibits RDP-activity. This approach reduced response time and improved accuracy of the reaction [252]. Application of fluorescence-labelled probes enables the quantification of the amplified DNA in real time. It is therefore referred to as real-time or quantitative PCR (qPCR). In this process, the fluorescence increases in proportion to the number of PCR products. This project used so-called FAM probes. These probes are coupled to a

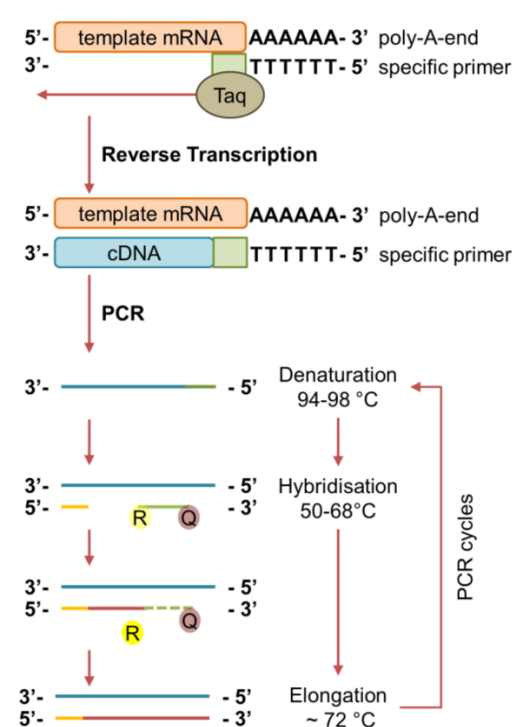


**Figure 3-2: Schematic representation of the qRT-PCR process.** Taq-polymerase (Taq) recognizes the target specific primers (green) that bind to the template mRNA (red). Taq, by its RDP-activity, synthesizes a cDNA (blue), thereby constructing an mRNA:cDNA hybrid. This hybrid, and later the double-stranded DNA fragments, is separated by heat. This is called denaturation. Probes and sequence-specific primers hybridize at approx. 50–68 °C. The optimum temperature is slightly below the melting temperature of the primer, which depends on its length. Extension of primer-DNA (elongation) by Taq occurs at approx. 72 °C. In this process, the attached probe is gradually replaced by newly-synthesized DNA. The separation of the reporter fluorophore (R, e. g. FAM) and the quencher (Q) eliminates the quencher's inhibitory effect thus enabling the detection of the fluorescence signal. After elongation, the next PCR cycle starts with the denaturation of the synthesized products.

quencher at the 3' end and to the reporter fluorescent dye FAM (6-carboxyfluorescein) at the 5' end. The 5'-3'-exonuclease activity of the Taq-polymerase separates the reporter fluorophores from the probe during DNA synthesis. The increasing distance between quencher and fluorophores enables the measurement of reporter fluorescence. This occurs at the end of each elongation cycle.

### *Sample preparation*

For quantification of mRNA expressions, 33,000 cells were seeded in 24-well format and treated as described above (see chap. 3.2.1, page 24). After exposure to test substances or vehicles, the total RNA was isolated using the RNeasy Mini kit according to the manufacturer's instructions. Briefly, the supernatant was removed and cells were covered with 350 µl of RLT lysis buffer. If necessary, the plates were sealed and stored at -80 °C until further processing. Thawed lysates were covered with 350 µl of 70 % ethanol. The mixture was transferred into centrifugation columns and centrifuged at 800 x g for 20 s. The fluid has been discarded. The columns were washed initially with 500 µl of the RW1 buffer and subsequently two times with 500 µl of RPE buffer. The last washing step was followed by centrifugation at 8,000 x g for 2 min. The liquid flow was discarded and the column was centrifuged dry at 14,000 x g. The RNA was eluted with 30 µl of RNase-free water and centrifugation at 8,000 x g for 1 min. The RNA was collected in a RNase-free reaction vial and stored at -80 °C until further analysis. Expression levels of target mRNAs were determined by qRT-PCR using the TaqMan® RNA-to-C<sub>T</sub>™ 1-Step kit. Primers and probes for human β-actin, HO-1 and HO-2 were TaqMan® gene expression assays. All experiments were performed according to the manufacturer's instructions. Briefly, a RNA template-free master mix was prepared as listed in Table 3-1.

Then, 5 µl of RNA template were transferred to a MicroAmp™ reaction plate prior to the addition of 15 µl master mix. All components were light-protected and kept on ice for the time of preparation. The reaction plate was sealed with optical adhesion film before starting the procedure.

**Table 3-1: Composition of qRT-PCR master mix**

Component	Volume for one reaction
TaqMan® RT-PCR mix (2X)	10.0 µl
TaqMan® gene expression assay (20X)	1.0 µl
TaqMan® RT enzyme mix (40X)	0.5 µl
RNase-free water	3.5 µl
Total volume	15.0 µl



The qRT-PCR, including 40 cycles of PCR, was run using the temperature protocol depicted in Figure 3-3. The levels of mRNA expression were analyzed by comparison of threshold cycle ( $C_t$ ) values<sup>k</sup>. HO-1 and HO-2 mRNA levels were normalized to  $\beta$ -actin and samples were compared to appropriate vehicle controls.

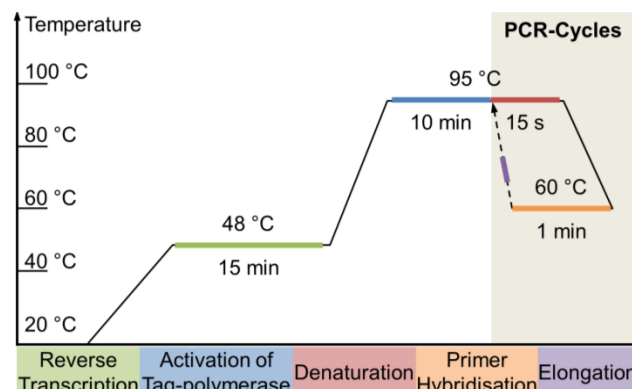


**Figure 3-3: Scheme of the qRT-PCR temperature profile.** Reverse transcription proceeded at 48 °C for 15 min. The Taq-polymerase was thermally activated at 95 °C for 10 min. This was followed by 40 PCR cycles. The DNA was denatured at 95 °C for 10 s. Hybridization of primers occurred after cooling to 60 °C. After 1 min the temperature was increased to 95 °C. Elongation occurred during the temperature increase.

### 3.2.4 Analysis of cell migration

#### *Principle of migration experiments*

Migration is the active locomotion of cells resulting in a change of place. The term migration includes the undirected spontaneous (random) migration, the directed chemotactic movement and changes in chemokinesis. Using a modified Boyden chamber assay cellular motility was monitored as migration through Falcon® cell culture inserts (8  $\mu$ m pore size) towards the chemoattractant PDGF.

#### *Procedure of migration experiments*

In order to investigate the role of HO-1 in the migration of HUASMC, two different experimental settings were used. First, cells seeded in rSMCGM were subjected to treatment with the HO-1 activity inhibitor SnPPiX and test substances as stated above (see chap. 3.2.1, page 24). After incubation, cells were counted and viable HUASMC (50,000 cells/0.5 ml rSMCGM) were seeded in Falcon® cell culture inserts. Migration was initiated subsequently. Second, after reversed transfection in rSMCGM (see chap. 3.2.2, page 26), viable HUASMC (30,000 cells/0.5 ml rSMCGM) were seeded in Falcon® cell culture inserts and incubated (37 °C, 5% CO<sub>2</sub>) with CBD (6  $\mu$ M and 10  $\mu$ M) or appropriate vehicle for 60 min before initiation of migration. In both setups, migration was initiated by addition of 500  $\mu$ l rSMCGM containing

<sup>k</sup> The  $C_t$  value is a theoretical quantity that describes the beginning of the exponential growth of a curve. In this method, the  $C_t$  value describes the part of the curve in which the fluorescence for the first time increases exponentially above the background value.

PDGF (20 ng/ml) or vehicle to the companion plate. Cells were further incubated (37 °C, 5% CO<sub>2</sub>) for 6 h. Then, supernatant medium was aspirated and non-migrated cells on the upper surface of the insert were removed with a cotton swab. Afterwards, the insert was carefully washed with DPBS. Cells on the lower surface of the inserts were fixed and stained with Diff-Quick staining according to the manufacturer's instructions. Briefly, the prepared inserts were successively dipped into fixation solution, staining solution I and staining solution II. The inserts were immersed for up to 10 s in each solution. Between the different steps, adhering excess of solutions was wiped off on a paper towel. Afterwards, fixed and stained inserts were washed in deionized water to remove excess dye. After complete drying, inserts were photographed at 10X magnification using a digital microscope camera. Five randomly selected fields per insert were counted.

### 3.2.5 Analysis of cell proliferation

#### *Principle of proliferation assay*

Bromodeoxyuridine (BrdU) is a synthetic nucleoside that is chemically analog to thymidine and deoxyuridine, respectively. BrdU is generated by connection of deoxyribose and the nucleobase 5-bromouracil and is used in the diagnostic labelling of proliferating cells in vital tissues [253]. BrdU is incorporated by cells and subsequently, its phosphorylated form is integrated into newly synthesized DNA thereby substituting the nucleotide deoxythymidine triphosphate (dTTP). Thus, BrdU labelling of cells directly correlates to the rate of DNA synthesis during the synthesis-(S-)phase of the cell cycle. Antibodies directed against BrdU are then used to detect the incorporated chemical, indicating actively replicating cells. Antibody labelling requires denaturation of DNA and opening of cell membranes, both realized by exposing the cells to acid.

#### *Procedure of the proliferation assay*

The impact of test substances on proliferation of HUASMC was quantified using BrdU Cell Proliferation enzyme-linked immunosorbent assay kit according to the manufacturer's instructions. Briefly, 5,000 cells were seeded into 96-well format and allowed to grow for 24 h. Then, the medium was refreshed and cells were challenged to test substances or vehicles for the indicated times. 1X BrdU reagent was added 6-24 h prior to analysis. After incubation, the medium was removed and the cells were covered with fixing solution and incubated for at least 30 min at room temperature. Then, the samples were washed three times with 1X wash buffer and incubated with pre-diluted anti-BrdU detection antibody for 1 h at room temperature.

Afterwards, the samples were washed three times with 1X wash buffer and incubated with HRP-conjugated secondary detection antibody (30 min, room temperature). Then, the samples were washed three times with 1X wash buffer plus an additional washing using distilled water. Then, samples were incubated with substrate solution for a maximum of 30 min light-protected. The stop solution was added at the end of the incubation period or when the samples turned blue. The absorption was measured at 450/550 nm using a plate reader. Cells that did not receive BrdU reagent served as blank. Each experiment consisted of four repeats per sample.

### 3.2.6 Protein expression analysis

The evaluation of the influences of the test substances on cellular protein expression patterns was carried out using the Western blot technique. For this purpose, cellular proteins were isolated, separated and detected to ensure a specific and quantitative analysis.

#### *Isolation of cellular proteins*

Whole cell culture lysates were prepared by combining floating and adherent cells. Briefly, the supernatant containing floating cells was collected and adherent cells were washed with pre-warmed DPBS before being detached using 1X TE. Trypsin activity was inhibited by addition of 10% DMEM and cells were rinsed off the wells and combined with the collected floating cells. After centrifugation (800 x g, 5 min), the cell pellet was resuspended in 50 µl sample buffer. Cells were then lysed by sonication, heated for 5 min at 95 °C and centrifuged at 20,000 x g for 5 min at 4 °C. Supernatants were stored at -20 °C until further analysis.

#### *Principle and procedure of protein concentration analysis*

The protein concentrations of cellular lysates were determined using the Pierce® bicinchoninic acid (BCA) protein assay kit according to the manufacturer's protocol. This assay relies on two distinct reactions (Figure 3-4) [254]. First, peptide bonds in the proteins reduce  $\text{Cu}^{2+}$  ions from copper (II) sulfate to  $\text{Cu}^+$  in a temperature-dependent reaction and proportional to the amount of protein present in the sample. In a ratio of 1:2  $\text{Cu}^+$  ions and BCA form a purple-colored complex with a maximum absorption at approx. 570 nm. Briefly, 5 µl of lysate were mixed with aqua ad injectabilia yielding a final dilution of 1:10. Then, 10 µl of the diluted lysate were mixed with 200 µl of working solution (50:1-mixture of reagent A and reagent B as provided in the kit) after transfer into 96-wells.

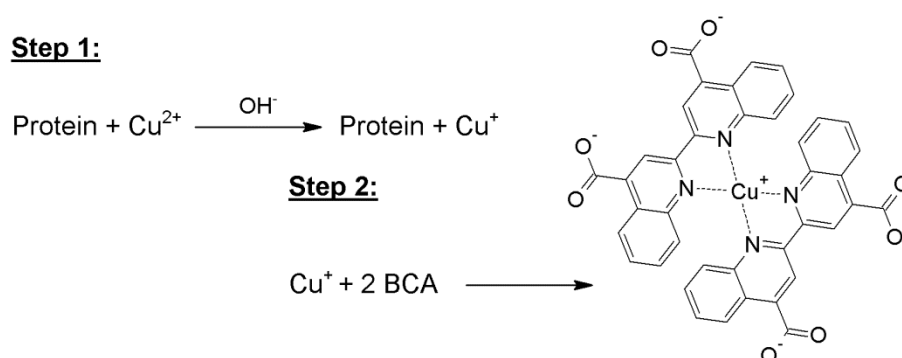


**Figure 3-4: Chemical reaction of the BCA protein assay.** Reaction equation according to [254]. See text for details.  $\text{Cu}^{2+}$ : divalent copper ion;  $\text{OH}^-$ : hydroxide ion;  $\text{Cu}^+$ : monovalent copper ion; BCA: bicinchoninic acid

Protein concentrations of samples were quantified under consideration of the sample dilution using the calibration function of a standard curve from 0–1 mg/ml bovine serum albumin. Standards and samples were analyzed in duplicates and triplicates, respectively. After incubation (37 °C, 30 min), absorbance was measured at 570 nm using a plate reader.

### *Protein separation*

Sodium dodecyl sulfate-polyacrylamide gel electrophoresis (SDS-PAGE), invented by Ulrich K. Laemmli, enables the separation of proteins in an electrical field according to their molecular weight [255]. The separating matrix used in this electrophoresis was a discontinuous gel based on poly acrylamide. By use of the anionic detergent SDS, the charge of the proteins is covered resulting in negatively charged SDS-protein complexes. Proteins and SDS bind in a ratio of 1.4 g SDS/g protein [256]. Both, negative SDS charge (causes repulsion) and heating of the samples, lead to the denaturation (i. e. linearisation) of the proteins. This procedure allows protein separation according to protein length, which is proportional to the molecular weight. Large proteins have a higher retention than small proteins, which leads to different migration patterns.

SDS-PAGE was conducted using either Bio-Rad Mini-PROTEAN® Tetra Cell System or SE 250 Mini-Vertical Unit. For electrophoresis, gels with 10% or 12% acrylamide content and 1 mm or 1.5 mm thickness were used to separate samples containing 50 µg of total protein. Samples were adjusted to equal protein concentration and sample volumes by mixing with aqua ad injectabilia. Permanent breakdown of disulfide bonds was ensured by addition of 5% [v/v] β-mercaptoethanol to each sample. Samples were additionally supplemented with 1–2 µl bromophenol blue to visualize the migration front. Then, protein samples were carefully transferred into the pockets of the gel using a microliter syringe.

For the approximation of the protein size, a prestained SDS-PAGE standard was run simultaneously. Gels were run in 1X electrophoresis buffer at 15 mA/gel (stacking gel) and 25 mA/gel (separation gel), respectively. Electrophoresis was stopped before the migration front reached the end of the gel.

#### *Western blot protein transfer*

Immediately after electrophoretic separation, proteins were transferred onto a nitrocellulose membrane by Western blot technique using a semi-dry transfer system. Therefore, extra-thick blotting paper and nitrocellulose membrane were cut to the size of the gel and pre-incubated in transfer buffer for 5–30 min. Excess of buffer solution was removed from blotting papers prior to transfer preparation. Then, a blotting sandwich was assembled by stacking following layers from bottom to top: blotting paper - nitrocellulose membrane - gel - blotting paper. Air bubbles were removed and the blotting sandwich was compressed by carefully rolling over every layer using a glass tube. Transfer was run for 70 min at 41 mW/cm<sup>2</sup>, 2.73 mA/cm<sup>2</sup> and 15 V (constant).

#### *Immunologic detection of proteins (chemiluminescence)*

After the transfer was completed, membranes were put into 50 ml centrifuge tubes to remove residual transfer buffer by washing with TRIS-buffered saline/Tween®20 (TBS-T). All washing and incubation steps were performed on a roller mixer at 30 rotations per minute. Blocking of free nitrocellulose binding sites was ensured by incubation for 1 h in blocking solution (BS). Then, membranes were incubated with specific primary antibodies at 4 °C overnight. Afterwards, membranes were washed with TBS-T and probed with appropriate horseradish peroxidase-linked secondary antibodies. All antibody dilutions used here are listed in Table 3-2. Antibody binding was visualized by enhanced chemiluminescence (ECL) reaction (see suppl. Figure 12-3, page 113) and quantified by densitometric analysis using Quantity One 1-D analysis software. Therefore, membranes were placed in an unlighted Bio-Rad universal hood and covered with 2 ml of ECL detection solution. Emission of light was detected in intervals for up to 300 s (e.g. for HO-1, HO-2) or a maximum of 60 s (for  $\beta$ -actin) with starting times dependent on the signal strength. Images that did not show overexposed signals were used for quantification. After analysis, membranes were prepared for reprobing or storage as described below. Expressions of proteins were normalized to  $\beta$ -actin and compared to the appropriate vehicle controls.

**Table 3-2: Antibody dilutions used for immunologic detection.**

Primary antibody	Dilution in 5% BS	Secondary antibody	Dilution in 1% BS
HO-1	1:1,000	anti-rabbit IgG	1:1,000
HO-2	1:1,000		
TRPV1	1:500		
GPR55	1:500		
CB <sub>1</sub> R	1:200	anti-mouse IgG	1:1,000
CB <sub>2</sub> R	1:200		
β-actin	1:10,000		

### *Stripping and storage of membranes*

The removal or inactivation of primary and secondary antibodies from a membrane is termed “stripping”. This operation is used in order to investigate more than one protein on the same blot. Therefore, the membranes were incubated twice with 5 ml of 1X stripping buffer for 15 minutes. Then, the membranes were washed three times with TBS-T. Subsequently, the membranes were incubated in 3–5 ml of BS and reprobed with another primary antibody. If no reprobing was required, membranes were stripped and washed gradually with TBS-T and deionized water, respectively. Then, membranes were air dried on paper towels and stored in transparent pockets at 4 °C.

### 3.2.7 Flow cytometry analyses

#### *Operating principle of flow cytometry*

The flow cytometry analysis is based on the detection of optical signals emitted by single cells after passing a laser beam (for detailed illustrations refer to suppl. Figure 12-4, page 114). The sheath fluid hydrodynamically focuses the cell suspension. This divides the cell population into single cells, which are then directed into the measuring cuvette (i. e. flow cell). Herein, the single cells pass a laser beam and thus scatter the light. The forward scatter, which is measured along the path of the laser, allows the discrimination of cells by size. The side scatter, which is measured at a 90-degree angle relative to the laser, provides information about the internal complexity (i. e. granularity) of a cell. Measurement of both light scatters in conjunction allows simple cellular differentiation within a heterogeneous cell

population. Additionally, the measurement of emitted fluorescence signals, induced by labelling with fluorescent probes, allows further distinctions by detection of e. g. cell surface markers (such as the cluster of differentiation [CD]), membrane integrity (a parameter for cell viability), DNA content and others.

#### *Detection of oxidative stress using CellROX™ green staining*

Analysis of oxidative stress in HUASMC was performed using the CellROX™ green flow cytometry assay kit according to the manufacturer's instructions. The CellROX™ green reagent is a cell-permeable probe that, when oxidized in presence of ROS, binds to DNA and exhibits a strong fluorogenic signal with absorption/emission maxima of 508/525 nm. Co-staining with SYTOX™ red dead cell stain allows distinction between oxidative stressed, non-stressed and dead cells. Briefly, HUASMC were seeded in 12-well plates and allowed to adhere for 24 h. Then, medium was refreshed and cells were pre-incubated with NAC (0.5–3 mM) or vehicle for 1 h. Cells were then co-incubated with CBD (6 µM, 10 µM) for 3 h before addition of CellROX™ green reagent (500 nM). After 1 h, floating cells were collected and combined with the adherent cells that were harvested by detachment with accutase solution according to the manufacturer's instructions. Cells were pelleted by centrifugation (200 x g, 5 min) and carefully resuspended in 200 µl cSMCGM. Finally, SYTOX™ red dead cell stain (5 nM) was added and cells were incubated in the dark for 15 min at room temperature. Subsequently, 10,000 cells per sample were analyzed with an AccuriC6™ flow cytometer. Appropriate gating of cell populations and compensation was ensured by analysis of unstained and single-stained cells, respectively. HUASMC that were treated with the ROS inducer tert-butyl hydroperoxide (TBHP, 250 µM) for 1 h prior to sample preparation served as a positive control. Negative control cells were pre-incubated with NAC (0.5 mM) prior to stimulation with TBHP.

#### *Detection of apoptosis by Annexin V/propidium iodide staining*

Detection of apoptosis was accomplished by flow cytometry using Fluorescein isothiocyanate-(FITC-)Annexin V (AV) apoptosis detection kit I according to the manufacturer's instructions. During apoptosis, cells undergo certain morphological changes such as loss of plasma membrane asymmetry, cell shrinkage and condensation of cytoplasm and nucleus. AV is a phospholipid-binding protein with high affinity for phosphatidylserine, which is exposed on the outer side of apoptotic but not viable cells. Both, progression of apoptosis and necrosis lead to loss of membrane integrity of cells. Therefore, co-staining with propidium iodide (PI), a membrane-impermeable dye, allows distinction between early- and late-apoptotic

cells. Cells that are considered viable are negative for both FITC-AV and PI; cells in early apoptosis are positive for FITC-AV but negative for PI. However, due to the loss of membrane integrity and binding of both FITC-AV and PI, there is no exact differentiation between late-apoptotic and necrotic cell populations in this assay. Briefly, HUASMC were seeded in 12-well plates and allowed to adhere for 24 h. After incubation with test substances, floating cells were collected and combined with the adherent cells that were harvested by detachment with accutase solution according to the manufacturer's instructions. Cells were pelleted by centrifugation (400 x *g*, 4 °C, and 5 min) and were then washed twice in 500 µl DPBS. Afterwards, cells were carefully resuspended in 200 µl 1X AV-binding buffer and incubated with 2 µl FITC-AV and 1 µl PI solution. Following 15 min of incubation in the dark, 10,000 cells per sample were analyzed with an AccuriC6™ flow cytometer. Appropriate gating of cell populations and compensation was ensured by analysis of unstained and single-stained cells, respectively. HUASMC that were fixed with ethanol prior to incubation with AV and PI served as a staining control.

### 3.2.8 Statistics

Measurement values of cell proliferation assay were analyzed for statistical outliers in each experiment using Nalimov test. Statistical analysis was performed using GraphPad Prism 6.01. One-way ANOVA plus Dunnett post hoc test was used for comparison of samples to vehicle control. Comparison among selected groups was carried out by Student's two-tailed *t* test (for kinetics) or with one-way ANOVA plus Šidák post hoc test. All values are presented as mean ± standard error of the mean (SEM). A *p* value  $P < 0.05$  was considered significant.



## 4 Results

### 4.1 Effects of cannabinoids on HO protein expression in HUASMC

A first experimental approach aimed to investigate the potential of four different cannabinoids, the phytocannabinoids CBD and THC (CB<sub>1</sub>R/CB<sub>2</sub>R agonist) as well as the synthetic cannabinoids R(+)-methanandamide (MA, CB<sub>1</sub>R agonist) and JWH-133 (CB<sub>2</sub>R agonist), to influence HO-1 and HO-2 protein expression in HUASMC. Therefore, the cells were incubated for 24 h with increasing concentrations (0.1–10  $\mu$ M) of the substances or respective vehicles followed by Western blot analysis (Figure 4-1).

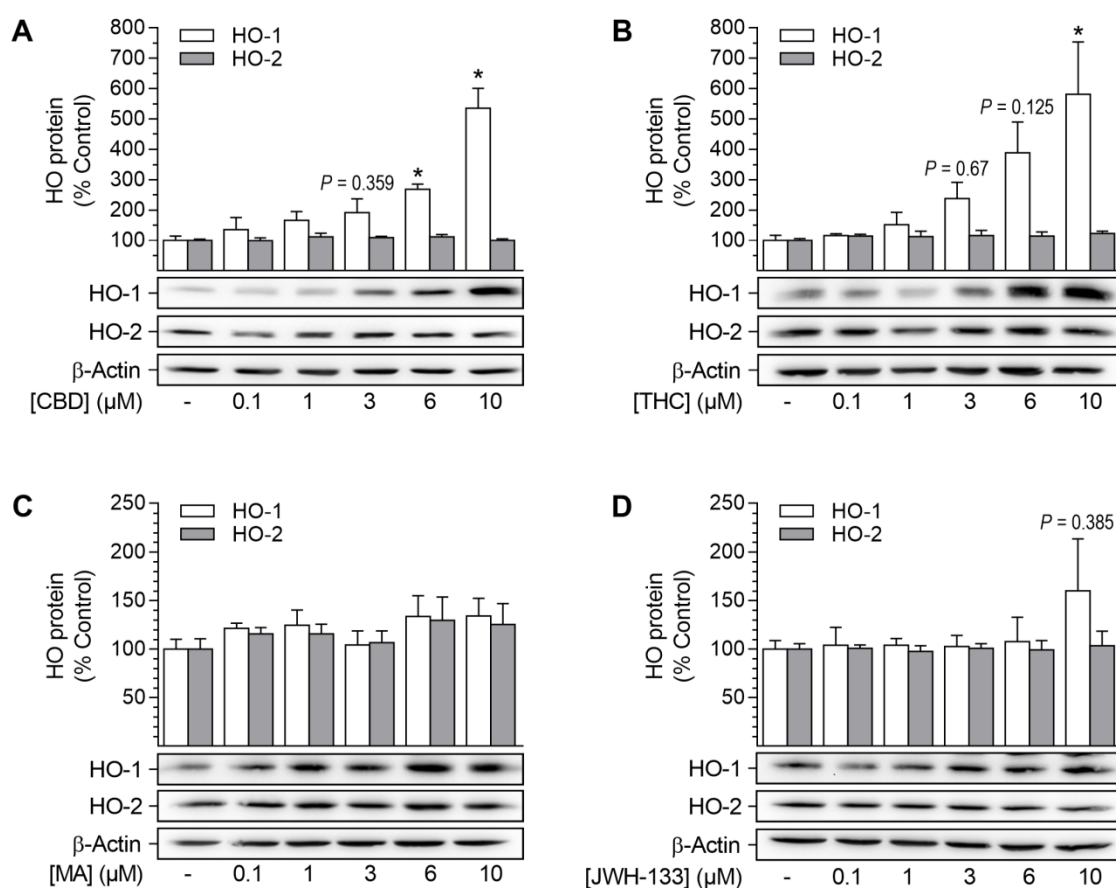


**Figure 4-1: Effects of cannabinoids on HO-1 and HO-2 protein expression in HUASMC.**

Cells were incubated for 24 h with CBD (A), THC (B), R(+)-methanandamide (MA) (C) or JWH-133 at the indicated concentrations. Following incubation, cells were harvested and lysates were analyzed for protein expression of HO-1 and HO-2 by Western blot. Protein expression values were normalized to  $\beta$ -actin. Percent control represents comparison with the corresponding vehicle-treated, time-matched group (set as 100%). Values are means  $\pm$  SEM of  $n = 4$  (A, HO-1),  $n = 5$  (A, HO-2) or  $n = 3$  (B, C, D) experiments. \* $P < 0.05$  vs. time-matched vehicle control; one-way ANOVA plus Dunnett post hoc test.

HO-1 protein expression was significantly increased in a concentration-dependent manner by both CBD (Figure 4-1A) and THC (Figure 4-1B). The CBD-mediated induction of HO-1 was significant at concentrations of 6  $\mu$ M and 10  $\mu$ M CBD, resulting in 2.7-fold and 5.4-fold increases of HO-1 protein, respectively (Figure 4-1A). Similarly, HO-1 protein expression was strongly increased at 6  $\mu$ M THC (3.9-fold) (Figure 4-1B). The THC-mediated induction of HO-1 protein became significant at 10  $\mu$ M, resulting in a 5.8-fold increase (Figure 4-1B). Conversely, neither R(+)-methanandamide (Figure 4-1C) nor JWH-133 (Figure 4-1D) led to a significant enhancement of HO-1 protein expression in the cells. Finally, HO-2 protein expression of HUASMC was not altered after incubation with increasing concentrations of any cannabinoid tested (Figure 4-1A–D).

CBD, due to its lack of psychoactivity and the potent induction of HO-1 shown in these experiments, displays an interesting candidate substance for therapeutic applications. CBD was therefore selected for further investigations in this study.

## 4.2 Characteristics of CBD-mediated HO-1 induction

Additional analyses targeted to characterize the CBD-mediated induction of HO-1 in HUASMC (Figure 4-2). First, investigations regarding an involvement of mRNA expression were performed following incubation with increasing concentrations (0.1–10  $\mu$ M) of CBD or the corresponding vehicle (Figure 4-2A).

After a 24-h incubation with CBD, HO-1 mRNA expression was strongly enhanced at 6  $\mu$ M (4.8-fold) and became significant after incubation with 10  $\mu$ M CBD which resulted in an 8.1-fold increase (Figure 4-2A). In consistence to the results of the protein expression analysis (Figure 4-1A, page 37), there was no increase of HO-2 mRNA expression in HUASMC following incubation with CBD at any concentration tested (Figure 4-2A). Next, kinetic studies were performed to investigate possible time-dependent effects of CBD on HO-1 mRNA and protein expression (Figure 4-2B–C). Therefore, cells were incubated for 6 h, 24 h or 48 h with 6  $\mu$ M CBD, a concentration that significantly induced HO-1 protein in previous experiments (Figure 4-1A). Kinetic studies revealed the CBD-mediated induction of HO-1 mRNA to be time-dependent. The enhancement of HO-1 mRNA expression was significant after 6 h (2.7-fold), peaked after 24 h with a 7.3-fold increase and then declined to a 4.2-fold increase during the 48-h incubation (Figure 4-2B). Accordingly, HO-1 protein expression was progressively increased up to 6.3-fold during a 48-h incubation with 6  $\mu$ M CBD (Figure 4-2C). Again, and in consistence to the data obtained previously (Figure 4-1A, page 37; Figure 4-2A), there was no induction of HO-2 mRNA or protein expression at any incubation time tested (see suppl. Figure 12-5, page 115).

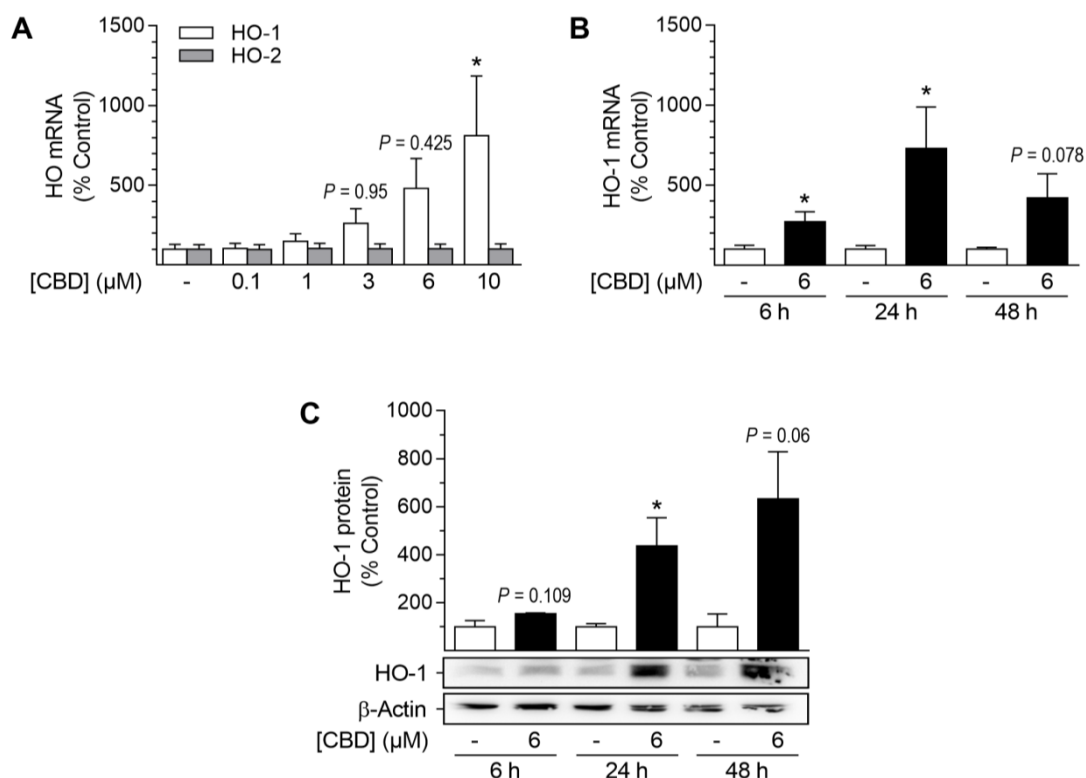


**Figure 4-2: Effect of CBD on HO-1 and HO-2 mRNA and protein expression in HUASMC.**

Cells were incubated for 24 h with increasing concentrations (0.1–10 μM) of CBD (A) or with 6 μM CBD for the indicated times (B, C). After incubation, cells were analyzed for mRNA expression of HO-1 (A, B) and HO-2 (B) or protein expression of HO-1 (C). Expression values were normalized to β-actin. Percent control represents comparison with the corresponding vehicle-treated, time-matched group (set as 100%). Values are means ± SEM of  $n = 6$  (A),  $n = 3$ –5 (B) or  $n = 3$  (C) experiments. \* $P < 0.05$  vs. time-matched vehicle control; one-way ANOVA plus Dunnett post hoc test (A) or Student's two-tailed  $t$  test (B, C).

### 4.3 Involvement of cannabinoid-receptor signaling in CBD-mediated induction of HO-1

The underlying mechanisms of CBD's action as well as its molecular targets in cells are still not fully identified and may vary dependent on cell type and conditions. Therefore, a potential participation of important and well-known cannabinoid-activated receptors in CBD-mediated induction of HO-1 was investigated (Figure 4-3).

To this end, HUASMC, treated with 10 μM CBD or the corresponding vehicle, were first analyzed for the presence of CB<sub>1</sub>R, CB<sub>2</sub>R, GPR55, and TRPV1 (Figure 4-3A, A<sub>1</sub>). All of the above-mentioned target receptors were expressed by HUASMC (Figure 4-3A, A<sub>1</sub>). Additionally, the protein expressions of these receptors were neither increased nor decreased after a 24-h incubation with CBD as shown by Western blot analysis (Figure 4-3A, A<sub>1</sub>).

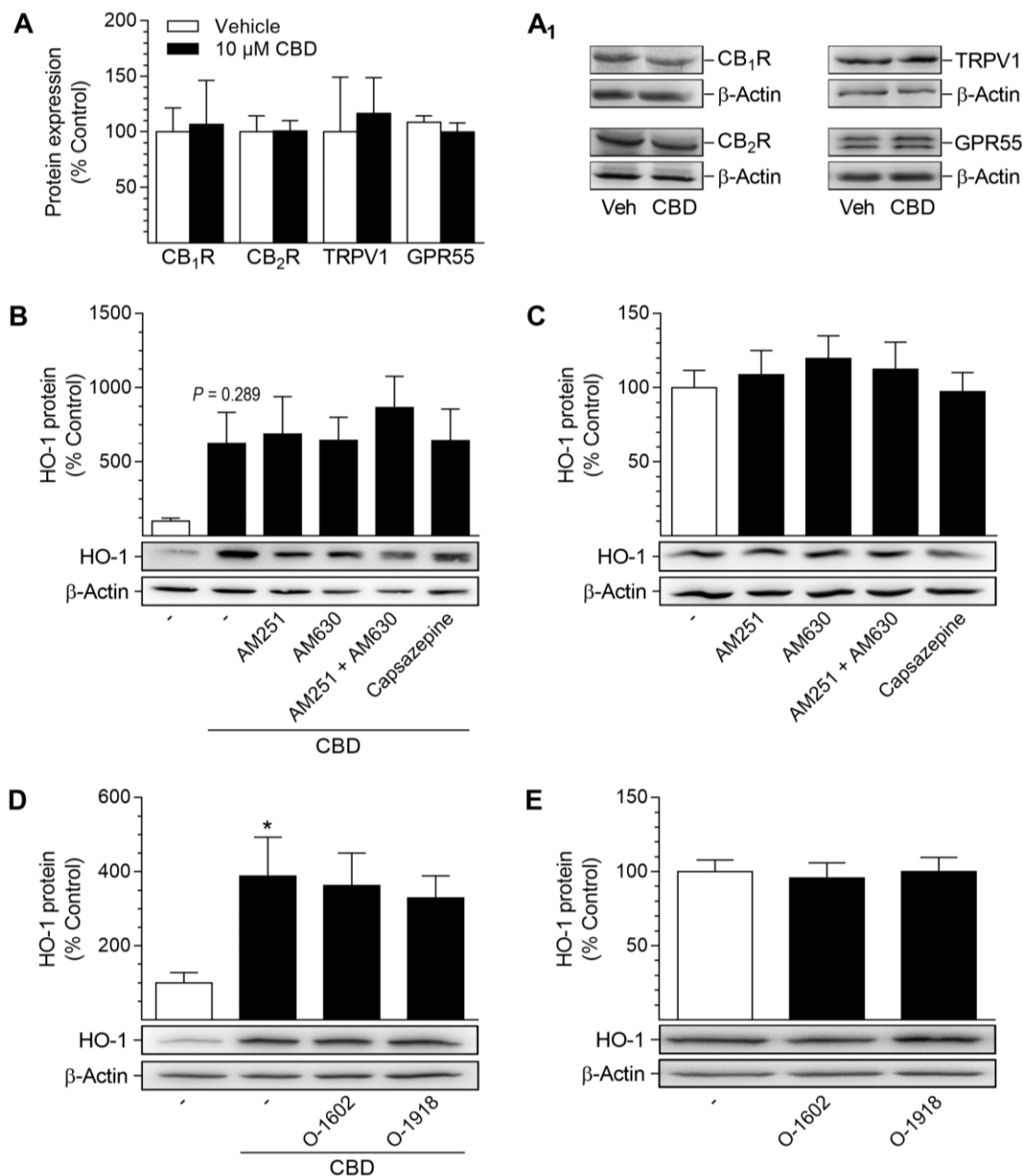


**Figure 4-3: Presence of potential target receptors of CBD in HUASMC and investigation of their involvement in CBD-mediated induction of HO-1 protein.** Analysis of target receptor presence was performed by Western blot following a 24-h incubation with 10 μM CBD or the corresponding vehicle (A, A<sub>1</sub>). For investigation of receptor involvement, HUASMC were pre-incubated with AM251 (CB<sub>1</sub>R antagonist), AM630 (CB<sub>2</sub>R antagonist), capsazepine (TRPV1 antagonist) O-1602 (GPR55 agonist) or O-1918 (GPR55 antagonist) for 1 h and then further co-incubated with (B, D) or without (C, E) 10 μM CBD for 24 h. Following incubation, cells were harvested and lysates were analyzed for protein expression of target receptors (A, A<sub>1</sub>) or HO-1 (B–E) via Western blot. Samples and control were adjusted to equal amounts of the respective vehicles. Protein expression values were normalized to β-actin. Percent control represents the comparison with the corresponding vehicle-treated, time-matched group (set as 100%). Values are means ± SEM of  $n = 3$  (A),  $n = 5$  (B, C, D) or  $n = 6$  (E) experiments. \* $P < 0.05$  vs. time-matched vehicle control; one-way ANOVA plus Šidák post hoc test. Statistical analysis was performed using Student's two tailed  $t$  test (A), one-way ANOVA plus Šidák post hoc test (B, D) or one-way ANOVA plus Dunnett post hoc test (C, E) and revealed no other significant differences between the analyzed groups.

Further experiments aimed to investigate the involvement of these cannabinoid-activated receptors in the CBD-mediated induction of HO-1 protein in HUASMC (Figure 4-3B, D). In order to block the receptor signaling, HUASMC were pre-incubated for 1 h with antagonists targeting CB<sub>1</sub>R (AM251), CB<sub>2</sub>R (AM630), TRPV1 (capsazepine) and GPR55 (O-1918) followed by a 24-h co-incubation with CBD (10  $\mu$ M, Figure 4-3B, D). Additionally, a potential antagonistic effect of CBD on GPR55 was investigated using the GPR55 agonist O-1602 (Figure 4-3D). Blocking of receptor signaling by pre-incubation with antagonists targeting CB<sub>1</sub>R, CB<sub>2</sub>R, TRPV1 and GPR55 did not alter the CBD-mediated induction of HO-1 protein in HUASMC after a 24-h co-incubation with 10  $\mu$ M CBD (Figure 4-3B, D). Similarly, pre-incubation with the GPR55 agonist O-1602 prior to treatment with 10  $\mu$ M CBD did not alter the CBD-mediated induction of HO-1 protein expression (Figure 4-3D). Finally, a 24-h incubation with the receptor activity-modulating substances (1  $\mu$ M) alone had no impact on HO-1 protein expression compared to the corresponding vehicle-treated groups (Figure 4-3C, D).

#### 4.4 Involvement of ROS in CBD-mediated induction of HO-1

The general mechanism leading to the induction of HO-1 is described to involve a ROS-dependent electrophilic attack leading to an Nrf2-mediated activation of *HMOX1* transcription [61, 63–65]. In order to examine an involvement of ROS in the CBD-mediated induction of HO-1, the oxidant-scavenging glutathione system was strengthened by pre-incubation with the glutathione precursor NAC (for details see suppl. Figure 12-2, page 112) prior to a 24-h co-incubation with CBD at 10  $\mu$ M (Figure 4-4A). The Western blot analysis of HO-1 protein revealed that the CBD-mediated HO-1 induction, which resulted in a 3.7-fold increase (vs. control), was significantly reduced by pre-incubation with NAC at 0.5–3 mM (Figure 4-4A). Herein, NAC, at any concentration tested, did not alter HO-1 protein expression *per se*<sup>1</sup> (Figure 4-4A). Based on these results, the potential pro-oxidant capability of CBD was investigated in subsequent flow cytometry-based analyses using the ROS-sensitive probe CellROX™ green (Figure 4-4B–E). In an exemplary experiment, HUASMC were pre-incubated with NAC or CBD prior to a 1-h co-incubation with the ROS inducer TBHP (Figure 4-4C). TBHP strongly increased the mean fluorescence intensity (MFI) of CellROX™ green-stained HUASMC (Figure 4-4C, red line), whereby the MFI of CellROX™ green in TBHP-treated cells was reduced by pre-incubation with NAC (0.5  $\mu$ M, Figure 4-4C, green line).

---

<sup>1</sup> from the Latin: by or of itself

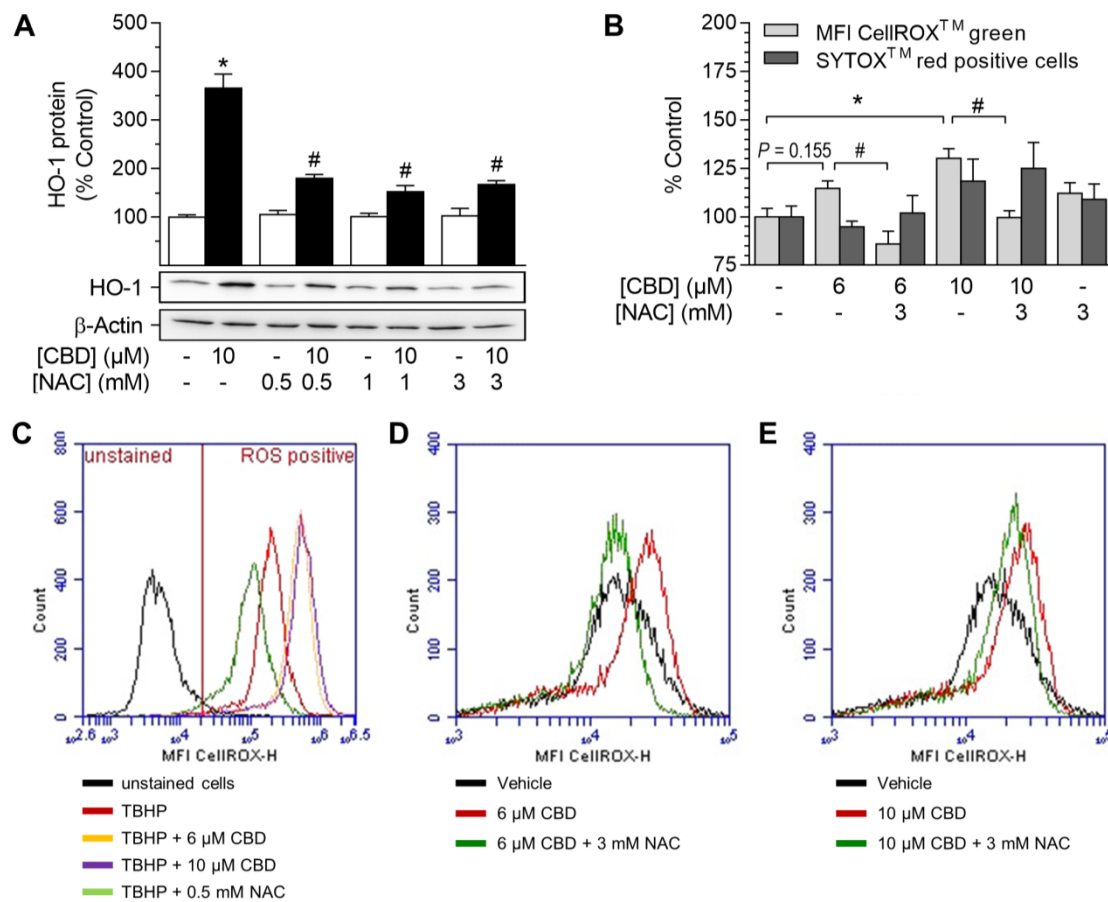


**Figure 4-4: Effect of NAC on CBD-mediated induction of HO-1 protein and ROS generation in HUASMC.** Cells were pre-incubated for 1 h with NAC at indicated concentrations prior to co-incubation with 10 μM CBD for 24 h (A). For detection of ROS generation (B–E), cells were pre-incubated with 0.5 mM (C) or 3 mM NAC (B, D–E) followed by a 4-h co-incubation with CBD as indicated. The ROS-inducing substance TBHP (250 μM) was added as a positive control 1 h prior to sample preparation. Following incubation, cells were harvested and analyzed for HO-1 protein expression (A) or oxidative stress level using flow cytometry (B–E). Protein expression values were normalized to β-actin. Percent control represents the comparison with the corresponding vehicle-treated, time-matched group (set as 100%). Values are means ± SEM of  $n = 4$  (A),  $n = 6$  (B, D–E) or  $n = 1$  (C) experiments. \* $P < 0.05$  vs. time-matched vehicle control; # $P < 0.05$  vs. CBD-treated group; one-way ANOVA plus Šidák post hoc test.

In contrast, pre-incubation with CBD at 6 μM (Figure 4-4C, yellow line) or 10 μM (Figure 4-4C, violet line) further enhanced the TBHP-mediated increase in the MFI of CellROX™ green-stained HUASMC.

Additional experiments were performed to further substantiate the relation between ROS generation and HO-1 induction mediated by CBD (Figure 4-4B, D–E). For that reason, cells were pre-incubated for 1 h with 3 μM NAC prior to a 4-h co-incubation with CBD at 6 μM (Figure 4-4B, D) or 10 μM (Figure 4-4B, E) followed by flow cytometry analysis. The MFI of CellROX™ green-stained HUASMC was raised by 15% after a 4-h incubation with 6 μM CBD (Figure 4-4B, D, red line) and was significantly increased to 130% at 10 μM CBD (Figure 4-4B, E, red line).

Additionally, the CBD-mediated enhancement in the MFI of CellROX™ green-stained HUASMC was significantly attenuated by the pre-incubation with 3 mM NAC at both 6  $\mu$ M and 10  $\mu$ M CBD (Figure 4-4B, D–E, green lines). The flow cytometry-based analysis of cell death, which was accomplished in parallel to ROS detection by co-staining with SYTOX™ red, however, revealed no significant increases of SYTOX™ red-stained cells after treatment with CBD alone or in combination with NAC (Figure 4-4B).

#### 4.5 Investigation of HUASMC phenotype in experimental conditions

Dependent on diverse circumstances, VSMC possess the ability to switch between a contractile/quiescent and a synthetic/proliferative phenotype [3, 257]. To classify the phenotype of HUASMC in these experiments, cells were subjected to differently composed media for 24 h followed by the analysis of proliferation using the BrdU incorporation assay (Table 4-1). The here used media were cSMCGM and rSMCGM (FCS content as indicated). Withdrawal of growth factors (rSMCGM, 5% FCS) significantly decreased proliferation of HUASMC to 60% compared to incubation in cSMCGM (5% FCS; set as 100%).

**Table 4-1: Effect of media composition on proliferation of HUASMC**

Medium	FCS content	BrdU incorporation (% Control)
cSMCGM	FCS (5%)	100.0 $\pm$ 1.1
rSMCGM	FCS (5%)	60 $\pm$ 3 *
rSMCGM	FCS (2%)	29 $\pm$ 3 #
rSMCGM	FCS (0%)	2.4 $\pm$ 0.6 #

Note: Cells were incubated in cSMCGM (containing supplements and 5% FCS) or rSMCGM (no supplements, FCS content as indicated) for 48 h followed by analysis of BrdU incorporation. Percent control represents comparison with the corresponding cSMCGM-incubated, time-matched group (set as 100%). Values are means  $\pm$  SEM of  $n = 8$  experiments. \* $P < 0.05$  vs. cSMCGM; # $P < 0.05$  vs. rSMCGM (5% FCS); one-way ANOVA plus Šidák post hoc test.

Comparison of the rSMCGM-incubated cells showed that the reduction of serum content further attenuated the proliferation of HUASMC. In detail, the proliferation was decreased by 52% (rSMCGM, 2% FCS) and 96% (rSMCGM, 0% FCS) when compared to incubation in rSMCGM containing 5% FCS (set as 100% in this comparison). Thus, HUASMC seeded in cSMCGM showed an enhanced proliferation dependent on the presence of growth factors and serum content. Another well-known stimulant of VSMC activation, resulting in increased proliferation and migration, is PDGF. The optimal concentration of PDGF to stimulate HUASMC was determined

in preliminary experiments (Table 4-2). Herein, proliferation was concentration-dependently increased after a 24-h incubation with PDGF resulting in a maximum proliferation of 219% vs. vehicle control (100%) at 60 ng/ml PDGF (Table 4-2). However, for specific stimulation of VSMC, a PDGF concentration of 20 ng/ml, resulting in a proliferation of 196% vs. vehicle control, was considered ideal.

These results suggest that HUASMC incubated in cSMCGM do also represent a synthetic/proliferative phenotype. Therefore, experiments investigating effects of CBD on potential disease-associated features of HUASMC were performed in either cSMCGM (5% FCS) or using a combination of rSMCGM (2% FCS) and treatment with PDGF (20 ng/ml) as a specific stimulator of the synthetic/proliferative phenotype.

**Table 4-2: Effect of PDGF on proliferation of HUASMC**

Treatment	BrdU incorporation (% Control)
Vehicle	100 ± 3
PDGF (10 ng/ml)	182 ± 12 *
PDGF (20 ng/ml)	196 ± 10 *
PDGF (40 ng/ml)	215 ± 14 *
PDGF (60 ng/ml)	219 ± 14 *

Note: Cells seeded in rSMCGM (no supplements, 2% FCS) were incubated with different concentrations of PDGF for 24 h prior to analysis of BrdU incorporation. Percent control represents comparison with the respective vehicle-treated group (set as 100%). Values are means ± SEM of  $n = 10$ –14 experiments. \* $P < 0.05$  vs. vehicle-treated group; one-way ANOVA plus Dunnett post hoc test.

#### 4.6 Effect of CBD on proliferation and viability of HUASMC

Further experiments analyzing cell viability and proliferation were performed to investigate the effects of CBD on cellular functions of HUASMC (Figure 4-5). As shown in Figure 4-5A, cell viability, as analyzed by trypan blue exclusion staining, was not affected after a 48-h incubation with CBD at concentrations of 0.1–10  $\mu$ M. Indeed, there was a slight, yet not significant, concentration-dependent increase in cell viability. In contrast, a 48-h incubation with CBD concentration-dependently inhibited proliferation of HUASMC (Figure 4-5B). Here, proliferation was significantly decreased to 75% and 62% vs. vehicle control (100%) at 6  $\mu$ M and 10  $\mu$ M CBD, respectively (Figure 4-5B). This anti-proliferative effect was also visible in microphotographs showing cell densities of the cultured monolayers (Figure 4-5D). Herein, vehicle-treated cells, which were seeded at subconfluence in the beginning of



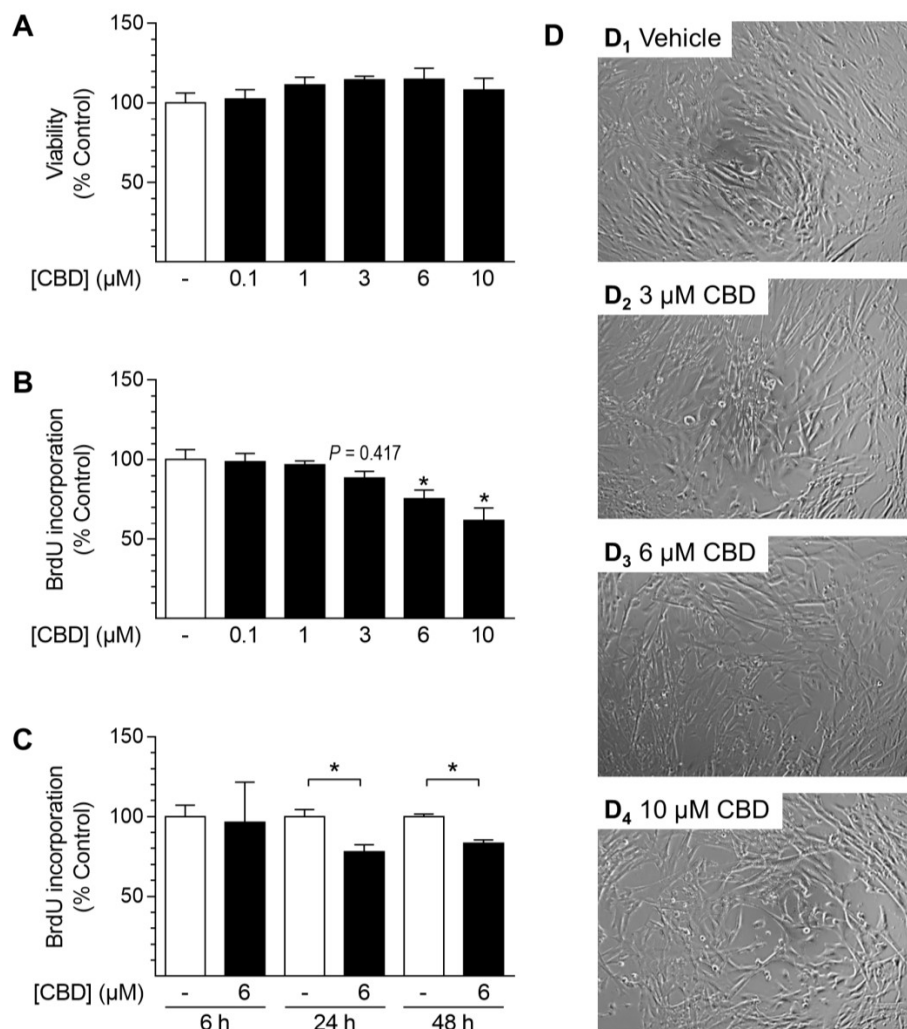


**Figure 4-5: Effect of CBD on viability and proliferation of HUASMC.** Cells were incubated for 48 h with indicated concentrations of CBD (A, B) or with 6 μM CBD for the indicated times (C). Following incubation, cells were analyzed for viability via trypan blue exclusion staining (A) or proliferation using BrdU incorporation assay (B, C). For visualization, unstained monolayers were photographed in culture at 10X magnification using a digital microscope camera (D). Percent control represents comparison with the corresponding vehicle-treated, time-matched group (set as 100%). Values are means  $\pm$  SEM of  $n = 4$  (A) or  $n = 10$ –12 (B, C) experiments. \* $P < 0.05$  vs. time-matched vehicle control; one-way ANOVA plus Dunnett post hoc test (A, B) or Student's two-tailed  $t$  test (C).

the experiment, formed a confluent monolayer (Figure 4-5D<sub>1</sub>). In contrast, the monolayer density was reduced after incubation with increasing concentrations of CBD (Figure 4-5D<sub>2</sub>–D<sub>4</sub>). Kinetic studies revealed that proliferation was significantly inhibited by 22% and 17% after incubation with 6 μM CBD for 24 h and 48 h, respectively (Figure 4-5C).

#### 4.7 Involvement of receptor-signaling in CBD-mediated anti-proliferative effects

In order to investigate the underlying mechanism of CBD-mediated anti-proliferative effects in HUASMC, cells were pre-incubated for 1 h with substances targeting CB<sub>1</sub>R (AM251), CB<sub>2</sub>R (AM630), TRPV1 (capsazepine) and GPR55 (O-1918, antagonist; O-1602; agonist) followed by a 24-h co-incubation with CBD (10  $\mu$ M, Figure 4-6A). Similar to the results mentioned before (Figure 4-5B, page 45), incubation with 10  $\mu$ M CBD significantly decreased the proliferation of HUASMC resulting in a maximum proliferation of 52% vs. vehicle-treated control (100%, Figure 4-6A). Pre-incubation with the corresponding receptor activity-modulating substances did not prevent or attenuate this effect (Figure 4-6A). Indeed, pre-incubation with the GPR55 agonist O-1602 enhanced the anti-proliferative effect of CBD by 2.1-fold, resulting in 24% BrdU incorporation vs. vehicle-treated control (100%, Figure 4-6A). Additionally, substance-specific effects on cell proliferation were excluded by incubation of HUASMC with these substances in the absence of CBD (Figure 4-6B). Herein, none of the receptor activity modulating substances *per se* significantly altered the proliferation of HUASMC after a 24-h incubation (Figure 4-6B).

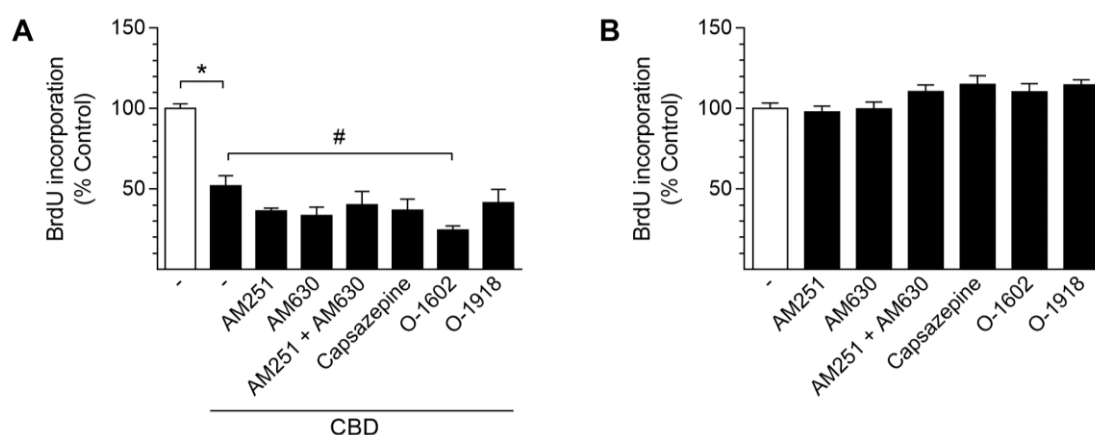


**Figure 4-6: Involvement of receptor-signaling in CBD-mediated anti-proliferative effects in HUASMC.** For investigation of receptor involvement in anti-proliferative effects of CBD, HUASMC were pre-incubated with AM251 (CB<sub>1</sub>R antagonist), AM630 (CB<sub>2</sub>R antagonist), capsazepine (TRPV1 antagonist), O-1602 (GPR55 agonist) or O-1918 (GPR55 antagonist) for 1 h and then further co-incubated with (A) or without (B) 10  $\mu$ M CBD for 24 h. Following incubation, cell proliferation was analyzed via BrdU incorporation assay. Percent control represents comparison with the corresponding vehicle-treated, time-matched group (set as 100%). Values are means  $\pm$  SEM of  $n=10-12$  (A) or  $n=7-8$  experiments. \* $P < 0.05$  vs. time-matched vehicle control; one-way ANOVA plus Šidák post hoc test (A) or one-way ANOVA plus Dunnett post hoc test (B).

#### 4.8 Involvement of HO-1 in CBD-mediated anti-proliferative effects and viability in HUASMC: The SnPPIX approach

The results mentioned before (chap. 4.7, page 46, Figure 4-6) indicate that the anti-proliferative effects of CBD are not mediated by the cannabinoid-activated receptors CB<sub>1</sub>R, CB<sub>2</sub>R, TRPV1, and GPR55. Therefore, additional experiments aimed to address a possible relation between the CBD-mediated anti-proliferative effects and the induction of HO-1 in HUASMC (Figure 4-7). The functional role of HO-1 in CBD's anti-proliferative effects was investigated using the two previously defined culturing setups to promote a disease-associated behavior of HUASMC (see chap. 4.5, page 43).

In order to block HO-1 activity, cells were pre-incubated with 10  $\mu$ M of the HO-1 inhibitor SnPPIX prior to a co-incubation with CBD. The proliferation of HUASMC was significantly attenuated after a 48-h incubation with 6  $\mu$ M and 10  $\mu$ M CBD, resulting in 87% and 68% BrdU incorporation vs. vehicle control (100%, Figure 4-7A). However, pre-incubation with SnPPIX did not prevent or attenuate the anti-proliferative effects of CBD. Indeed, the inhibition of HO-1 activity by SnPPIX alone decreased the proliferation of HUASMC (SnPPIX: 87% vs. vehicle control [100%]) and slightly enhanced the CBD-mediated anti-proliferative effects (Figure 4-7A). Additionally, the flow cytometry-based analyses of apoptosis revealed that the viability of HUASMC was not decreased after a 48-h incubation with CBD alone (6  $\mu$ M and 10  $\mu$ M, Figure 4-7B, C<sub>1-3</sub>). The mean amounts of viable cells were 89.2% (vehicle treated), 89.9% (6  $\mu$ M CBD) and 90.0% (10  $\mu$ M CBD, Figure 4-7B, C<sub>1-3</sub>). Conversely, the inhibition of HO-1 activity by SnPPIX significantly reduced the cell viability and increased the amount of the late apoptotic/necrotic cell population when administered alone or in combination with CBD (Figure 4-7B, C<sub>4-6</sub>). The mean amounts of viable cells after treatment with SnPPIX were 77.4% (vehicle treated), 79.1% (6  $\mu$ M CBD) and 82.3% (10  $\mu$ M CBD, Figure 4-7B, C<sub>4-6</sub>). The mean amounts of late apoptotic/necrotic cells after treatment with SnPPIX were 20.38% (vehicle treated), 18.64% (6  $\mu$ M CBD) and 15.4% (10  $\mu$ M CBD, Figure 4-7B, C<sub>4-6</sub>). In contrast, the mean amounts of the late apoptotic/necrotic cells in absence of SnPPIX were 8.1% (vehicle treated), 7.4% (6  $\mu$ M CBD) and 7.7% (10  $\mu$ M CBD, Figure 4-7B, C<sub>1-3</sub>). However, the mean proportion of early apoptotic cells, which are positive for Annexin V only, was not increased by any treatment and was below 2.1% (Figure 4-7B, C<sub>1-6</sub>). Additional experiments targeted to investigate the role of HO-1 in the impact of CBD on PDGF-mediated proliferation of HUASMC (Figure 4-7D). For this purpose, cells were cultured in rSMCGM and pre-incubated with SnPPIX for 1 h prior to a 24-h co-incubation period in presence of CBD and PDGF or corresponding vehicles (Figure 4-7D).

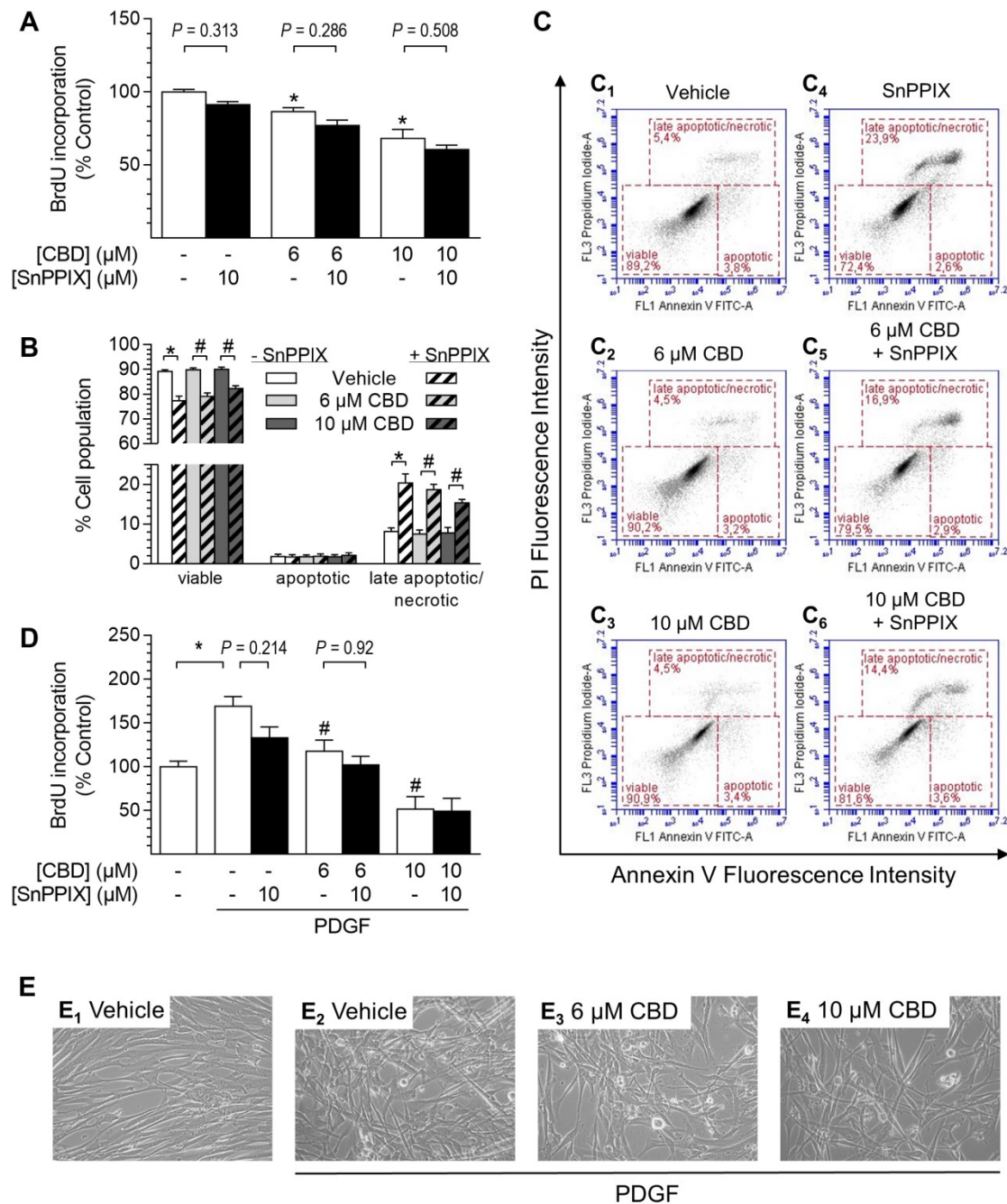


**Figure 4-7: Effect of HO-1 activity inhibitor SnPPIX on CBD-mediated anti-proliferative effects and viability of HUASMC.** Cells were pre-incubated for 1 h with 10 μM SnPPIX or the corresponding vehicle followed by a 48-h co-incubation period with vehicle or CBD as indicated before analysis of proliferation using BrdU incorporation assay (A) or flow cytometry-based analysis of apoptosis (B). Exemplary images of flow cytometry analysis are shown in (C). For specific stimulation, cells seeded in rSMCGM were pre-incubated for 1 h with 10 μM SnPPIX or the corresponding vehicle followed by a 24-h co-incubation period with vehicle or CBD as indicated prior to analysis of BrdU incorporation (D). For visualization, unstained monolayers were photographed in culture at 10X magnification using a digital microscope camera (E). Percent control represents comparison with the corresponding vehicle-treated, time-matched group (set as 100%). Values are means  $\pm$  SEM of  $n = 10-12$  (A, D) or  $n = 8$  (B) experiments. \* $P < 0.05$  vs. time-matched (PDGF-free) vehicle control or as indicated; # $P < 0.05$  vs. PDGF-treated vehicle control one-way ANOVA plus Šidák post hoc test.

Incubation with PDGF *per se* significantly enhanced the proliferation of HUASMC up to 170% vs. vehicle control (100%, Figure 4-7D). This effect was also visible by changes in monolayer density and cell organization compared to vehicle-treated cells (Figure 4-7E<sub>1-2</sub>). Presence of CBD at 6  $\mu$ M and 10  $\mu$ M significantly reduced this pro-proliferative effect of PDGF, resulting in 118% and 52% BrdU incorporation, respectively (Figure 4-7D). This anti-proliferative effect was also recognizable in microphotographs, showing a considerably reduced cell density in the presence of PDGF by CBD at 6  $\mu$ M and 10  $\mu$ M, respectively (Figure 4-7E<sub>2-4</sub>). Similar to the results in Figure 4-7A, presence of SnPPIX *per se* reduced the PDGF-induced proliferation of HUASMC to 133% (Figure 4-7D). According to the previous results, co-incubation with SnPPIX neither significantly enhanced nor attenuated the anti-proliferative effects of CBD under these conditions (Figure 4-7D).

#### 4.9 Involvement of HO-1 in CBD-mediated anti-proliferative effects and viability in HUASMC: The siRNA approach

In order to exclude possible off-target effects of SnPPIX, additional siRNA approaches were performed to knock down HO-1 protein expression (Figure 4-8). HO-1 protein was significantly increased to 180% and 280% by CBD at 6  $\mu$ M and 10  $\mu$ M, respectively (Figure 4-8A). Administration of siRNA specifically targeting HO-1 significantly attenuated the CBD-mediated induction of HO-1 by 75% and 50% at 6  $\mu$ M and 10  $\mu$ M CBD, respectively (Figure 4-8A). Likewise, the basal protein expression of HO-1 was reduced by 78% after transfection with HO-1 siRNA (Figure 4-8A).

Similar to the above-mentioned results using SnPPIX (see chap. 4.8, page 47, Figure 4-7A), knockdown of HO-1 further enhanced the CBD-mediated anti-proliferative effects after a 24-h incubation albeit being anti-proliferative *per se* (Figure 4-8B). According to the previous results (see chap. 4.8, page 47, Figure 4-7B), viability analyses using vital staining showed a significant loss of cell viability in HUASMC after knockdown of HO-1 in the presence of CBD at 6  $\mu$ M and 10  $\mu$ M, respectively (Figure 4-8C). However, administration of HO-1 siRNA *per se* did not affect cell viability (Figure 4-8C). Cell viability of control cells that were transfected with a non-targeting siRNA (NON) was not attenuated in presence of CBD (Figure 4-8C). Further characterization of the CBD-mediated cell death occurring in cells depleted of HO-1 was performed by flow cytometry-based analyses of apoptosis (Figure 4-8D). The results once more showed that the amount of viable cells was not decreased by CBD *per se* (Figure 4-8D).

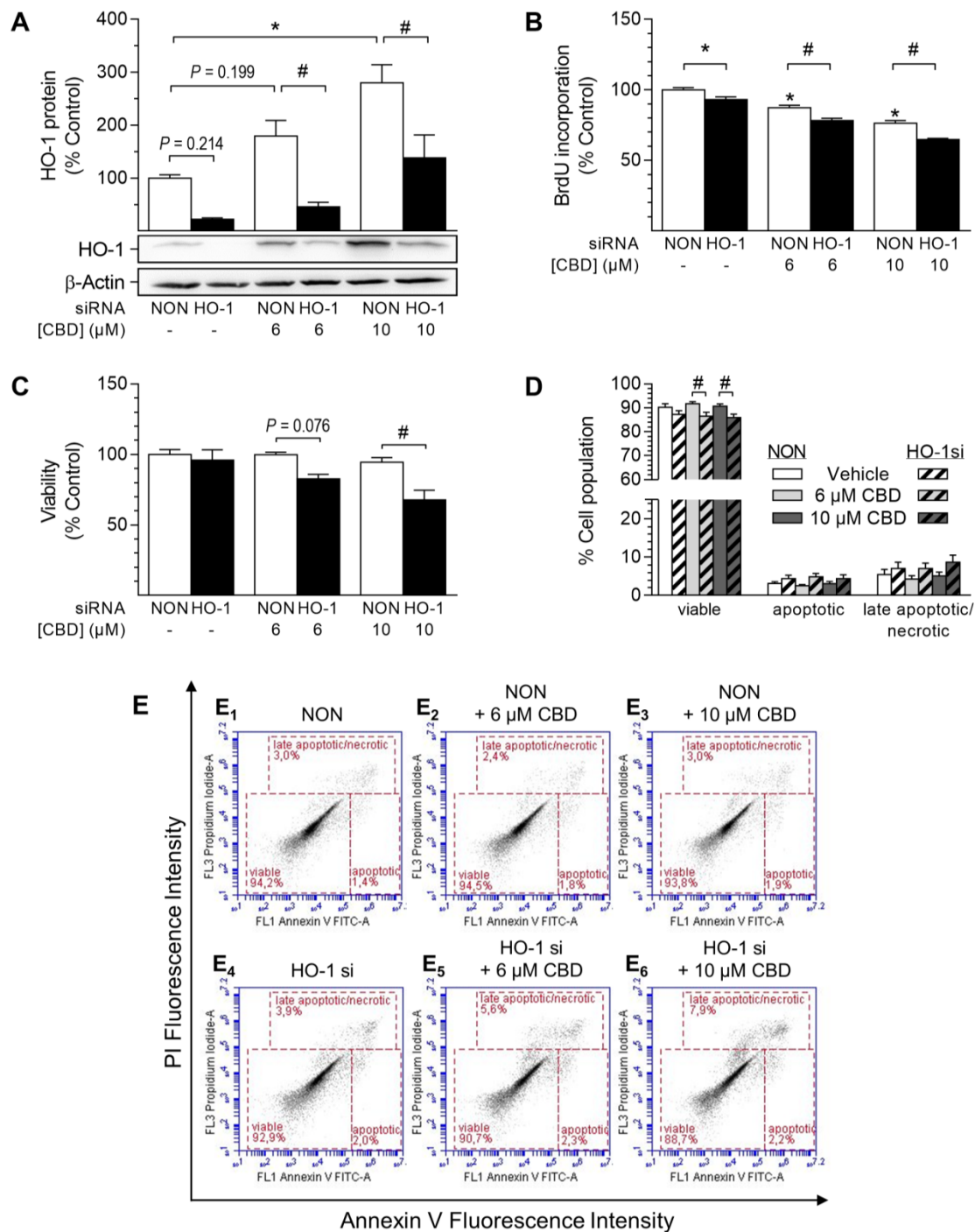


**Figure 4-8: Effect of HO-1 siRNA on CBD-mediated anti-proliferative effects and viability of HUASMC.** Cells were transfected with HO-1 specific or non-targeting siRNA (NON) prior to stimulation with CBD as indicated for 48 h (A, C, D) or 24 h (B). Following incubation, cells were analyzed for protein expression of HO-1 (A), BrdU incorporation (B), viability (C) or apoptosis (D). Representative images of flow cytometry-based analysis of apoptosis are shown in (E). Protein expression values were normalized to  $\beta$ -actin. Percent control represents comparison with the corresponding NON-transfected, time-matched group (set as 100%). Values are means  $\pm$  SEM of  $n = 4$  (A),  $n = 11$ –12 (B),  $n = 3$  (C) or  $n = 9$  (D) experiments.  $\ast P < 0.05$  vs. time-matched NON-transfected vehicle control;  $\# P < 0.05$  vs. concentration-matched NON-transfected sample; one-way ANOVA plus Šidák post hoc test.

The mean amounts of viable cells after transfection with the non-targeting siRNA (NON) were 90.2% (vehicle treated), 91.7% (6  $\mu$ M CBD) and 90.7% (10  $\mu$ M CBD, Figure 4-8D, E<sub>1-3</sub>). In contrast, the presence of HO-1 siRNA significantly reduced the number of viable cells Figure 4-8D, E<sub>4-6</sub>). The mean amounts of viable cells after transfection with HO-1 siRNA were 87.2% (vehicle treated), 86.5% (6  $\mu$ M CBD) and 85.9% (10  $\mu$ M CBD, Figure 4-8D, E<sub>4-6</sub>). The apoptotic or late apoptotic/necrotic cell populations of HUASMC were not increased after a 48-h treatment with CBD alone (Figure 4-8D, E<sub>1-3</sub>). However, in accordance to the drastic loss of cell viability (see vital-staining, Figure 4-8C), both apoptotic and late apoptotic/necrotic cell populations were increased in HO-1 siRNA-transfected cells in presence of CBD (Figure 4-8D, E<sub>4-6</sub>). The mean amounts of apoptotic cells after transfection with HO-1 siRNA were 4.4% (vehicle treated), 4.9% (6  $\mu$ M CBD) and 4.4% (10  $\mu$ M CBD, Figure 4-8D, E<sub>4-6</sub>). The mean amounts of late apoptotic/necrotic cells after transfection with HO-1 siRNA were 7.1% (vehicle treated), 7.1% (6  $\mu$ M CBD) and 8.7% (10  $\mu$ M CBD, Figure 4-8D, E<sub>4-6</sub>).

#### 4.10 Role of HO-1 in CBD-mediated anti-migratory effects

VSMC of the synthetic/proliferative phenotype are also capable of enhanced migration [3]. Therefore, effects of CBD on HUASMC migration towards PDGF (20 ng/ml) as a chemoattractant were analyzed using a modified Boyden chamber assay. The role of HO-1 in this process was investigated using both SnPPIX (Figure 4-9A, B<sub>1</sub>) and HO-1-specific siRNA (Figure 4-9C–F). To ensure specific migration towards the chemoattractant PDGF in both approaches, HUASMC were cultured in rSMCGM for the whole time of the experiment. As shown in Figure 4-9A, B<sub>1-2</sub>, migration of HUASMC was significantly increased in presence of PDGF resulting in 330% migration vs. PDGF-free vehicle control (100%). Pre-incubation with CBD (10  $\mu$ M) almost completely inhibited this pro-migratory effect, resulting in 139% migration (Figure 4-9A, B<sub>4</sub>). However, when tested at a concentration of 6  $\mu$ M, the anti-migratory effect of CBD did not reach significance ( $P = 0.366$ , one-way ANOVA plus Šidák post hoc test,  $n = 15$ , Figure 4-9A, B<sub>3</sub>). Similar to the previous results (chap. 4.8, page 47, Figure 4-7A, D), inhibition of HO-1 activity by pre-incubation with 10  $\mu$ M SnPPIX did not attenuate or prevent the CBD-mediated anti-migratory effect (Figure 4-9A, B<sub>2-7</sub>). Indeed, inhibition of HO-1 activity enhanced the anti-migratory effects of CBD, being slightly anti-migratory *per se* (Figure 4-9A, B<sub>2-7</sub>). Using HO-1-specific siRNA, both the CBD-mediated and the basal HO-1 protein expressions were significantly knocked down (Figure 4-9C, D). Herein, the CBD-mediated HO-1 protein expression (6  $\mu$ M CBD: 290% vs. vehicle control) was reduced to 30% (Figure 4-9C).



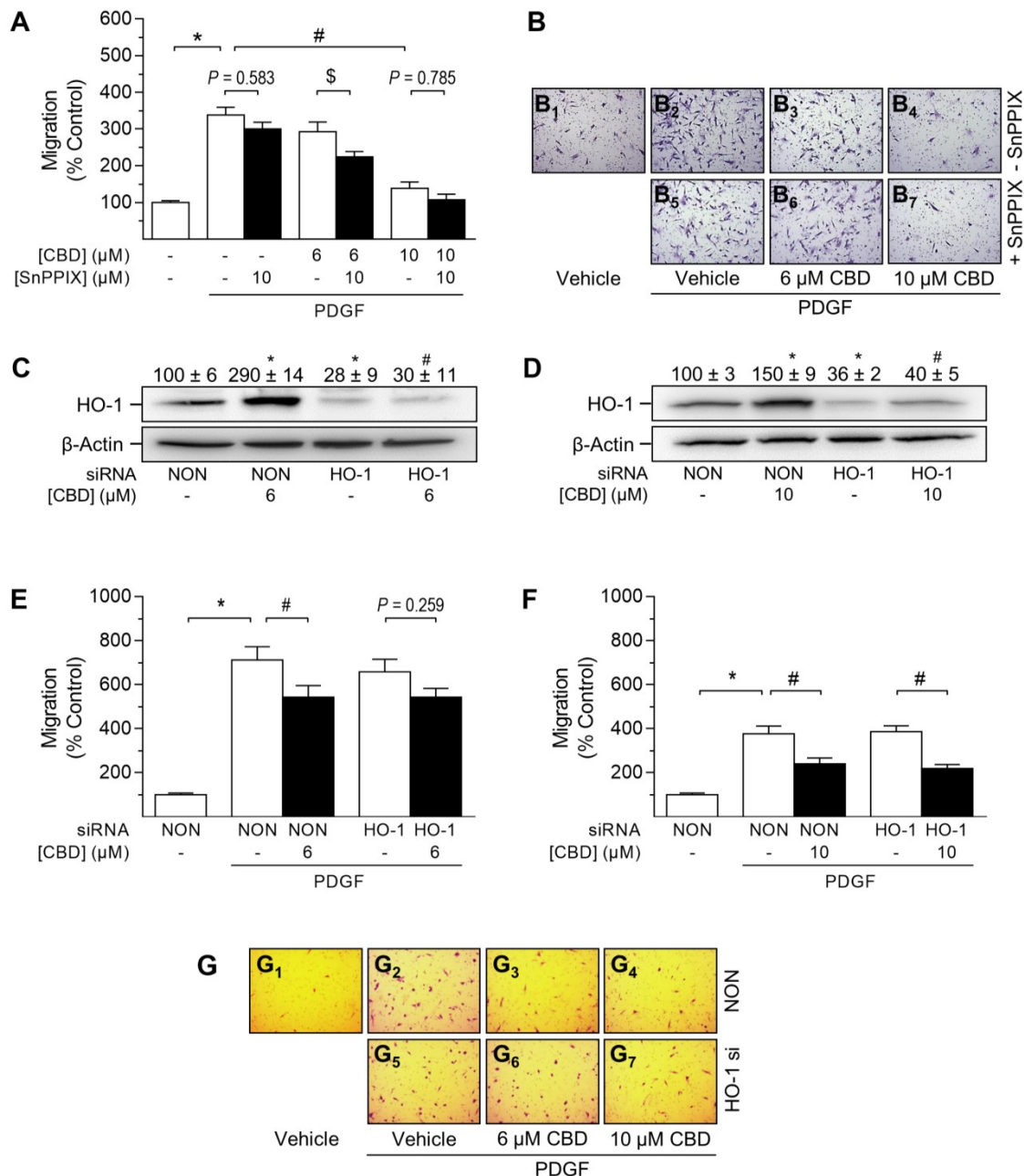


**Figure 4-9: Role of HO-1 in CBD-mediated anti-migratory effects in HUASMC.** Cells, seeded in rSMCGM (no supplements, 2% FCS), were pre-incubated for 1 h with the HO-1 activity inhibitor SnPPiX (10 μM) prior to a 24-h co-incubation period with vehicle or CBD at indicated concentrations. Afterwards, viable cells were transferred into Falcon® cell culture inserts and migration towards PDGF (20 ng/ml) or appropriate vehicle was run for 6 h (A, B). Cells were transfected with HO-1-specific or non-targeting siRNA (NON) and incubated in rSMCGM for 24 h. For Western blot analysis (C, D), viable cells were transferred into 6-wells and incubated with CBD or corresponding vehicle for 6 h prior to sample preparation. For migration (E, F), viable cells were transferred into Falcon® cell culture inserts and incubated with CBD or corresponding vehicle for 1 h prior to initiation of a 6-h migration towards PDGF (20 ng/ml). Inserts were prepared and cells in five randomly selected fields per insert were counted. Representative images of migration analyses are shown in (B, G). Percent control represents comparison with the corresponding NON-transfected, vehicle-treated group (set as 100%). Values are means ± SEM of  $n = 15$  (A),  $n = 3$  (C),  $n = 6$  (D),  $n = 28-36$  (E) or  $n = 25$  (F) experiments. \* $P < 0.05$  vs. PDGF-free vehicle control or as indicated; # $P < 0.05$  vs. PDGF-treated vehicle control; \$ $P < 0.05$  as indicated; one-way ANOVA plus Šidák post hoc test.



Similarly, 10  $\mu$ M CBD enhanced the HO-1 protein expression in HUASMC to 150% vs. vehicle control (Figure 4-9D). This effect was significantly attenuated (40% vs. vehicle control) by HO-1 siRNA (Figure 4-9D). Similar to the above-mentioned results (Figure 4-9A), migration of HUASMC was significantly enhanced in presence of PDGF (Figure 4-9E, F, G<sub>1-2</sub>). Accordingly, CBD at 6  $\mu$ M (Figure 4-9E, G<sub>3</sub>) or 10  $\mu$ M (Figure 4-9F, G<sub>4</sub>) significantly inhibited the PDGF-induced migration of HUASMC transfected with non-targeting siRNA (NON). However, using this approach, knockdown of HO-1 protein expression did not alter the CBD-mediated inhibition of PDGF-induced migration (Figure 4-9E–F, G<sub>5-7</sub>).

#### 4.11 Role of CBD-mediated ROS in anti-proliferative effects and cell death of HUASMC

Since anti-proliferative and anti-migratory effects of CBD could not be assigned to HO-1 by the previous experiments, additional experiments aimed to investigate the role of the CBD-mediated ROS-signaling with regard to proliferation and cell death of HUASMC (Figure 4-10A–D). In order to examine the effects mediated by CBD-mediated ROS production or ROS-signaling, cells were pre-incubated with the glutathione precursor NAC (for details see suppl. Figure 12-2, page 112). According to the previous results showing the correlation between CBD-treatment, ROS-signaling and induction of HO-1 (chap. 4.4, page 41), pre-treatment with NAC at a concentration of 0.1 mM significantly attenuated the CBD-mediated induction of HO-1, indicating a reduction of ROS-signaling under these conditions (Figure 4-10A). Herein, HO-1 protein expression was not altered after incubation with NAC alone (Figure 4-10A). Analysis of cell proliferation by BrdU incorporation assay after a 24-h incubation confirmed the previously detected anti-proliferative effect of CBD, which was significant at concentrations of 6  $\mu$ M and 10  $\mu$ M, respectively (Figure 4-10B). Herein, proliferation of HUASMC was reduced to 81% and 71% vs. vehicle control (100%). However, the CBD-mediated anti-proliferative effect was neither attenuated nor enhanced in presence of NAC, indicating that ROS-signaling may not contribute to this effect (Figure 4-10B).

Referring to the previous results investigating the cell death of CBD-treated HUASMC in the absence of functional HO-1 (chap. 4.8, page 47; chap. 4.9, page 49), further experiments targeted to examine the role of the CBD-mediated increase of ROS in cell death of HUASMC (Figure 4-10C, D). Similar to the previous results, administration of CBD alone did not decrease the number of viable cells in the analyzed population (Figure 4-10C, D<sub>1-3</sub>). Although pre-treatment with NAC inhibited the CBD-mediated induction of HO-1 (Figure 4-10A), viability and both apoptotic and late apoptotic/necrotic cell populations of HUASMC were virtually

unaffected in presence of CBD (Figure 4-10C, D<sub>4-6</sub>). Consequently, these results suggest that the CBD-mediated ROS production contributes to induction of the anti-oxidant enzyme HO-1 and thus protection of cells against ROS-dependent apoptosis.

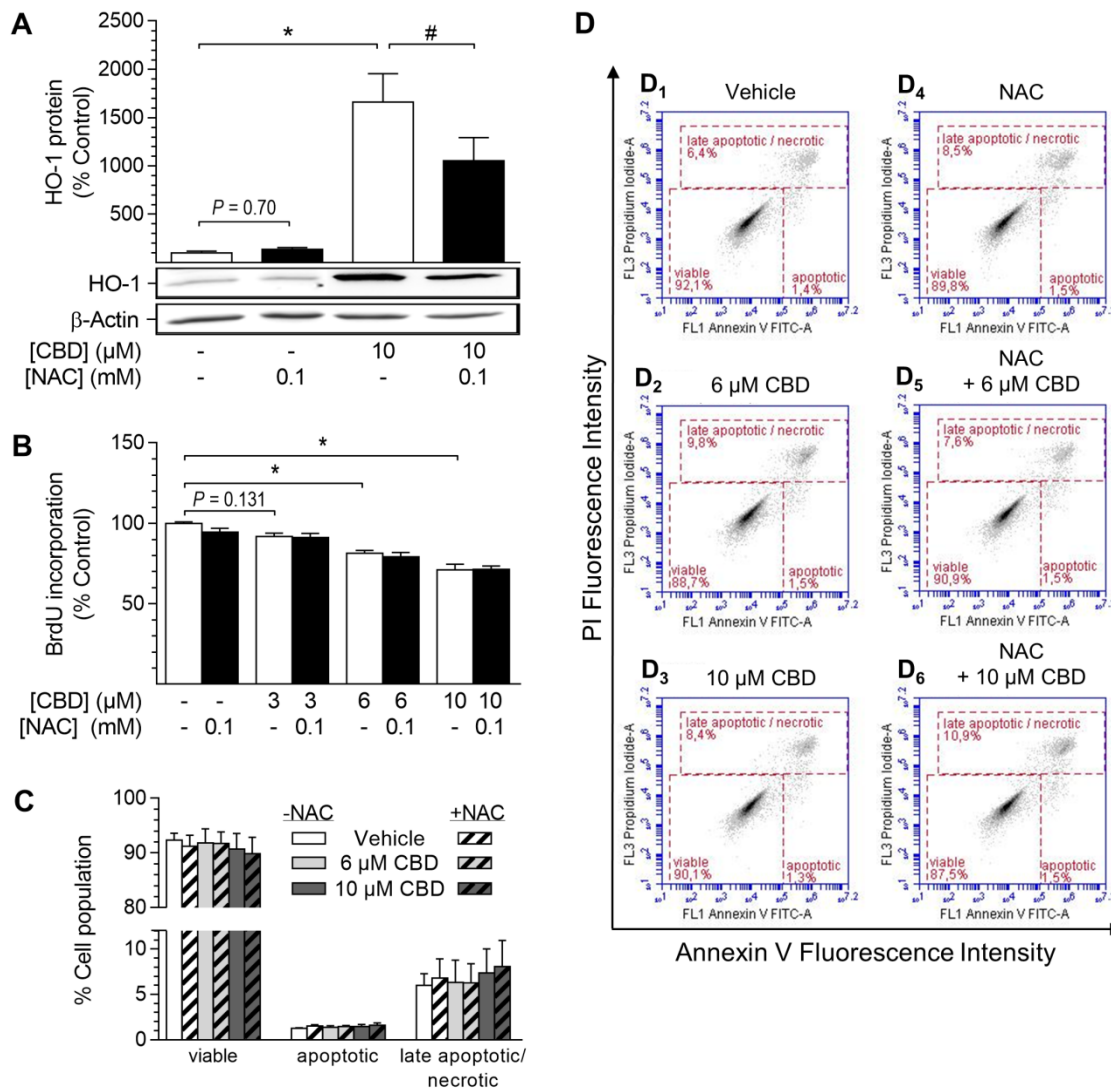


**Figure 4-10: Impact of N-acetylcysteine (NAC) on CBD-mediated anti-proliferative effects and viability of HUASMC.** Cells were pre-incubated with 0.1 mM NAC or vehicle for 1 h prior to a 24-h co-incubation with CBD or the corresponding vehicle. This was followed by analysis of HO-1 protein via Western blot (A), analysis of proliferation using BrdU incorporation assay (B) or flow cytometry-based analysis of apoptosis (C) with the representative images shown in (D). Protein expression values were normalized to β-actin. Percent control represents comparison with the corresponding vehicle-treated, time-matched group (set as 100%). Values are means ± SEM of  $n = 6$  (A),  $n = 11-12$  (B) or  $n = 4$  (C) experiments. \* $P < 0.05$  vs. vehicle control; # $P < 0.05$  vs. CBD-treated sample; one-way ANOVA plus Šidák post hoc test.

## 5 Discussion

This project investigated the effect of the phytocannabinoid CBD on the proliferation and migration of VSMC, which are both disease-associated features of these cells. Aberrant proliferation and migration of VSMC, triggered in particular by inflammatory mediators and growth factors, are closely related to the main causes of acute cardiovascular events: atherosclerosis and restenosis [31, 258–260]. By participating in blood vessel formation, VSMC contribute in providing access to nutrients and routes of distribution for solid tumors [261, 262]. Thus, recruited and activated VSMC are involved in tumour development and cancer progression. Strengthening the cellular anti-inflammatory capacity and/or inhibiting the excessive proliferation and migration of VSMC may therefore provide benefits in the treatment of progressive vascular diseases and cancer. This thesis especially focused the role of the anti-oxidant enzyme HO-1 in the CBD-mediated effects in VSMC. The results of this work are schematically summarized in Figure 5-1 and discussed below.

The present study demonstrates that CBD mediates the induction of HO-1 via a ROS-dependent mechanism. Additionally, CBD attenuates the disease-associated behaviour of VSMC by inhibiting growth factor-initiated proliferation and migration. Since both events occurred independently, this study suggests a HO-1-independent mechanism that confers the anti-proliferative and anti-migratory effects of CBD.

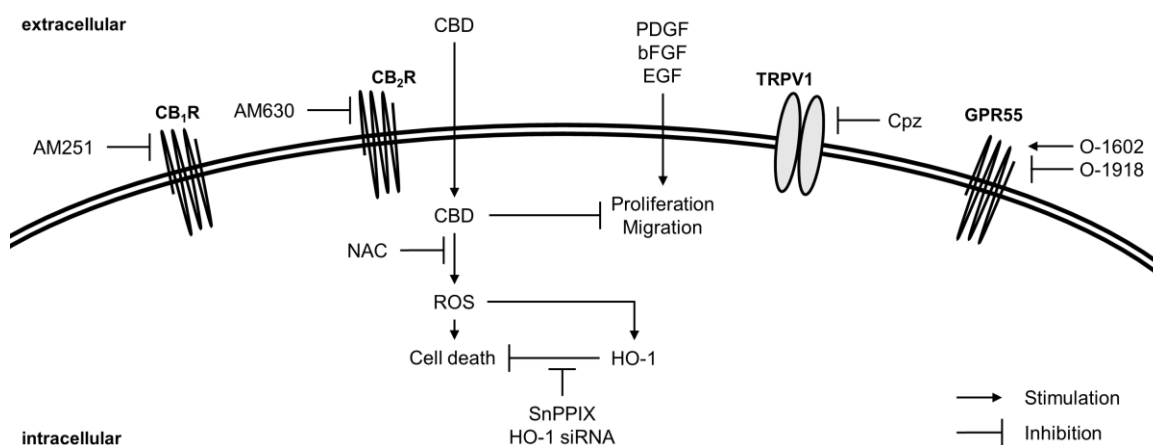


**Figure 5-1: Schematic representation of the experimental outcomes of this thesis.** CBD enters the cell and induces the production of ROS in HUASMC. As a protective mechanism, the expression of HO-1 is stimulated in a counter-regulatory manner. The glutathione precursor NAC prevents the CBD-mediated ROS generation and induction of HO-1. Inhibition of HO-1 by SnPPiX or HO-1 knockdown by siRNA causes cell death of HUASMC. CBD promotes anti-proliferative and anti-migratory effects in HUASMC independent of cannabinoid-activated receptors (CB<sub>1</sub>R, CB<sub>2</sub>R, TRPV1 and GPR55), ROS and HO-1. AM251: CB<sub>1</sub>R antagonist; AM630: CB<sub>2</sub>R antagonist; bFGF: basic fibroblast growth factor; Cpz: capsazepine, TRPV1 antagonist; EGF: epidermal growth factor; HO-1: heme oxygenase-1; GPR55: G protein-coupled receptor 55; NAC: N-acetylcysteine; O-1602: GPR55 agonist; O-1918: GPR55 antagonist; PDGF: platelet-derived growth factor; ROS: reactive oxygen species; SnPPiX: tin protoporphyrin IX, inhibitor of HO activity; TRPV1: transient receptor potential vanilloid 1

Initial experiments examined the potential of synthetic and plant-derived cannabinoids to modulate the proteins of the HO system in HUASMC. The results demonstrated that the two phytocannabinoids tested, CBD and THC, induced the expression of HO-1 but not HO-2. In contrast, the two synthetic cannabinoids tested, R(+)-methanandamide and JWH-133, were virtually inactive in this respect. Although few studies have been investigating a relation between synthetic cannabinoids and HO-1, some have shown that JWH-133, via the induction of HO-1, has positive effects in animal models of alcohol- and inflammation-induced liver disease [263, 264]. Interestingly, another study reported HO-1 induction in human breast cancer cell lines that was induced by JWH-133 but not R(+)-methanandamide [265]. Indeed, these reports are, at least in parts, in contrast to the data shown in the present study. However, this is the first study providing evidence of a phytocannabinoid-mediated HO-1 induction in human VSMC.

The present study concentrated on CBD, which unlike THC lacks psychoactivity. At the same time, CBD exerts numerous positive pharmacological effects as assessed in animal studies and clinical trials (recently reviewed in [205]). In subsequent analyses, the impact of CBD on HO-1 was further characterised. The experimental results revealed a CBD-mediated concentration- and time-dependent up-regulation of both, HO-1 mRNA and protein level. These results correspond to several studies showing a comparable modulation of HO-1 in VSMC by other plant-derived substances [14, 15, 17, 21, 68, 97, 99].

Another set of experiments aimed to investigate the involvement of typical cannabinoid-activated receptors, CB<sub>1</sub>R and CB<sub>2</sub>R, GPR55 or TRPV1 in the CBD-mediated HO-1 induction. The experimental approaches with antagonists targeting CB<sub>1</sub>R, CB<sub>2</sub>R, TRPV1 and GPR55 and a GPR55 agonist showed no changes in the CBD-mediated induction of HO-1. Thus, the participation of these established cannabinoid-activated receptors in the HO-1-inducing effect of CBD was excluded.

Likewise, an induction of HO-1 was observed after chemical inhibition or knockdown of the endocannabinoid-degrading enzyme fatty acid amide hydrolase (FAAH) or exogenous addition of AEA in MCF-7 and MDA-MB-231 human breast cancer cell lines [265]. Similar to the present study, the induction of HO-1 was independent of the cannabinoid-activated receptors CB<sub>1</sub>R, CB<sub>2</sub>R and TRPV1 and involved the activation of Nrf2 [265]. In accordance with these observations, others have described several CB<sub>1</sub>R/CB<sub>2</sub>R-independent actions of CBD. For example, CBD at concentrations of 1-3  $\mu$ M led to a reduction of the infarct volume by activating the 5-HT<sub>1A</sub> receptor [266]. Thus, CBD contributed to neuroprotection of mice after occlusion of cerebral arteries [266]. Similarly, CBD (2.5–5 mg/kg) prevented chemotherapy-induced neuropathic pain in female C57BL/6 mice by 5-HT<sub>1A</sub> signaling [267]. This effect was observed when CBD was administered either before or after the injection of standard doses of paclitaxel, suggesting both the therapeutic

and protective potential of CBD in this context [267]. In this study, CBD (0.6–2.7  $\mu$ M) also exerted positive additive effects by significantly improving the paclitaxel-mediated reduction of viability in mouse and human breast cancer cells [267]. Thus, CBD contributed to strengthening the effectiveness of chemotherapy [267]. Finally, CBD at concentrations of 3–9  $\mu$ M impaired migration of U87 human glioma cells in a Boyden chamber assay [268]. It was shown that this anti-migratory effect of CBD occurred independent of CB<sub>1</sub>R, CB<sub>2</sub>R and TRPV1, and in a PTX-insensitive manner, thereby excluding an involvement of classical cannabinoid receptors and/or other G<sub>i/o</sub> protein-coupled receptors [268]. Interestingly, controversial data were observed in a study reporting CBD-mediated anti-proliferative effects, accompanied by an  $\alpha$ -tocopherol-reversible induction of apoptosis, in U86 and U373 human glioma [269]. Herein, the anti-proliferative effect on cancer cells, that was also present in an *in vivo* xenograft model of human glioma using athymic CD-1 nude mice, was partially prevented by the CB<sub>2</sub>R antagonist SR144528 [269]. However, as this anti-proliferative effect of CBD was also insensitive against PTX, a G<sub>i/o</sub> protein-coupled receptor-dependent mechanism was finally excluded [269]. In contrast, and despite its low affinity to CB<sub>1</sub>R and CB<sub>2</sub>R [165, 270], some studies also reported cannabinoid receptor-dependent effects of CBD. For example, CBD reduced the *in vitro* chemotaxis of peritoneal murine macrophages via CB<sub>2</sub>R signaling [271]. In addition, CBD-mediated activation of both CB<sub>1</sub>R and TRPV1 led to endothelium-dependent vasorelaxation in pre-constricted human mesenteric arteries [272]. In contrast, an *in vitro* GTP $\gamma$ S binding assay revealed that CBD antagonized the CP55,940- and WIN55,212-mediated agonistic actions at CB<sub>1</sub>R and CB<sub>2</sub>R and additionally displayed inverse agonism at CB<sub>2</sub>R [273]. Likewise, CBD behaved as a non-competitive negative allosteric modulator of the THC- and 2-AG-induced actions at CB<sub>1</sub>R in human embryonic kidney cell line HEK293A and in *STHdb*<sup>Q7/Q7</sup> striatal neurons [274]. Although excluded in the present study, CBD was shown to exert some effects via TRPV1. For example, CBD at a dose of 10 mg/kg mediated an anti-hyperalgesic effect in a rat model of acute inflammation via activation of TRPV1 that was independent of both CB<sub>1</sub>R and CB<sub>2</sub>R [182]. Agonism of CBD at TRPV1 also increased endocannabinoid levels by inhibition of AEA uptake and hydrolysis [195]. Concerning GPR55, CBD antagonised the agonist effect of CP55,940 at this receptor in an *in vitro* GTP $\gamma$ S binding assay [184]. Additionally, an antagonistic action of CBD at GPR55 induced mesenchymal stem cell migration by activating ERK MAPK [228]. In the present study, the use of GPR55 agonist O-1602 and GPR55 antagonist O-1918 excluded GPR55's involvement in the CBD-mediated induction of HO-1, as this effect was neither reversed nor amplified.

Considering the evolutionarily conserved mechanism of HO-1 induction [63], an involvement of ROS in the CBD-mediated induction of HO-1 was examined in subsequent experiments. Strengthening the anti-oxidative capability of VSMC by the

glutathione precursor NAC countered the CBD-induced HO-1 expression. This indicated an involvement of ROS signaling in this process. Accordingly, subsequent flow cytometry-based analyses showed that CBD increased the ROS generation in HUASMC in a NAC-reversible manner. With regard to oxidative stress, the role of CBD has been described as ambivalent as its different effects on the cannabinoid-activated receptors. For example, the metabolism of CBD by hepatic mouse microsomes led to the suppression of lipid peroxidation in the presence and absence of a NADPH-generating system [275]. This indicated potential anti-oxidant properties of the phytocannabinoid [275]. In contrast, inhibition of some radical scavenging enzymes, such as superoxide dismutase (SOD) and catalase, and CBD metabolism-dependent generation of ROS have been found in the same study [275]. Additionally, CB<sub>1</sub>R/CB<sub>2</sub>R-independent ER stress-induced apoptosis in activated but not in control hepatic stellate cells or primary hepatocytes was observed after treatment with CBD [276]. These results demonstrated potential beneficial effects of CBD on the resolution of liver fibrosis [276]. However, contrasting effects of CBD were reported for oligodendrocyte progenitor cells [232]. Herein, CBD at a concentration of 1  $\mu$ M reduced apoptosis following both inflammation-induced ER stress and hydrogen peroxide-(H<sub>2</sub>O<sub>2</sub>)-induced ROS generation [232]. Likewise, intraperitoneal pre-administration of CBD at doses of 2.5–10 mg/kg countered the cisplatin-mediated oxidative/nitrative stress-induced inflammation and nephropathy in male C57BL/6J mice [277]. Similarly, an *intravital* microscopy-study showed that CBD-mediated the attenuation of lipopolysaccharide<sup>m</sup>-(LPS)-induced vascular changes and inflammation in mouse brain [229]. These findings thus suggest beneficial neuroprotective effects in severe complications of bacterially induced endotoxic shock [229]. In addition, positive anti-inflammatory effects of CBD were also observed in a rat model of I/R injury [243], a mouse model of type I diabetic cardiomyopathy [278], and in primary human cardiomyocytes exposed to high glucose [278], with CBD reducing inflammation and oxidative/nitrative stress in each of these studies.

This project next aimed to examine the impact of CBD on proliferation and migration of HUASMC. Therefore, the proliferative capacity of VSMC was investigated in preliminary experiments using different culture conditions. In these experiments, the proliferation of HUASMC cultured in cSMCGM was increased compared to cells that were cultured under growth factor- and serum-deprivation. Accordingly, Proudfoot *et al.* (2012) described the de-differentiation along with the enhanced proliferation of isolated human VSMC, stating that isolated and cultured VSMC represent a disease-associated synthetic/proliferative rather than a contractile/quiescent phenotype [279]. It was additionally verified by several studies, that the VSMC

---

<sup>m</sup> Endotoxin component of the outer membrane of Gram-negative bacteria.

phenotype can be modulated by mitogens<sup>n</sup> including growth factors such as bFGF and EGF (reviewed in [3, 257, 280–282]). These both were present in the here used cSMCGM. In accordance to several other studies, HUASMC cultured under growth factor- and serum-deprivation (rSMCGM conditions) specifically responded to stimulation with PDGF by increasing both proliferation and migration [16–19, 21, 23, 24]. In the present study, cultivation in cSMCGM or the combination of rSMCGM and PDGF-stimulation conferred an amplification of the proliferative capacity in HUASMC. These conditions were therefore considered suitable models to investigate the effects of CBD against the disease-associated aberrant proliferation and migration of VSMC.

In subsequent functional analyses, this study revealed a CBD-mediated concentration-dependent inhibition of growth factor-initiated proliferation and migration of HUASMC. Analyses using substances targeting CB<sub>1</sub>R, CB<sub>2</sub>R, TRPV1, and GPR55 excluded an involvement of these cannabinoid-activated receptors in the CBD-mediated anti-proliferative effect. Interestingly, the decrease of HUASMC proliferation/migration apparently correlated with the CBD-mediated induction of HO-1. Therefore, an involvement of HO-1 was considered a potential mechanism of CBD's anti-proliferative/anti-migratory effects observed in these experiments. However, this hypothesis was rejected by experiments targeting both HO-1 activity and HO-1 protein expression. In detail, neither HO-1 siRNA nor the inhibitor of HO-1 activity, SnPPiX, antagonized the CBD-mediated anti-proliferative/anti-migratory responses. Since ROS were involved in the CBD-mediated induction of HO-1, additional experiments were performed to examine the role of ROS in the CBD-mediated modulation of HUASMC proliferation. One study previously reported that initiation of ER stress following administration of the potent ER stress inducer tunicamycin led to up-regulation of HO-1, inhibition of mitochondrial ROS production and modulation of cell cycle-regulatory proteins [19]. Thereby, CBD inhibited the PDGF-induced proliferation/migration in rat thoracic aorta SMC (RTASMC) without showing significant apoptosis [19]. Although emphasizing the anti-oxidant and cytoprotective role of HO-1, it was assumed that the area, where positive and negative effects of ER stress are separated, is narrow and requires a fine adjustment [19]. In the present study, NAC, at a concentration that sufficiently blocked the CBD-mediated ROS-dependent induction of HO-1, failed to attenuate the CBD-mediated anti-proliferative effects in HUASMC. Even if not explicitly examined here, a ROS-independent effect could also apply to the here reported CBD-mediated anti-migratory effects in HUASMC. This study thus demonstrates that neither HO-1 nor ROS contributed to CBD's anti-proliferative effects in HUASMC.

---

<sup>n</sup> Mitogens are chemical substances that stimulate a cell to initiate cell division (mitosis). This is referred to as mitogenesis.

Similarly, experiments using wild-type and HO-1-null mouse aortic SMC excluded a relation between extracellular acidosis-(EA-)mediated induction of HO-1 and inhibition of the PDGF-induced proliferation/migration [283]. An involvement of multiple intracellular pathways was thus suggested [283]. Conversely, several other studies reported an anti-proliferative/anti-migratory effect of HO-1 in VSMC originating from rat thoracic aorta [14, 17, 19, 21, 99, 101, 284], human aorta [15], and human saphenous vein [284]. Herein, some plant-derived substances, such as the citrus flavonoid naringenin [14], the sesquiterpene lactone eupatolide from *Inula britannica* [21], and the green tea-derived epigallocatechin gallate [15], conferred up-regulation of HO-1 and inhibited cytokine- or PDGF-induced proliferation and migration in VSMC of different origin. Likewise, atractylenolide I<sup>o</sup> (AO-I) prevented oxidized-low-density lipoprotein-(ox-LDL-)induced production of inflammatory cytokines and proliferation in RTASMC via induction of HO-1 [100]. Furthermore, AO-1 inhibited foam cell formation and lipid accumulation in peritoneal mice macrophages, thereby mediating beneficial anti-atherosclerotic effects [100]. Additionally, overexpression of human HO-1 following retroviral transduction of RTASMC inhibited cell cycle progression and protected against H<sub>2</sub>O<sub>2</sub>-induced oxidative injury [95].

Consistent to the positive findings, chemical inhibition of HO-1 by SnPPIX intensified the heme-induced ROS production and the increases of proliferation and migration in RTASMC [285]. Accordingly, administration of the HO reaction product bilirubin inhibited neointima formation and intimal thickening following carotid artery balloon-injury in rats [84]. The underlying mechanism involved the inhibition of both cell cycle progression and proliferation of human vascular SMC, thus providing beneficial effects against unwanted vascular remodeling after therapeutic intervention [84]. Likewise, the exogenous exposure to the gaseous HO reaction product CO inhibited the proliferation of HUASMC and human umbilical vein endothelial cells (HUVEC) [286].

The apparently contradictory results for the role of HO-1 may root in substance-dependent divergent mechanisms conferring the anti-proliferative and anti-migratory effects in SMC. As a matter of fact, anti-proliferative effects in SMC were ascribed to both HO-1-dependent and -independent actions. Likewise, it was demonstrated that different inducers of HO-1 triggered divergent effects in one cell type [287]. In more detail, Loboda *et al.* (2005) investigated the mechanism of VEGF-production in human microvascular endothelial cells using two different inducers of HO-1, namely cobalt (II) chloride (CoCl<sub>2</sub>) and cobalt protoporphyrin IX (CoPPIX) [287]. Although both compounds induced HO-1 in these cells, the CoCl<sub>2</sub>-mediated production of VEGF did not involve HO-1 and rather relied on the

---

° One of the major bioactive components of plant rhizomes from *Atractylodes macrocephaly*.



activation of hypoxia-inducible factor 1 $\alpha$  (HIF1 $\alpha$ ) [287]. In contrast, they also showed that CoPPIX-mediated VEGF production originated from HO-1 activity and did not involve HIF1 $\alpha$  [287]. It was further reported that genetic differences in GT-repeat length influence the activity of the HO-1 promotor in human VSMC [66]. Consequently, species- and donor-dependent genetic differences may affect the transcriptional responses and thus the strength of HO-1 activity. These genetic factors may be the cause of the divergent outcomes in different studies.

In terms of the functional investigations in the present study, it is worth mentioning that a greater loss in cell viability was observed by use of the chemical inhibitor SnPPIX, in contrast to the siRNA-mediated knockdown of HO-1. The loss of viability under SnPPIX conditions exclusively increased the late apoptotic/necrotic but not the apoptotic cell population. Possibly, this is a consequence of an acceleration of apoptosis or toxicity. In contrast, the targeted knockdown of HO-1 by siRNA led to a slight reduction in cell viability, but both apoptotic and necrotic fractions were increased. This seemed more likely to be the normal course of the apoptotic cell death. In the present study, SnPPIX was used at a concentration of 10  $\mu$ M. For HO inhibitors, including SnPPIX and zinc protoporphyrin IX (ZnPPIX), this concentration is commonly used in *in vitro* studies investigating the role of HO-1 in VSMC [17, 18, 21, 21, 68, 97, 99, 246, 285, 288]. The efficiency of SnPPIX to inhibit the HO-catalyzed heme degradation reaction has been proven in several studies by activity assays [244, 289, 290]. However, studies regarding the selectivity of these substances are rare. Nevertheless, non-selective but very potent inhibitory effects of SnPPIX on both HO isoenzymes were described [291]. It is therefore conceivable that not only the stress response, but also the basic anti-oxidant capacity of the cells will decrease. This may explain the resulting differences and the drastic loss of cell viability even in the absence of CBD. On the other hand, the targeted knockdown of HO-1 significantly reduced the corresponding protein. However, both, the residual activity of the remaining HO-1 and a possible compensation by HO-2, could mitigate the potential toxic conditions in the presence of CBD. These processes may lead to the different outcomes of these experiments. A possible compensatory role for HO-2 has been described for human endothelial cells under hypoxic conditions [292]. Herein, the expression of HO-1 was decreased under hypoxic conditions, whereas the translation of HO-2 transcripts, and thus HO-2 protein synthesis, was up-regulated and preserved cell viability under these conditions [292]. However, by pointing out that inhibition or knockdown of HO-1 further enhances the anti-proliferative and anti-migratory effects of CBD together with the induction of apoptotic cell death, the present study substantiates the fundamental cytoprotective role of HO-1. Similarly, treatment with the plant-derived triterpenoids maslinic acid and oleanolic acid confirmed a protective role of the HO-1 pathway against H<sub>2</sub>O<sub>2</sub>-induced oxidative stress and apoptosis in RTASMC [68, 97].

A protective role of HO-1 has been likewise reported regarding other disease-models or cell types. For example, CoPPIX-mediated induction of HO-1 or treatment with the CO-releasing molecule-(CORM-)A1 prevented oxidative stress and hepatocyte cell death *in vitro* and in an *in vivo* model of alcoholic liver disease using female C57BL/6J mice [87]. Similarly, CoPPIX-mediated induction of HO-1 protected HUVEC against high glucose-mediated oxidative and ER stress and activation of inflammatory and apoptotic reactions [90]. It was thereby suggested that HO-1 mediates positive effects against diabetes-induced endothelial dysfunction and cardiovascular complications [90]. Additionally, endogenous and overexpressed HO-1 prevented hypoxia/reoxygenation-(H/R)-induced cell death by inhibiting mitochondrial ROS production and stabilization of mitochondrial membrane in H9C2 rat cardiomyocytes [293]. Thus, HO-1 provided beneficial effects against myocardial H/R-injury [293].

In the present study, subsequent experiments further substantiated the cytoprotective role of HO-1 and its compensatory induction following the CBD-mediated ROS production. NAC, by mitigating ROS production, prevented both the compensatory up-regulation of HO-1 and the cell death mediated by CBD in absence of HO-1.

According to the results of the study presented here, Scott *et al.* (2015) observed CBD-specific changes in expression and up-regulation of several heat shock proteins (HSPs) including HO-1 by ROS generation in T98G and U87MG human glioblastoma cell lines [294]. Despite structural similarities between CBD and THC, these effects were not observed using THC [294]. In detail, co-incubation with non-cytotoxic concentrations of inhibitors targeting some of these HSPs reduced the mean inhibitory concentration (IC<sub>50</sub>) of CBD and markedly induced apoptosis [294]. The latter effect was evoked by an increase in the cells' sensitivity to radiation, which may provide an interesting approach for future irradiative glioblastoma therapies [294]. Finally, the CBD-mediated increase of HSPs was sensitive against the ROS scavenger NAC [294]. This result is in line with the NAC-sensitive CBD-mediated induction of HO-1 observed in the present study. The apoptosis-inducing mechanism of some cannabinoid receptor agonists, such as THC, AEA and the synthetic THC analog HU-210, was investigated in H460 human lung cancer cells [295]. The study revealed an increased mitochondrial H<sub>2</sub>O<sub>2</sub> production that was caused by the inhibition of the respiratory chain's mitochondrial complex I [295]. In the case of CBD, however, an opposite effect was observed in a model of chemotherapy-induced cardiomyopathy in male C57BL/6J mice [296]. Herein, pre-treatment with intraperitoneally administered CBD at a dose of 10 mg/kg preserved doxorubicin-induced cardiotoxicity by several protective mechanisms [296]. These included, for example, the reduction of oxidative/nitrative stress, the improvement of mitochondrial biogenesis and an increased activity of the respiratory chain's mitochondrial complexes I and II [296]. Similar, a recent study reported that CBD at a concentration of 5  $\mu$ M prevented cytotoxicity and cell death in an oxygen-glucose-

deprivation/reperfusion- (OGD/R-)model using HT22 mouse hippocampal neuronal cells [297]. Herein, the in-depth analyses showed that CBD protected cells from OGD/R-induced loss of mitochondrial bioenergetics by stimulating the pentose-phosphate pathway of glucose metabolism and reducing oxidative stress [297]. Thus, CBD exerted a strong and potential neuroprotective effect against I/R injury [297], which is in line with some other studies [221, 223]. Interestingly, in animal studies of cerebral ischemia CBD, given at doses of 1 mg/kg or 5 mg/kg, also exerted neuroprotective effects even when given after the ischemic insult [220, 222]. It was therefore assumed that CBD might also mediate beneficial therapeutic effects when used as an anti-ischemic drug [220, 222].

Regarding the cytoprotective role of HO-1, the suppression of *HMOX1* gene translation after transfection with the hypoxia-inducible miR-24 showed anti-proliferative and anti-migratory effects in human aortic SMC [298]. However, this was accompanied by the induction of apoptosis [298]. In addition, Wu *et al.* (2008) reported CBD-dependent cytotoxicity in primary lymphocytes of mice due to oxidative stress and induction of apoptosis-indicating caspase-8 [299]. Similar to the present study, the CBD-mediated oxidative stress and apoptosis were prevented by the pre-treatment with NAC at concentrations up to 1 mM [299]. The same group later described a CBD-induced contrasting pro-apoptotic effect between freshly isolated and pre-cultured human monocytes [300]. The investigations of this study showed a significant decrease in the glutathione content in the freshly isolated monocytes [300]. In contrast, the pre-cultured monocytes were insensitive to the CBD-induced cytotoxicity due to higher glutathione and HO-1 values [300]. In the present study, however, VSMC treated with CBD alone did not undergo apoptosis as analyzed by flow cytometry and vital staining, even though CBD intensely induced the ROS production.

CBD appears to perform various actions that may depend on the species and cell types analyzed and are particularly evident when comparing cancer and non-neoplastic cells. Nevertheless, the role of HO-1 in cancer and non-neoplastic cells is also regarded as ambivalent. Since HO-1 has positive cell-protective properties, it can also protect degenerated cells, thus promoting undesirable effects such as chemoresistance, tumor growth and cancer angiogenesis (reviewed in [301, 302]). Recently, potent anti-tumor effects of paeonol<sup>p</sup> in MDA-MB-231 human breast cancer cells were correlated with a down-regulation of HO-1 [303]. On the other hand, the up-regulation of HO-1 by piperlongumine<sup>q</sup> selectively induced ROS generation and apoptosis in MCF-7 human breast cancer but not in MCF10-A human breast epithelial cells [304].

---

<sup>p</sup> A phenolic compound in root barks of *Paeonia montan.*

<sup>q</sup> A natural alkaloid derived from long pepper.

Additionally, in a recent study, the flavonoid fisetin<sup>r</sup> induced HO-1 up-regulation in 4T1 and JC mouse breast cancer cells and inhibited matrix metalloproteinases, enzymes that are commonly up-regulated in cell migration processes [305]. These results therefore indicate also beneficial anti-metastatic effects of HO-1 with respect to breast cancer therapy [305].

Noteworthy, the up-regulation of HO-1 and the anti-proliferative/anti-migratory effects of CBD were significantly detectable at concentrations of 6  $\mu\text{M}$  and 10  $\mu\text{M}$ . Although representative of the usual CBD concentrations that range from 0.1–100  $\mu\text{M}$  in *in vitro* experiments [232, 242, 269, 272, 275, 294, 299, 300], these concentrations are indeed above the therapeutic plasma concentrations of the drug. Accordingly, six weeks of oral treatment of Huntington's disease patients with CBD at a dose of 10 mg/kg/day (approx. 700 mg/d) resulted in maximum mean CBD plasma peak values of 0.036  $\mu\text{M}$  (equivalent to 11.2 ng/ml) as investigated by gas chromatography-mass spectrometry (GC-MS) analysis [306]. Interestingly, another recent study reported approximately 20-fold higher maximum CBD plasma concentrations of 0.7  $\mu\text{M}$  (equivalent to 221 ng/ml) [307]. This was measured 3 hours after simultaneous administration of a single oral dose of CBD (800 mg; equivalent to 10–15 mg/kg) and a single intravenous dose of fentanyl<sup>s</sup> (0.5  $\mu\text{g/kg}$ ) [307]. Given the conditions and limitations of cell culture experiments, a direct correlation of *in vitro* to *in vivo* is rather critical anyway. For example, diverging outcomes between *in vivo* and *in vitro* studies investigating the CBD-induced production of interleukin (IL) in murine macrophages have been shown [271]. Herein, antagonists targeting CB<sub>1</sub>R and CB<sub>2</sub>R prevented the CBD-mediated increase of IL-12 and the CBD-mediated decrease of IL-10 in *in vitro* experiments, but not in *in vivo* models [271].

In summary, the various complex effects of CBD appear to depend on cell type, species and experimental conditions. These dependencies complicate both the understanding and the targeted investigation of the underlying mechanisms of the CBD-mediated anti-proliferative and anti-migratory effects in HUASMC. Although cannabinoids have been the focus of research in recent decades, there are likely some unexplored targets and mechanisms underlying the cannabinoid-mediated actions. However, this study provides the first evidence of a phytocannabinoid-induced increase of HO-1 in VSMC by both, CBD and THC. Accompanying the increase in HO-1, CBD exerted positive anti-proliferative and anti-migratory effects without showing cytotoxicity *per se*. However, aside from the protection against oxidative stress-induced cell death, HO-1 did not contribute to the positive effects mediated by CBD in HUASMC. Further studies on the potential vasculoprotective and anti-angiogenic properties of CBD are therefore justified.

---

<sup>r</sup> A flavonoid found in a variety of plants.

<sup>s</sup> Opioid. Used for pain-medication and anesthesia.

## 6 Summary

Cardiovascular diseases and cancer are the most frequent causes of death worldwide. Vascular smooth muscle cells (VSMC) are involved in their underlying mechanisms. VSMC, physiologically contributing to the maintenance of the vascular tone and the regulation of blood pressure, are assigned to a contractile/quiescent phenotype. Inflammatory processes and/or released growth factors lead to phenotypic changes in VSMC and thus support, for example, wound healing processes. This activated phenotype is characterized by a high proliferation and migration rate. It is referred to as a synthetic/proliferative or disease-associated phenotype. Uncontrolled activation and promotion of this phenotype occurs, for example, in chronic inflammatory vascular diseases such as arteriosclerosis. Growth factors, released during tumor progression, also support this process and thus enable the development of a tumor blood supply. The inhibition of abnormal proliferation and migration of VSMC represents a strategy to slow down or even prevent the progression of these diseases. Several studies attributed such an anti-proliferative/anti-migratory effect in VSMC to heme oxygenase-1 (HO-1). This enzyme is primarily induced under conditions of oxidative cell stress and contributes significantly to cell protection through its potentially anti-oxidative products.

Medical research increasingly proves the benefit of cannabinoids, which, among other things, have spasmolytic, analgesic, and anti-inflammatory properties. However, psychoactive effects limit the therapeutic benefits of several cannabinoids. In contrast, the phytocannabinoid cannabidiol (CBD) does not exhibit psychoactivity. It therefore represents a particularly interesting candidate for medical purposes. Recently, the American approval authority, FDA, licensed a pure CBD preparation for the treatment of severe, therapy-resistant forms of epilepsy.

In the context of this work, the effects of cannabinoids regarding an induction of HO-1 in VSMC were examined for the first time. In addition, the effects of CBD on proliferation and migration of VSMC and the role of HO-1 in these effects were evaluated. Initial experiments demonstrated a strong concentration- and time-dependent induction of HO-1 in VSMC by the two phytocannabinoids THC and CBD, but not by the synthetic cannabinoids R-(+)-methanandamide and JWH-133. This induction could also be demonstrated for CBD at the mRNA level. A participation of the cannabinoid-activated receptors CB<sub>1</sub>R, CB<sub>2</sub>R, TRPV1 and GPR55 in the HO-1 induction was experimentally excluded. The use of the glutathione precursor *N*-acetylcysteine (NAC) indicated a participation of reactive oxygen species (ROS) in the CBD-mediated induction of HO-1. A CBD-mediated formation of ROS was confirmed in flow cytometry-based investigations also using NAC. Based on proliferation analyses, experimental conditions promoting the synthetic/proliferative

phenotype of VSMC were determined. Subsequent functional analyses showed a significant inhibition of proliferation/migration of VSMC by treatment with CBD while maintaining cell viability. The role of HO-1 in these effects was investigated by both chemical inhibition of activity and by targeted knockdown of HO-1 via RNA interference. The inhibition of the activity/expression of HO-1 led to a severe reduction of cell viability after treatment with CBD in both experimental approaches. Accordingly, the anti-proliferative/anti-migratory effects of CBD were not eliminated, but partially enhanced. A participation of ROS in the CBD-mediated anti-proliferative effects was excluded by the use of NAC. The use of NAC inhibited both the CBD-mediated ROS formation and the HO-1 induction. Nevertheless, cell viability was maintained under treatment of CBD. From this, the role of HO-1 as a cytoprotective enzyme was demonstrated. A participation of HO-1 in the CBD-mediated anti-proliferative/anti-migratory effects was contradicted by the investigations.

Summarizing, this study shows that CBD mediates beneficial effects with regard to the excessive proliferation and migration, i. e. disease-associated behavior of VSMC. The compensatory induction of HO-1 contributes to the protection of the cells against the formation of ROS mediated by CBD. Due to the lack of psychoactivity, CBD is still a promising candidate for the treatment of various diseases. The mechanism by which CBD mediates its shown anti-proliferative and anti-migratory effects needs to be further investigated.

## 7 Zusammenfassung

Kardiovaskuläre Erkrankungen und Krebs gehören zu den häufigsten Todesursachen weltweit. An den zugrundeliegenden Mechanismen sind vaskuläre glatte Muskelzellen (VSMC, engl.: vascular smooth muscle cells) beteiligt. VSMC tragen physiologischerweise zum Erhalt des Gefäßtonus und zur Regulation des Blutdrucks bei und werden einem kontraktile/ruhemdem Phänotyp zugeordnet. Entzündliche Prozesse oder freigesetzte Wachstumsfaktoren führen zur phänotypischen Veränderung der VSMC und fördern so beispielsweise die Wundheilung. Dieser aktivierte Phänotyp zeichnet sich u. a. durch eine hohe Proliferations- und Migrationsrate aus. Er wird als synthetischer/proliferierender bzw. als krankheitsassoziierter Phänotyp bezeichnet. Eine unkontrollierte Aktivierung und Förderung dieses Phänotyps tritt beispielsweise bei chronisch-entzündlichen Gefäßerkrankungen wie der Arteriosklerose auf. Auch im Rahmen der Tumorprogression freigesetzte Wachstumsfaktoren unterstützen diesen Prozess und ermöglichen so den Aufbau einer Tumor-Blutversorgung. Die Hemmung der abnormalen Proliferation und Migration der VSMC stellt eine Strategie dar, das Fortschreiten dieser Erkrankungen zu verlangsamen oder gar zu verhindern.

In diversen Untersuchungen konnte ein derartiger anti-proliferativer/anti-migrativer Effekt in VSMC der Hämooxygenase-1 (HO-1) zugeschrieben werden. Dieses Enzym wird vorrangig unter Bedingungen des oxidativen Zellstress induziert und trägt durch seine potenziell anti-oxidativen Produkte maßgeblich zum Zellschutz bei.

Medizinische Forschungen belegen wiederholt den Nutzen von Cannabinoiden, die u. a. krampflösende, schmerzstillende und anti-entzündliche Eigenschaften aufweisen. Der therapeutische Nutzen vieler Cannabinoide wird allerdings durch psychoaktive Eigenschaften limitiert, die das Phytocannabinoid Cannabidiol (CBD) jedoch nicht aufweist. Es stellt somit einen besonders interessanten Kandidaten für medizinische Zwecke dar. Erst kürzlich wurde durch die amerikanische Lebensmittelüberwachungs- und Arzneimittelbehörde (FDA, engl. Food and Drug Administration) ein reines CBD-Präparat zur Behandlung schwerer, therapieresistenter Epilepsieformen zugelassen.

Im Rahmen dieser Arbeit wurden erstmals die Effekte von Cannabinoiden hinsichtlich einer Induktion der HO-1 in VSMC untersucht. Zudem sollte die Wirkung von CBD auf Proliferation und Migration der VSMC sowie die Rolle der HO-1 in diesen Effekten evaluiert werden. Erste Untersuchungen zeigten eine starke konzentrations- und zeitabhängige Induktion der HO-1 in VSMC durch die beiden Phytocannabinoide THC und CBD, nicht jedoch durch die synthetischen Cannabinoide R-(+)-Methanandamid und JWH-133. Diese Induktion konnte für

CBD auch auf mRNA-Ebene nachgewiesen werden. Eine Beteiligung der Cannabinoid-aktivierten Rezeptoren CB<sub>1</sub>R, CB<sub>2</sub>R, TRPV1 und GPR55 an der HO-1-Induktion konnte experimentell ausgeschlossen werden. Die Verwendung des Glutathionvorläufers *N*-Acetylcystein (NAC) wies auf eine Beteiligung reaktiver Sauerstoffspezies (ROS) an der CBD-vermittelten Induktion der HO-1 hin. Eine CBD-vermittelte Bildung von ROS wurde in durchflusszytometrischen Untersuchungen ebenso unter Verwendung von NAC belegt. Anhand von Proliferationsanalysen wurden experimentelle Bedingungen ermittelt, welche den synthetischen/proliferativen Phänotyp der VSMC fördern. Anschließend funktionelle Analysen zeigten eine starke Hemmung von Proliferation und Migration der VSMC durch Behandlung mit CBD, bei gleichbleibender Viabilität der Zellen. Die Rolle der HO-1 in diesen Effekten wurde sowohl durch chemische Hemmung der Aktivität als auch durch ein gezieltes Knockdown der HO-1 via RNA-Interferenz untersucht. Eine Hemmung der Aktivität/Expression der HO-1 führte in beiden experimentellen Ansätzen zu einer starken Reduktion der Zellviabilität nach Behandlung mit CBD. Die anti-proliferativen/anti-migrativen Effekte von CBD wurden dementsprechend nicht aufgehoben, sondern teilweise verstärkt. Eine Beteiligung von ROS an den CBD-vermittelten anti-proliferativen Effekten wurde durch den Einsatz von NAC ausgeschlossen. NAC führte sowohl zur Hemmung der CBD-vermittelten ROS-Bildung als auch der HO-1 Induktion. Dennoch blieb die Zellviabilität unter Behandlung von CBD erhalten. Hieraus lässt sich die Rolle der HO-1 als Zellschutz-Enzym belegen. Eine Beteiligung der HO-1 an den CBD-vermittelten anti-proliferativen/anti-migrativen Effekten wurde durch die Untersuchungen widerlegt.

Zusammenfassend konnte in dieser Arbeit gezeigt werden, dass CBD vorteilhafte Effekte hinsichtlich der überschießenden Proliferation und Migration, also einem krankheitsassoziierten Verhalten von VSMC, vermittelt. Die kompensatorische Induktion der HO-1 trägt hierbei zum Schutz der Zellen vor der durch CBD vermittelten Bildung von ROS bei. Aufgrund fehlender Psychoaktivität ist CBD weiterhin ein vielversprechender Kandidat für die Behandlung verschiedener Erkrankungen. Der Mechanismus, über den CBD seine hier gezeigten anti-proliferativen und anti-migrativen Effekte vermittelt, muss noch näher untersucht werden.



## 8 References

1. Ross R, Glomset JA. The pathogenesis of atherosclerosis (first of two parts). *N Engl J Med*. 1976; 295: 369–377.
2. Rensen SSM, Doevendans PAFM, van Eys GJJM. Regulation and characteristics of vascular smooth muscle cell phenotypic diversity. *NHJL*. 2007; 15: 100–108.
3. Beamish JA, He P, Kottke-Marchant K, Marchant RE. Molecular regulation of contractile smooth muscle cell phenotype: implications for vascular tissue engineering. *Tissue Eng Part B Rev*. 2010; 16: 467–491.
4. Chamley-Campbell J, Campbell GR, Ross R. The smooth muscle cell in culture. *Physiol Rev*. 1979; 59: 1–61.
5. Bochaton-Piallat ML, Ropraz P, Gabbiani F, Gabbiani G. Phenotypic heterogeneity of rat arterial smooth muscle cell clones. Implications for the development of experimental intimal thickening. *Arterioscler Thromb Vasc Biol*. 1996; 16: 815–820.
6. Frid MG, Aldashev AA, Dempsey EC, Stenmark KR. Smooth muscle cells isolated from discrete compartments of the mature vascular media exhibit unique phenotypes and distinct growth capabilities. *Circ Res*. 1997; 81: 940–952.
7. Li S, Fan YS, Chow LH, van den Diepstraten C, van der Veer E, Sims SM, Pickering JG. Innate diversity of adult human arterial smooth muscle cells. Cloning of distinct subtypes from the internal thoracic artery. *Circ Res*. 2001; 89: 517–525.
8. Hao H, Ropraz P, Verin V, Camenzind E, Geinoz A, Pepper MS, Gabbiani G, Bochaton-Piallat M-L. Heterogeneity of smooth muscle cell populations cultured from pig coronary artery. *Arterioscler Thromb Vasc Biol*. 2002; 22: 1093–1099.
9. Alexander MR, Owens GK. Epigenetic control of smooth muscle cell differentiation and phenotypic switching in vascular development and disease. *Annu Rev Physiol*. 2012; 74: 13–40.
10. Qiu J, Zheng Y, Hu J, Liao D, Gregersen H, Deng X, Fan Y, Wang G. Biomechanical regulation of vascular smooth muscle cell functions. From *in vitro* to *in vivo* understanding. *J R Soc Interface*. 2014; 11: 20130852.
11. Hedin U, Bottger BA, Forsberg E, Johansson S, Thyberg J. Diverse effects of fibronectin and laminin on phenotypic properties of cultured arterial smooth muscle cells. *J Cell Biol*. 1988; 107: 307–319.
12. Evanko SP, Angello JC, Wight TN. Formation of hyaluronan- and versican-rich pericellular matrix is required for proliferation and migration of vascular smooth muscle cells. *Arterioscler Thromb Vasc Biol*. 1999; 19: 1004–1013.

13. Chai S, Chai Q, Danielsen CC, Hjorth P, Nyengaard JR, Ledet T, Yamaguchi Y, Rasmussen LM, Wogensen L. Overexpression of hyaluronan in the tunica media promotes the development of atherosclerosis. *Circ Res.* 2005; 96: 583–591.
14. Chen S, Ding Y, Tao W, Zhang W, Liang T, Liu C. Naringenin inhibits TNF- $\alpha$  induced VSMC proliferation and migration via induction of HO-1. *Food Chem Toxicol.* 2012; 50: 3025–3031.
15. Liu P-L, Liu J-T, Kuo H-F, Chong I-W, Hsieh C-C. Epigallocatechin gallate attenuates proliferation and oxidative stress in human vascular smooth muscle cells induced by interleukin-1 $\beta$  via heme oxygenase-1. *Mediators Inflamm.* 2014; 2014: 1–8.
16. Roos TU, Heiss EH, Schwaiberger AV, Schachner D, Sroka IM, Oberan T, Vollmar AM, Dirsch VM. Caffeic acid phenethyl ester inhibits PDGF-induced proliferation of vascular smooth muscle cells via activation of p38 MAPK, HIF-1 $\alpha$ , and heme oxygenase-1. *J Nat Prod.* 2011; 74: 352–356.
17. Lee S, Seo J, Ryoo S, Cuong TD, Min B-S, Lee J-H. Malabaricone C inhibits PDGF-induced proliferation and migration of aortic smooth muscle cells through induction of heme oxygenase-1. *J Cell Biochem.* 2012; 113: 2866–2876.
18. Cheng C, Haasdijk RA, Tempel D, den Dekker WK, Chrifi I, Blonden LAJ, van de Kamp EHM, Boer M de, Burgisser PE, Noorderloos A, Rens JAP, Hagen TLM ten, Duckers HJ. PDGF-induced migration of vascular smooth muscle cells is inhibited by heme oxygenase-1 via VEGFR2 upregulation and subsequent assembly of inactive VEGFR2/PDGFR $\beta$  heterodimers. *Arterioscler Thromb Vasc Biol.* 2012; 32: 1289–1298.
19. Yi N, Chen S-Y, Ma A, Chen P-S, Yao B, Liang T-M, Liu C. Tunicamycin inhibits PDGF-BB-induced proliferation and migration of vascular smooth muscle cells through induction of HO-1. *Anat Rec (Hoboken).* 2012; 295: 1462–1472.
20. Salabei JK, Cummins TD, Singh M, Jones SP, Bhatnagar A, Hill BG. PDGF-mediated autophagy regulates vascular smooth muscle cell phenotype and resistance to oxidative stress. *Biochem. J.* 2013; 451: 375–388.
21. Kim N, Hwangbo C, Lee S, Lee J-H. Eupatolide inhibits PDGF-induced proliferation and migration of aortic smooth muscle cells through ROS-dependent heme oxygenase-1 induction. *Phytother. Res.* 2013; 27: 1700–1707.
22. Ha JM, Yun SJ, Kim YW, Jin SY, Lee HS, Song SH, Shin HK, Bae SS. Platelet-derived growth factor regulates vascular smooth muscle phenotype via mammalian target of rapamycin complex 1. *Biochem Biophys Res Commun.* 2015; 464: 57–62.
23. Li J, Zhang M, Ma J. Myricitrin inhibits PDGF-BB-stimulated vascular smooth muscle cell proliferation and migration through suppressing PDGFR $\beta$ /Akt/Erk signaling. *Int J Clin Exp Med.* 2015; 8: 21715–21723.

24. Liu W, Kong H, Zeng X, Wang J, Wang Z, Yan X, Wang Y, Xie W, Wang H. Iptakalim inhibits PDGF-BB-induced human airway smooth muscle cells proliferation and migration. *Exp Cell Res*. 2015; 336: 204–210.
25. Global Health Estimates 2016. Deaths by cause, age, sex, by country and by religion, 2000-2016. 2018; [http://www.who.int/healthinfo/global\\_burden\\_disease/estimates/en/](http://www.who.int/healthinfo/global_burden_disease/estimates/en/). recorded on: 27.06.2018 at 13:45 MEZ.
26. Ross R. The pathogenesis of atherosclerosis--an update. *N Engl J Med*. 1986; 314: 488–500.
27. Ross R. Atherosclerosis - an inflammatory disease. *N Engl J Med*. 1999; 340: 115–126.
28. Bennett MR, Sinha S, Owens GK. Vascular smooth muscle cells in atherosclerosis. *Circ Res*. 2016; 118: 692–702.
29. Cerrito MG, Scagliarini A, Froio A, Liloia A, Busnelli M, Giovannoni R, Le Otterbein, Mainetti L, Villa M, Bach FH, Eugenio L, Biasi GM, Lavitrano M. Heme oxygenase-1 inhibition prevents intimal hyperplasia enhancing nitric oxide-dependent apoptosis of vascular smooth muscle cells. *Biol. Pharm. Bull*. 2011; 34: 1204–1214.
30. Hyvelin J-M, Maurel B, Uzbekov R, Motterlini R, Lermusiaux P. Hemin prevents in-stent stenosis in rat and rabbit models by inducing heme oxygenase-1. *J Vasc Surg*. 2010; 51: 417–428.
31. Marx SO, Totary-Jain H, Marks AR. Vascular smooth muscle cell proliferation in restenosis. *Circ Cardiovasc Interv*. 2011; 4: 104–111.
32. Carmeliet P. Angiogenesis in life, disease and medicine. *Nature*. 2005; 438: 932–936.
33. Carmeliet P, Jain RK. Angiogenesis in cancer and other diseases. *Nature*. 2000; 407: 249–257.
34. El-Kenawi AE, El-Remessy AB. Angiogenesis inhibitors in cancer therapy. Mechanistic perspective on classification and treatment rationales. *Br J Pharmacol*. 2013; 170: 712–729.
35. Vasudev NS, Reynolds AR. Anti-angiogenic therapy for cancer. Current progress, unresolved questions and future directions. *Angiogenesis*. 2014; 17: 471–494.
36. Tenhunen R, Marver HS, Schmid R. The enzymatic conversion of heme to bilirubin by microsomal heme oxygenase. *Proc Natl Acad Sci U S A*. 1968; 61: 748–755.
37. Loboda A, Jazwa A, Grochot-Przeczek A, Rutkowski AJ, Cisowski J, Agarwal A, Jozkowicz A, Dulak J. Heme oxygenase-1 and the vascular bed: from molecular mechanisms to therapeutic opportunities. *Antioxid Redox Signal*. 2008; 10: 1767–1812.
38. Araujo JA, Zhang M, Yin F. Heme oxygenase-1, oxidation, inflammation, and atherosclerosis. *Front Pharmacol*. 2012; 3: 119.

39. Zelenka J, Koncošová M, Ruml T. Targeting of stress response pathways in the prevention and treatment of cancer. *Biotechnol Adv.* 2018; 36: 583–602.
40. Kumar S, Bandyopadhyay U. Free heme toxicity and its detoxification systems in human. *Toxicol Lett.* 2005; 157: 175–188.
41. Lin Y-W, Wang J. Structure and function of heme proteins in non-native states. A mini-review. *J Inorg Biochem.* 2013; 129: 162–171.
42. Jeney V, Balla J, Yachie A, Varga Z, Vercellotti GM, Eaton JW, Balla G. Pro-oxidant and cytotoxic effects of circulating heme. *Blood.* 2002; 100: 879–887.
43. Tenhunen R, Marver H, Pinstone NR, Trager WF, Cooper DY, Schmid R. Enzymic degradation of heme. Oxygenative cleavage requiring cytochrome P-450. *Biochemistry.* 1972; 11: 1716–1720.
44. Tenhunen R, Marver HS, Schmid R. Microsomal heme oxygenase. Characterization of the enzyme. *J Biol Chem.* 1969; 244: 6388–6394.
45. Singleton JW, Laster L. Biliverdin reductase of guinea pig liver. *J Biol Chem.* 1965; 240: 4780–4789.
46. Granick S. Ferritin; its properties and significance for iron metabolism. *Chem Rev.* 1946; 38: 379–403.
47. Maines MD, Trakshel GM, Kutty RK. Characterization of two constitutive forms of rat liver microsomal heme oxygenase. Only one molecular species of the enzyme is inducible. *J Biol Chem.* 1986; 261: 411–419.
48. McCoubrey WK, Huang TJ, Maines MD. Isolation and characterization of a cDNA from the rat brain that encodes hemoprotein heme oxygenase-3. *Eur J Biochem.* 1997; 247: 725–732.
49. Hayashi S, Omata Y, Sakamoto H, Higashimoto Y, Hara T, Sagara Y, Noguchi M. Characterization of rat heme oxygenase-3 gene. Implication of processed pseudogenes derived from heme oxygenase-2 gene. *Gene.* 2004; 336: 241–250.
50. Cruse I, Maines MD. Evidence suggesting that the two forms of heme oxygenase are products of different genes. *J Biol Chem.* 1988; 263: 3348–3353.
51. Keyse SM, Tyrrell RM. Heme oxygenase is the major 32-kDa stress protein induced in human skin fibroblasts by UVA radiation, hydrogen peroxide, and sodium arsenite. *Proc Natl Acad Sci U S A.* 1989; 86: 99–103.
52. McCoubrey WK, Ewing JF, Maines MD. Human heme oxygenase-2. Characterization and expression of a full-length cDNA and evidence suggesting that the two HO-2 transcripts may differ by choice of polyadenylation signal. *Arch Biochem Biophys.* 1992; 295: 13–20.
53. Rotenberg MO, Maines MD. Characterization of a cDNA-encoding rabbit brain heme oxygenase-2 and identification of a conserved domain among mammalian heme oxygenase isozymes. Possible heme-binding site? *Arch Biochem Biophys.* 1991; 290: 336–344.
54. Kutty RK, Kutty G, Rodriguez IR, Chader GJ, Wiggert B. Chromosomal localization of the human heme oxygenase genes. Heme oxygenase-1

- (*HMOX1*) maps to chromosome 22q12 and heme oxygenase-2 (*HMOX2*) maps to chromosome 16p13.3. *Genomics*. 1994; 20: 513–516.
55. Kuwano A, Ikeda H, Takeda K, Nakai H, Kondo I, Shibahara S. Mapping of the human gene for inducible heme oxygenase to chromosome 22q12. *Tohoku J Exp Med*. 1994; 172: 389–392.
  56. Zhang L, Guarente L. Heme binds to a short sequence that serves a regulatory function in diverse proteins. *EMBO J*. 1995; 14: 313–320.
  57. Yi L, Ragsdale SW. Evidence that the heme regulatory motifs in heme oxygenase-2 serve as a thiol/disulfide redox switch regulating heme binding. *J Biol Chem*. 2007; 282: 21056–21067.
  58. McCoubrey WK, Huang TJ, Maines MD. Heme oxygenase-2 is a hemoprotein and binds heme through heme regulatory motifs that are not involved in heme catalysis. *J Biol Chem*. 1997; 272: 12568–12574.
  59. Shibahara S, Han F, Li B, Takeda K. Hypoxia and heme oxygenases: oxygen sensing and regulation of expression. *Antioxid Redox Signal*. 2007; 9: 2209–2226.
  60. Ding Y, Zhang YZ, Furuyama K, Ogawa K, Igarashi K, Shibahara S. Down-regulation of heme oxygenase-2 is associated with the increased expression of heme oxygenase-1 in human cell lines. *FEBS J*. 2006; 273: 5333–5346.
  61. Zhong JL, Raval C, Edwards GP, Tyrrell RM. A role for Bach1 and HO-2 in suppression of basal and UVA-induced HO-1 expression in human keratinocytes. *Free Radic Biol Med*. 2010; 48: 196–206.
  62. Alam J, Cook JL. How many transcription factors does it take to turn on the heme oxygenase-1 gene? *Am J Respir Cell Mol Biol*. 2007; 36: 166–174.
  63. Loboda A, Damulewicz M, Pyza E, Jozkowicz A, Dulak J. Role of Nrf2/HO-1 system in development, oxidative stress response and diseases. An evolutionarily conserved mechanism. *Cell Mol Life Sci*. 2016; 73: 3221–3247.
  64. Sun J, Hoshino H, Takaku K, Nakajima O, Muto A, Suzuki H, Tashiro S, Takahashi S, Shibahara S, Alam J, Taketo MM, Yamamoto M, Igarashi K. Hemoprotein Bach1 regulates enhancer availability of heme oxygenase-1 gene. *EMBO J*. 2002; 21: 5216–5224.
  65. Abate A, Zhao H, Wong RJ, Stevenson DK. The role of Bach1 in the induction of heme oxygenase by tin mesoporphyrin. *Biochem Biophys Res Commun*. 2007; 354: 757–763.
  66. Chen W-J, Chen Y-H, Lai Y-J, Hsu Y-J, Yeh Y-H, Tsai C-S, Lin C-Y. GT-repeat length polymorphism in heme oxygenase-1 promoter determines the effect of cilostazol on vascular smooth muscle cells. *Int J Cardiol*. 2016; 222: 407–415.
  67. Kietzmann T, Samoylenko A, Immenschuh S. Transcriptional regulation of heme oxygenase-1 gene expression by MAP kinases of the JNK and p38 pathways in primary cultures of rat hepatocytes. *J Biol Chem*. 2003; 278: 17927–17936.

68. Feng J, Zhang P, Chen X, He G. PI3K and ERK/Nrf2 pathways are involved in oleanolic acid-induced heme oxygenase-1 expression in rat vascular smooth muscle cells. *J. Cell. Biochem.* 2011; 112: 1524–1531.
69. Schwartz M, Böckmann S, Borchert P, Hinz B. SB202190 inhibits endothelial cell apoptosis via induction of autophagy and heme oxygenase-1. *Oncotarget.* 2018; 9: 23149–23163.
70. Muñoz-Sánchez J, Chánez-Cárdenas ME. A review on hemeoxygenase-2. Focus on cellular protection and oxygen response. *Oxid Med Cell Longev.* 2014; 2014: 604981.
71. Parfenova H, Neff RA, Alonso JS, Shlopov BV, Jamal CN, Sarkisova SA, Leffler CW. Cerebral vascular endothelial heme oxygenase. Expression, localization, and activation by glutamate. *Am J Physiol, Cell Physiol.* 2001; 281: C1954-63.
72. Boehning D, Sedaghat L, Sedlak TW, Snyder SH. Heme oxygenase-2 is activated by calcium-calmodulin. *J Biol Chem.* 2004; 279: 30927–30930.
73. Vukomanovic D, McLaughlin BE, Rahman MN, Szarek WA, Brien JF, Jia Z, Nakatsu K. Selective activation of heme oxygenase-2 by menadione. *Can J Physiol Pharmacol.* 2011; 89: 861–864.
74. Yachie A, Niida Y, Wada T, Igarashi N, Kaneda H, Toma T, Ohta K, Kasahara Y, Koizumi S. Oxidative stress causes enhanced endothelial cell injury in human heme oxygenase-1 deficiency. *J Clin Invest.* 1999; 103: 129–135.
75. Radhakrishnan N, Yadav SP, Sachdeva A, Pruthi PK, Sawhney S, Piplani T, Wada T, Yachie A. Human heme oxygenase-1 deficiency presenting with hemolysis, nephritis, and asplenia. *J Pediatr Hematol Oncol.* 2011; 33: 74–78.
76. Kawashima A, Oda Y, Yachie A, Koizumi S, Nakanishi I. Heme oxygenase-1 deficiency. The first autopsy case. *Human Pathol.* 2002; 33: 125–130.
77. Poss KD, Tonegawa S. Reduced stress defense in heme oxygenase 1-deficient cells. *Proc Natl Acad Sci U S A.* 1997; 94: 10925–10930.
78. Balla G, Jacob HS, Eaton JW, Belcher JD, Vercellotti GM. Hemin: A possible physiological mediator of low density lipoprotein oxidation and endothelial injury. *Arterioscler Thromb.* 1991; 11: 1700–1711.
79. Camejo G, Halberg C, Manschik-Lundin A, Hurt-Camejo E, Rosengren B, Olsson H, Hansson GI, Forsberg GB, Ylhen B. Hemin binding and oxidation of lipoproteins in serum: mechanisms and effect on the interaction of LDL with human macrophages. *J Lipid Res.* 1998; 39: 755–766.
80. Lee PJ, Alam J, Wiegand GW, Choi AM. Overexpression of heme oxygenase-1 in human pulmonary epithelial cells results in cell growth arrest and increased resistance to hyperoxia. *Proc Natl Acad Sci U S A.* 1996; 93: 10393–10398.
81. Zhu H, Wang J, Jiang H, Ma Y, Pan S, Reddy S, Sun X. Bilirubin protects grafts against nonspecific inflammation-induced injury in syngeneic intraportal islet transplantation. *Exp Mol Med.* 2010; 42: 739–748.

82. Zhu HQ, Gao Y, Guo HR, Kong QZ, Ma Y, Wang JZ, Pan SH, Jiang HC, Dai WJ. Pretreatment with bilirubin protects islet against oxidative injury during isolation and purification. *Transplant Proc.* 2011; 43: 1810–1814.
83. Cai C, Teng L, Vu D, He J-Q, Guo Y, Li Q, Tang X-L, Rokosh G, Bhatnagar A, Bolli R. The heme oxygenase-1 inducer (CoPP) protects human cardiac stem cells against apoptosis through activation of the extracellular signal-regulated kinase (ERK)/NRF2 signaling pathway and cytokine release. *J Biol Chem.* 2012; 287: 33720–33732.
84. Peyton KJ, Shebib AR, Azam MA, Liu XM, Tulis DA, Durante W. Bilirubin inhibits neointima formation and vascular smooth muscle cell proliferation and migration. *Front Pharmacol.* 2012; 3: 48.
85. Andria B, Bracco A, Attanasio C, Castaldo S, Cerrito MG, Cozzolino S, Di Napoli D, Giovannoni R, Mancini A, Musumeci A, Mezza E, Nasti M, Scuderi V et al. Biliverdin protects against liver ischemia reperfusion injury in swine. *PLOS ONE.* 2013; 8: e69972.
86. Zhao Y, Zhang L, Qiao Y, Zhou X, Wu G, Wang L, Peng Y, Dong X, Huang H, Si L, Zhang X, Zhang L, Li J et al. Heme oxygenase-1 prevents cardiac dysfunction in streptozotocin-diabetic mice by reducing inflammation, oxidative stress, apoptosis and enhancing autophagy. *PLOS ONE.* 2013; 8: e75927.
87. Bakhautdin B, Das D, Mandal P, Roychowdhury S, Danner J, Bush K, Pollard K, Kaspar JW, Li W, Salomon RG, McMullen MR, Nagy LE. Protective role of HO-1 and carbon monoxide in ethanol-induced hepatocyte cell death and liver injury in mice. *J Hepatol.* 2014; 61: 1029–1037.
88. Hettiarachchi N, Dallas M, Al-Owais M, Griffiths H, Hooper N, Scragg J, Boyle J, Peers C. Heme oxygenase-1 protects against Alzheimer's amyloid- $\beta$ (1-42)-induced toxicity via carbon monoxide production. *Cell Death Dis.* 2014; 5: e1569.
89. Kim HJ, Joe Y, Yu JK, Chen Y, Jeong SO, Mani N, Cho GJ, Pae H-O, Ryter SW, Chung HT. Carbon monoxide protects against hepatic ischemia/reperfusion injury by modulating the miR-34a/SIRT1 pathway. *Biochim Biophys Acta.* 2015; 1852: 1550–1559.
90. Maamoun H, Zachariah M, McVey JH, Green FR, Agouni A. Heme oxygenase (HO)-1 induction prevents endoplasmic reticulum stress-mediated endothelial cell death and impaired angiogenic capacity. *Biochem Pharmacol.* 2017; 127: 46–59.
91. Akamatsu Y, Haga M, Tyagi S, Yamashita K, Graça-Souza AV, Ollinger R, Czismadia E, May GA, Ifedigbo E, Otterbein LE, Bach FH, Soares MP. Heme oxygenase-1-derived carbon monoxide protects hearts from transplant associated ischemia reperfusion injury. *FASEB J.* 2004; 18: 771–772.

92. Nassour I, Kautza B, Rubin M, Escobar D, Luciano J, Loughran P, Gomez H, Scott J, Gallo D, Brumfield J, Otterbein LE, Zuckerbraun BS. Carbon monoxide protects against hemorrhagic shock and resuscitation-induced microcirculatory injury and tissue injury. *Shock*. 2015; 43: 166–171.
93. He M, Nitti M, Piras S, Furfaro AL, Traverso N, Pronzato MA, Mann GE. Heme oxygenase-1-derived bilirubin protects endothelial cells against high glucose-induced damage. *Free Radic Biol Med*. 2015; 89: 91–98.
94. Motterlini R, Foresti R. Heme oxygenase-1 as a target for drug discovery. *Antioxid Redox Signal*. 2014; 20: 1810–1826.
95. Zhang M, Zhang BH, Chen L, An W. Overexpression of heme oxygenase-1 protects smooth muscle cells against oxidative injury and inhibits cell proliferation. *Cell Res*. 2002; 12: 123–132.
96. Hwang SM, Lee YJ, Lee YP, Yoon JJ, Lee SM, Cha JD, Choi KM, Kang DG, Lee HS. Anti-proliferative effect of an aqueous extract of *Prunella vulgaris* in vascular smooth muscle cells. *Evid Based Complement and Alternat Med*. 2013; 2013: 1–10.
97. Qin X, Qiu C, Zhao L. Maslinic acid protects vascular smooth muscle cells from oxidative stress through Akt/Nrf2/HO-1 pathway. *Mol Cell Biochem*. 2014; 390: 61–67.
98. Je J-Y, Lee D-B. *Nelumbo nucifera* leaves protect hydrogen peroxide-induced hepatic damage via antioxidant enzymes and HO-1/Nrf2 activation. *Food Funct*. 2015; 6: 1911–1918.
99. Liu R, Heiss EH, Sider N, Schinkovitz A, Gröblacher B, Guo D, Bucar F, Bauer R, Dirsch VM, Atanasov AG. Identification and characterization of [6]-shogaol from ginger as inhibitor of vascular smooth muscle cell proliferation. *Mol Nutr Food Res*. 2015; 59: 843–852.
100. Li W, Zhi W, Liu F, He Z, Wang X, Niu X. Atractylenolide I restores HO-1 expression and inhibits Ox-LDL-induced VSMCs proliferation, migration and inflammatory responses *in vitro*. *Exp Cell Res*. 2017; 353: 26–34.
101. Lee DH, Choi HC, Lee KY, Kang YJ. Aprotinin inhibits vascular smooth muscle cell inflammation and proliferation via induction of HO-1. *Korean J Physiol Pharmacol*. 2009: 123–129.
102. Migula W and Thomé OW. Prof. Dr. Thomé's Flora von Deutschland, Österreich und der Schweiz, in Wort und Bild, für Schule und Haus. F.E. Köhler. Gera-Untermhaus. 1886.
103. Li H-L. An archaeological and historical account of *Cannabis* in China. *Economic Botany*. 1973; 28: 437–448.
104. Kalant H. Medicinal use of *cannabis*. History and current status. *Pain Res Manag*. 2001; 6: 80–91.
105. Elsohly MA, Slade D. Chemical constituents of marijuana. The complex mixture of natural cannabinoids. *Life Sci*. 2005; 78: 539–548.



106. Appendino G, Chianese G, Tagliatela-Scafati O. Cannabinoids. Occurrence and medicinal chemistry. *Curr Med Chem*. 2011; 18: 1085–1099.
107. O'Shaughnessy WB. On the preparations of the Indian hemp, or Gunjah. *Cannabis Indica* their effects on the animal system in health, and their utility in the treatment of Tetanus and other convulsive diseases. *Prov Med J Retrospect Med Sci*. 1843; 5: 363–369.
108. Elsohly MA, Radwan MM, Gul W, Chandra S, Galal A. Phytochemistry of *Cannabis sativa* L. *Prog Chem Org Nat Prod*. 2017; 103: 1–36.
109. Flores-Sanchez IJ, Verpoorte R. Secondary metabolism in *Cannabis*. *Phytochemistry Reviews*. 2008; 7: 615–639.
110. Sirikantaramas S, Taura F, Tanaka Y, Ishikawa Y, Morimoto S, Shoyama Y. Tetrahydrocannabinolic acid synthase, the enzyme controlling Marijuana psychoactivity, is secreted into the storage cavity of the glandular trichomes. *Plant Cell Physiol*. 2005; 46: 1578–1582.
111. Gertsch J, Pertwee RG, Di Marzo V. Phytocannabinoids beyond the *Cannabis* plant - do they exist? *Br J Pharmacol*. 2010; 160: 523–529.
112. Petrocellis L de, Cascio MG, Di Marzo V. The endocannabinoid system. A general view and latest additions. *Br J Pharmacol*. 2004; 141: 765–774.
113. Croxford JL, Yamamura T. Cannabinoids and the immune system. Potential for the treatment of inflammatory diseases? *J Neuroimmunol*. 2005; 166: 3–18.
114. Bari M, Battista N, Fezza F, Gasperi V, Maccarrone M. New insights into endocannabinoid degradation and its therapeutic potential. *Mini Rev Med Chem*. 2006; 6: 257–268.
115. Lu Y, Anderson HD. Cannabinoid signaling in health and disease. *Can J Physiol Pharmacol*. 2017; 95: 311–327.
116. Toczek M, Malinowska B. Enhanced endocannabinoid tone as a potential target of pharmacotherapy. *Life Sci*. 2018; 204: 20–45.
117. Schwarz R, Ramer R, Hinz B. Targeting the endocannabinoid system as a potential anticancer approach. *Drug Metab Rev*. 2018; 50: 26–53.
118. Devane WA, Dysarz FA, Johnson MR, Melvin LS, Howlett AC. Determination and characterization of a cannabinoid receptor in rat brain. *Mol Pharmacol*. 1988; 34: 605–613.
119. Matsuda LA, Lolait SJ, Brownstein MJ, Young AC, Bonner TI. Structure of a cannabinoid receptor and functional expression of the cloned cDNA. *Nature*. 1990; 346: 561–564.
120. Gérard CM, Mollereau C, Vassart G, Parmentier M. Molecular cloning of a human cannabinoid receptor which is also expressed in testis. *Biochem J*. 1991; 279 (Pt 1): 129–134.
121. Munro S, Thomas KL, Abu-Shaar M. Molecular characterization of a peripheral receptor for cannabinoids. *Nature*. 1993; 365: 61–65.

122. Galiègue S, Mary S, Marchand J, Dussossoy D, Carrière D, Carayon P, Bouaboula M, Shire D, Le Fur G, Casellas P. Expression of central and peripheral cannabinoid receptors in human immune tissues and leukocyte subpopulations. *Eur J Biochem.* 1995; 232: 54–61.
123. Núñez E, Benito C, Pazos MR, Barbachano A, Fajardo O, González S, Tolón RM, Romero J. Cannabinoid CB<sub>2</sub> receptors are expressed by perivascular microglial cells in the human brain. An immunohistochemical study. *Synapse.* 2004; 53: 208–213.
124. van Sickle MD, Duncan M, Kingsley PJ, Mouihate A, Urbani P, Mackie K, Stella N, Makriyannis A, Piomelli D, Davison JS, Marnett LJ, Di Marzo V, Pittman QJ et al. Identification and functional characterization of brainstem cannabinoid CB<sub>2</sub> receptors. *Science.* 2005; 310: 329–332.
125. Beltramo M, Bernardini N, Bertorelli R, Campanella M, Nicolussi E, Fredduzzi S, Reggiani A. CB<sub>2</sub> receptor-mediated antihyperalgesia. Possible direct involvement of neural mechanisms. *Eur J Neurosci.* 2006; 23: 1530–1538.
126. Onaivi ES, Ishiguro H, Gong J-P, Patel S, Perchuk A, Meozzi PA, Myers L, Mora Z, Tagliaferro P, Gardner E, Brusco A, Akinshola BE, Liu Q-R et al. Discovery of the presence and functional expression of cannabinoid CB<sub>2</sub> receptors in brain. *Ann N Y Acad Sci.* 2006; 1074: 514–536.
127. Howlett AC, Qualy JM, Khachatrian LL. Involvement of G<sub>i</sub> in the inhibition of adenylate cyclase by cannabimimetic drugs. *Mol Pharmacol.* 1986; 29: 307–313.
128. Bayewitch M, Avidor-Reiss T, Levy R, Barg J, Mechoulam R, Vogel Z. The peripheral cannabinoid receptor. Adenylate cyclase inhibition and G protein coupling. *FEBS Letters.* 1995; 375: 143–147.
129. Slipetz DM, O'Neill GP, Favreau L, Dufresne C, Gallant M, Gareau Y, Guay D, Labelle M, Metters KM. Activation of the human peripheral cannabinoid receptor results in inhibition of adenylyl cyclase. *Mol Pharmacol.* 1995; 48: 352–361.
130. Bouaboula M, Poinot-Chazel C, Bourrié B, Canat X, Calandra B, Rinaldi-Carmona M, Le Fur G, Casellas P. Activation of mitogen-activated protein kinases by stimulation of the central cannabinoid receptor CB<sub>1</sub>. *Biochem. J.* 1995; 312 (Pt 2): 637–641.
131. Bouaboula M, Bianchini L, McKenzie FR, Pouyssegur J, Casellas P. Cannabinoid receptor CB<sub>1</sub> activates the Na<sup>+</sup>/H<sup>+</sup> exchanger NHE-1 isoform via G<sub>i</sub>-mediated mitogen activated protein kinase signaling transduction pathways. *FEBS Letters.* 1999; 449: 61–65.
132. Rueda D, Galve-Roperh I, Haro A, Guzmán M. The CB<sub>1</sub> cannabinoid receptor is coupled to the activation of c-Jun N-terminal kinase. *Mol Pharmacol.* 2000; 58: 814–820.
133. Kobayashi Y, Arai S, Waku K, Sugiura T. Activation by 2-arachidonoylglycerol, an endogenous cannabinoid receptor ligand, of p42/44 mitogen-activated protein kinase in HL-60 cells. *J Biochem.* 2001; 129: 665–669.

134. Derkinderen P, Ledent C, Parmentier M, Girault JA. Cannabinoids activate p38 mitogen-activated protein kinases through CB<sub>1</sub> receptors in hippocampus. *J Neurochem.* 2001; 77: 957–960.
135. Galve-Roperh I, Rueda D, Gómez del Pulgar T, Velasco G, Guzmán M. Mechanism of extracellular signal-regulated kinase activation by the CB<sub>1</sub> cannabinoid receptor. *Mol Pharmacol.* 2002; 62: 1385–1392.
136. Davis MI, Ronesi J, Lovinger DM. A predominant role for inhibition of the adenylate cyclase/protein kinase A pathway in ERK activation by cannabinoid receptor 1 in N1E-115 neuroblastoma cells. *J Biol Chem.* 2003; 278: 48973–48980.
137. Mackie K, Lai Y, Westenbroek R, Mitchell R. Cannabinoids activate an inwardly rectifying potassium conductance and inhibit Q-type calcium currents in AtT20 cells transfected with rat brain cannabinoid receptor. *J Neurosci.* 1995; 15: 6552–6561.
138. Twitchell W, Brown S, Mackie K. Cannabinoids inhibit N- and P/Q-type calcium channels in cultured rat hippocampal neurons. *J Neurophysiol.* 1997; 78: 43–50.
139. Coutts AA, Pertwee RG. Inhibition by cannabinoid receptor agonists of acetylcholine release from the guinea-pig myenteric plexus. *Br J Pharmacol.* 1997; 121: 1557–1566.
140. Gerdeman G, Lovinger DM. CB<sub>1</sub> cannabinoid receptor inhibits synaptic release of glutamate in rat dorsolateral striatum. *J Neurophysiol.* 2001; 85: 468–471.
141. Vásquez C, Navarro-Polanco RA, Huerta M, Trujillo X, Andrade F, Trujillo-Hernández B, Hernández L. Effects of cannabinoids on endogenous K<sup>+</sup> and Ca<sup>2+</sup> currents in HEK293 cells. *Can J Physiol Pharmacol.* 2003; 81: 436–442.
142. Boychuk CR, Zsombok A, Tasker JG, Smith BN. Rapid Glucocorticoid-induced activation of TRP and CB<sub>1</sub> receptors causes biphasic modulation of glutamate release in gastric-related hypothalamic preautonomic neurons. *Front Neurosci.* 2013; 7: 3.
143. Dazzi L, Talani G, Biggio F, Utzeri C, Lallai V, Licheri V, Lutz S, Mostallino MC, Secci PP, Biggio G, Sanna E. Involvement of the cannabinoid CB<sub>1</sub> receptor in modulation of dopamine output in the prefrontal cortex associated with food restriction in rats. *PLOS ONE.* 2014; 9: e92224.
144. Polissidis A, Chouliara O, Galanopoulos A, Naxakis G, Papahatjis D, Papadopoulou-Daifoti Z, Antoniou K. Cannabinoids negatively modulate striatal glutamate and dopamine release and behavioural output of acute D-amphetamine. *Behav Brain Res.* 2014; 270: 261–269.
145. Felder CC, Briley EM, Axelrod J, Simpson JT, Mackie K, Devane WA. Anandamide, an endogenous cannabimimetic eicosanoid, binds to the cloned human cannabinoid receptor and stimulates receptor-mediated signal transduction. *Proc Natl Acad Sci U S A.* 1993; 90: 7656–7660.

146. Felder CC, Joyce KE, Briley EM, Mansouri J, Mackie K, Blond O, Lai Y, Ma AL, Mitchell RL. Comparison of the pharmacology and signal transduction of the human cannabinoid CB<sub>1</sub> and CB<sub>2</sub> receptors. *Mol Pharmacol*. 1995; 48: 443–450.
147. Mu J, Zhuang SY, Kirby MT, Hampson RE, Deadwyler SA. Cannabinoid receptors differentially modulate potassium A and D currents in hippocampal neurons in culture. *J Pharmacol Exp Ther*. 1999; 291: 893–902.
148. Devane WA, Hanus L, Breuer A, Pertwee RG, Stevenson LA, Griffin G, Gibson D, Mandelbaum A, Etinger A, Mechoulam R. Isolation and structure of a brain constituent that binds to the cannabinoid receptor. *Science*. 1992; 258: 1946–1949.
149. Mackie K, Devane WA, Hille B. Anandamide, an endogenous cannabinoid, inhibits calcium currents as a partial agonist in N18 neuroblastoma cells. *Mol Pharmacol*. 1993; 44: 498–503.
150. Gonsiorek W, Lunn C, Fan X, Narula S, Lundell D, Hipkin RW. Endocannabinoid 2-arachidonoyl glycerol is a full agonist through human type 2 cannabinoid receptor. Antagonism by anandamide. *Mol Pharmacol*. 2000; 57: 1045–1050.
151. Sugiura T, Kondo S, Kishimoto S, Miyashita T, Nakane S, Kodaka T, Suhara Y, Takayama H, Waku K. Evidence that 2-arachidonoylglycerol but not *N*-palmitoylethanolamine or anandamide is the physiological ligand for the cannabinoid CB<sub>2</sub> receptor. Comparison of the agonistic activities of various cannabinoid receptor ligands in HL-60 cells. *J Biol Chem*. 2000; 275: 605–612.
152. Mechoulam R, Ben-Shabat S, Hanus L, Ligumsky M, Kaminski NE, Schatz AR, Gopher A, Almog S, Martin BR, Compton DR. Identification of an endogenous 2-monoglyceride, present in canine gut, that binds to cannabinoid receptors. *Biochem Pharmacol*. 1995; 50: 83–90.
153. Sugiura T, Kodaka T, Nakane S, Miyashita T, Kondo S, Suhara Y, Takayama H, Waku K, Seki C, Baba N, Ishima Y. Evidence that the cannabinoid CB<sub>1</sub> receptor is a 2-arachidonoylglycerol receptor. Structure-activity relationship of 2-arachidonoylglycerol, ether-linked analogues, and related compounds. *J Biol Chem*. 1999; 274: 2794–2801.
154. Hanus L, Gopher A, Almog S, Mechoulam R. Two new unsaturated fatty acid ethanolamides in brain that bind to the cannabinoid receptor. *J Med Chem*. 1993; 36: 3032–3034.
155. Bisogno T, Melck D, Bobrov M, Gretskaya NM, Bezuglov VV, Petrocellis L de, Di Marzo V. *N*-acyl-dopamines. Novel synthetic CB<sub>1</sub> cannabinoid-receptor ligands and inhibitors of anandamide inactivation with cannabimimetic activity *in vitro* and *in vivo*. *Biochem. J*. 2000; 351 Pt 3: 817–824.

156. Huang SM, Bisogno T, Trevisani M, Al-Hayani A, Petrocellis L de, Fezza F, Tognetto M, Petros TJ, Krey JF, Chu CJ, Miller JD, Davies SN, Geppetti P et al. An endogenous capsaicin-like substance with high potency at recombinant and native vanilloid VR1 receptors. *Proc Natl Acad Sci U S A*. 2002; 99: 8400–8405.
157. Porter AC, Sauer J-M, Knierman MD, Becker GW, Borna MJ, Bao J, Nomikos GG, Carter P, Bymaster FP, Leese AB, Felder CC. Characterization of a novel endocannabinoid, virodhamine, with antagonist activity at the CB<sub>1</sub> receptor. *J Pharmacol Exp Ther*. 2002; 301: 1020–1024.
158. Hanus L, Abu-Lafi S, Fride E, Breuer A, Vogel Z, Shalev DE, Kustanovich I, Mechoulam R. 2-arachidonyl glyceryl ether, an endogenous agonist of the cannabinoid CB<sub>1</sub> receptor. *Proc Natl Acad Sci U S A*. 2001; 98: 3662–3665.
159. Kleberg K, Hassing HA, Hansen HS. Classical endocannabinoid-like compounds and their regulation by nutrients. *Biofactors*. 2014; 40: 363–372.
160. Ben-Shabat S, Fride E, Sheskin T, Tamiri T, Rhee MH, Vogel Z, Bisogno T, Petrocellis L de, Di Marzo V, Mechoulam R. An entourage effect. Inactive endogenous fatty acid glycerol esters enhance 2-arachidonoyl-glycerol cannabinoid activity. *Eur J Pharmacol*. 1998; 353: 23–31.
161. Abadji V, Lin S, Taha G, Griffin G, Stevenson LA, Pertwee RG, Makriyannis A. (R)-Methanandamide. A chiral novel anandamide possessing higher potency and metabolic stability. *J Med Chem*. 1994; 37: 1889–1893.
162. Huffman JW, Liddle J, Yu S, Aung MM, Abood ME, Wiley JL, Martin BR. 3-(1',1'-Dimethylbutyl)-1-deoxy-delta<sup>8</sup>-THC and related compounds. Synthesis of selective ligands for the CB<sub>2</sub> receptor. *Bioorg Med Chem*. 1999; 7: 2905–2914.
163. Huffman JW, Mabon R, Wu MJ, Lu J, Hart R, Hurst DP, Reggio PH, Wiley JL, Martin BR. 3-Indolyl-1-naphthylmethanes. New cannabimimetic indoles provide evidence for aromatic stacking interactions with the CB<sub>(1)</sub> cannabinoid receptor. *Bioorg Med Chem*. 2003; 11: 539–549.
164. Huffman JW, Padgett LW, Isherwood ML, Wiley JL, Martin BR. 1-Alkyl-2-aryl-4-(1-naphthoyl)pyrroles. New high affinity ligands for the cannabinoid CB<sub>1</sub> and CB<sub>2</sub> receptors. *Bioorg Med Chem Lett*. 2006; 16: 5432–5435.
165. Showalter VM, Compton DR, Martin BR, Abood ME. Evaluation of binding in a transfected cell line expressing a peripheral cannabinoid receptor (CB<sub>2</sub>). Identification of cannabinoid receptor subtype selective ligands. *J Pharmacol Exp Ther*. 1996; 278: 989–999.
166. Little PJ, Compton DR, Mechoulam R, Martin BR. Stereochemical effects of 11-OH-delta<sup>8</sup>-THC-dimethylheptyl in mice and dogs. *Pharmacol Biochem Behav*. 1989; 32: 661–666.
167. Hillard CJ, Manna S, Greenberg MJ, DiCamelli R, Ross RA, Stevenson LA, Murphy V, Pertwee RG, Campbell WB. Synthesis and characterization of potent and selective agonists of the neuronal cannabinoid receptor (CB<sub>1</sub>). *J Pharmacol Exp Ther*. 1999; 289: 1427–1433.

168. Wiley JL, Marusich JA, Huffman JW, Balster RL, Thomas BF. Hijacking of basic research. The case of synthetic cannabinoids. *Methods Rep RTI Press*. 2011; 2011: pii: 17971.
169. Lapoint J, James LP, Moran CL, Nelson LS, Hoffman RS, Moran JH. Severe toxicity following synthetic cannabinoid ingestion. *Clin Toxicol (Phila)*. 2011; 49: 760–764.
170. Simmons J, Cookman L, Kang C, Skinner C. Three cases of "spice" exposure. *Clin Toxicol (Phila)*. 2011; 49: 431–433.
171. Tofighi B, Lee JD. Internet highs--seizures after consumption of synthetic cannabinoids purchased online. *J Addict Med*. 2012; 6: 240–241.
172. Rinaldi-Carmona M, Barth F, Héaulme M, Alonso R, Shire D, Congy C, Soubrié P, Brelière JC, Le Fur G. Biochemical and pharmacological characterisation of SR141716A, the first potent and selective brain cannabinoid receptor antagonist. *Life Sci*. 1995; 56: 1941–1947.
173. Lan R, Liu Q, Fan P, Lin S, Fernando SR, McCallion D, Pertwee R, Makriyannis A. Structure-activity relationships of pyrazole derivatives as cannabinoid receptor antagonists. *J Med Chem*. 1999; 42: 769–776.
174. Pertwee R, Griffin G, Fernando S, Li X, Hill A, Makriyannis A. AM630, a competitive cannabinoid receptor antagonist. *Life Sci*. 1995; 56: 1949–1955.
175. Pertwee RG. The therapeutic potential of drugs that target cannabinoid receptors or modulate the tissue levels or actions of endocannabinoids. *AAPS J*. 2005; 7: E625-54.
176. Pertwee RG. Receptors and channels targeted by synthetic cannabinoid receptor agonists and antagonists. *Curr Med Chem*. 2010; 17: 1360–1381.
177. Pertwee RG. Targeting the endocannabinoid system with cannabinoid receptor agonists. Pharmacological strategies and therapeutic possibilities. *Philos Trans R Soc Lond, B, Biol Sci*. 2012; 367: 3353–3363.
178. Zygmunt PM, Petersson J, Andersson DA, Chuang H, Sörgård M, Di Marzo V, Julius D, Högestätt ED. Vanilloid receptors on sensory nerves mediate the vasodilator action of anandamide. *Nature*. 1999; 400: 452–457.
179. Caterina MJ, Schumacher MA, Tominaga M, Rosen TA, Levine JD, Julius D. The capsaicin receptor. A heat-activated ion channel in the pain pathway. *Nature*. 1997; 389: 816–824.
180. Zsombok A. Vanilloid receptors--do they have a role in whole body metabolism? Evidence from TRPV1. *J Diabetes Complicat*. 2013; 27: 287–292.
181. Kaneko Y, Szallasi A. Transient receptor potential (TRP) channels. A clinical perspective. *Br J Pharmacol*. 2014; 171: 2474–2507.
182. Costa B, Giagnoni G, Franke C, Trovato AE, Colleoni M. Vanilloid TRPV1 receptor mediates the antihyperalgesic effect of the nonpsychoactive cannabinoid, cannabidiol, in a rat model of acute inflammation. *Br J Pharmacol*. 2004; 143: 247–250.

183. Sawzdargo M, Nguyen T, Lee DK, Lynch KR, Cheng R, Heng HH, George SR, O'Dowd BF. Identification and cloning of three novel human G protein-coupled receptor genes GPR52, PsiGPR53 and GPR55. GPR55 is extensively expressed in human brain. *Brain Res Mol Brain Res*. 1999; 64: 193–198.
184. Ryberg E, Larsson N, Sjögren S, Hjorth S, Hermansson N-O, Leonova J, Elebring T, Nilsson K, Drmota T, Greasley PJ. The orphan receptor GPR55 is a novel cannabinoid receptor. *Br J Pharmacol*. 2007; 152: 1092–1101.
185. O'Sullivan SE. An update on PPAR activation by cannabinoids. *Br J Pharmacol*. 2016; 173: 1899–1910.
186. Soderstrom K, Soliman E, van Dross R. Cannabinoids modulate neuronal activity and cancer by CB<sub>1</sub> and CB<sub>2</sub> receptor-independent mechanisms. *Front Pharmacol*. 2017; 8: 720.
187. Adams R, Hunt M, Clark JH. Structure of cannabidiol, a product isolated from the Marihuana extract of Minnesota wild hemp. I. *J. Am. Chem. Soc.* 1940; 62: 196–200.
188. Mechoulam R, Shvo Y. Hashish. I. The structure of cannabidiol. *Tetrahedron*. 1963; 19: 2073–2078.
189. Gaoni Y, Mechoulam R. Isolation, structure, and partial synthesis of an active constituent of hashish. *J. Am. Chem. Soc.* 1964; 86: 1646–1647.
190. Zimmerberg B, Glick SD, Jarvik ME. Impairment of recent memory by marihuana and THC in rhesus monkeys. *Nature*. 1971; 233: 343–345.
191. Ferraro DP, Grilly DM, Lynch WC. Effects of marihuana extract on the operant behavior of chimpanzees. *Psychopharmacologia*. 1971; 22: 333–351.
192. Karniol IG, Shirakawa I, Takahashi RN, Knobel E, Musty RE. Effects of delta<sup>9</sup>-tetrahydrocannabinol and cannabinol in man. *Pharmacology*. 1975; 13: 502–512.
193. Dornbush RL, Kokkevi A. Acute effects of *Cannabis* on cognitive, perceptual, and motor performance in chronic hashish users. *Ann N Y Acad Sci*. 1976; 282: 313–322.
194. Abood ME, Martin BR. Neurobiology of marijuana abuse. *Trends Pharmacol Sci*. 1992; 13: 201–206.
195. Bisogno T, Hanus L, Petrocellis L de, Tchilibon S, Ponde DE, Brandi I, Moriello AS, Davis JB, Mechoulam R, Di Marzo V. Molecular targets for cannabidiol and its synthetic analogues. Effect on vanilloid VR1 receptors and on the cellular uptake and enzymatic hydrolysis of anandamide. *Br J Pharmacol*. 2001; 134: 845–852.
196. Qin N, Neeper MP, Liu Y, Hutchinson TL, Lubin ML, Flores CM. TRPV2 is activated by cannabidiol and mediates CGRP release in cultured rat dorsal root ganglion neurons. *J Neurosci*. 2008; 28: 6231–6238.
197. Pertwee RG. Emerging strategies for exploiting cannabinoid receptor agonists as medicines. *Br J Pharmacol*. 2009; 156: 397–411.

198. Patil KR, Goyal SN, Sharma C, Patil CR, Ojha S. Phytocannabinoids for cancer therapeutics: Recent updates and future prospects. *Curr Med Chem.* 2015; 22: 3472–3501.
199. Goyal H, Awad HH, Ghali JK. Role of *Cannabis* in cardiovascular disorders. *J Thorac Dis.* 2017; 9: 2079–2092.
200. Hill KP, Palastro MD, Johnson B, Ditre JW. *Cannabis* and pain: a clinical review. *Cannabis Cannabinoid Res.* 2017; 2: 96–104.
201. Lochte BC, Beletsky A, Samuel NK, Grant I. The use of *Cannabis* for headache disorders. *Cannabis Cannabinoid Res.* 2017; 2: 61–71.
202. Stampanoni Bassi M, Sancesario A, Morace R, Centonze D, Iezzi E. Cannabinoids in Parkinson's disease. *Cannabis Cannabinoid Res.* 2017; 2: 21–29.
203. Müller-Vahl KR. Treatment of Tourette syndrome with cannabinoids. *Behav Neurol.* 2013; 27: 119–124.
204. Pichler E-M, Kawohl W, Seifritz E, Roser P. Pure delta-<sup>9</sup>-tetrahydrocannabinol and its combination with cannabidiol in treatment-resistant Tourette syndrome. A case report. *Int J Psychiatry Med.* 2018: 91217418791455.
205. Iffland K, Grotenhermen F. An update on safety and side effects of cannabidiol: a review of clinical data and relevant animal studies. *Cannabis Cannabinoid Res.* 2017; 2: 139–154.
206. Meuth SG, Vila C, Dechant KL. Effect of Sativex on spasticity-associated symptoms in patients with multiple sclerosis. *Expert Rev Neurother.* 2015; 15: 909–918.
207. Marková J, Essner U, Akmaz B, Marinelli M, Trompke C, Lentschat A, Vila Silván C. Sativex® as Add-on therapy Vs. further optimized first-line ANTispastics (SAVANT) in resistant multiple sclerosis spasticity. A double-blind, placebo-controlled randomised clinical trial. *Int J Neurosci.* 2018: 1–28.
208. Turri M, Teatini F, Donato F, Zanette G, Tugnoli V, Deotto L, Bonetti B, Squintani G. Pain modulation after oromucosal cannabinoid spray (SATIVEX®) in patients with Multiple Sclerosis. A study with quantitative sensory testing and laser-evoked potentials. *Medicines (Basel).* 2018; 5: pii: E59.
209. Costa B, Trovato AE, Comelli F, Giagnoni G, Colleoni M. The non-psychoactive *Cannabis* constituent cannabidiol is an orally effective therapeutic agent in rat chronic inflammatory and neuropathic pain. *Eur J Pharmacol.* 2007; 556: 75–83.
210. Consroe P, Wolkin A. Cannabidiol-antiepileptic drug comparisons and interactions in experimentally induced seizures in rats. *J Pharmacol Exp Ther.* 1977; 201: 26–32.
211. Cunha JM, Carlini EA, Pereira AE, Ramos OL, Pimentel C, Gagliardi R, Sanvito WL, Lander N, Mechoulam R. Chronic administration of cannabidiol to healthy volunteers and epileptic patients. *Pharmacology.* 1980; 21: 175–185.



212. Consroe P, Laguna J, Allender J, Snider S, Stern L, Sandyk R, Kennedy K, Schram K. Controlled clinical trial of cannabidiol in Huntington's disease. *Pharmacol Biochem Behav.* 1991; 40: 701–708.
213. Jones NA, Glyn SE, Akiyama S, Hill TDM, Hill AJ, Weston SE, Burnett MDA, Yamasaki Y, Stephens GJ, Whalley BJ, Williams CM. Cannabidiol exerts anti-convulsant effects in animal models of temporal lobe and partial seizures. *Seizure.* 2012; 21: 344–352.
214. O'Connell BK, Gloss D, Devinsky O. Cannabinoids in treatment-resistant epilepsy. A review. *Epilepsy Behav.* 2017; 70: 341–348.
215. Devinsky O, Verducci C, Thiele EA, Laux LC, Patel AD, Filloux F, Szaflarski JP, Wilfong A, Clark GD, Park YD, Seltzer LE, Bebin EM, Flamini R et al. Open-label use of highly purified CBD (Epidiolex®) in patients with CDKL5 deficiency disorder and Aicardi, Dup15q, and Doose syndromes. *Epilepsy Behav.* 2018: 131–137.
216. Guimarães FS, Aguiar JC de, Mechoulam R, Breuer A. Anxiolytic effect of cannabidiol derivatives in the elevated plus-maze. *Gen Pharmacol.* 1994; 25: 161–164.
217. Moreira FA, Aguiar DC, Guimarães FS. Anxiolytic-like effect of cannabidiol in the rat Vogel conflict test. *Prog Neuropsychopharmacol Biol Psychiatry.* 2006; 30: 1466–1471.
218. Campos AC, Ortega Z, Palazuelos J, Fogaça MV, Aguiar DC, Díaz-Alonso J, Ortega-Gutiérrez S, Vázquez-Villa H, Moreira FA, Guzmán M, Galve-Roperh I, Guimarães FS. The anxiolytic effect of cannabidiol on chronically stressed mice depends on hippocampal neurogenesis. Involvement of the endocannabinoid system. *Int J Neuropsychopharmacol.* 2013; 16: 1407–1419.
219. Mello Schier AR de, Oliveira Ribeiro NP de, Coutinho DS, Machado S, Arias-Carrión O, Crippa JA, Zuardi AW, Nardi AE, Silva AC. Antidepressant-like and anxiolytic-like effects of cannabidiol. A chemical compound of *Cannabis sativa*. *CNS Neurol Disord Drug Targets.* 2014; 13: 953–960.
220. Braidă D, Pegorini S, Arcidiacono MV, Consalez GG, Croci L, Sala M. Post-ischemic treatment with cannabidiol prevents electroencephalographic flattening, hyperlocomotion and neuronal injury in gerbils. *Neurosci Lett.* 2003; 346: 61–64.
221. Hayakawa K, Mishima K, Abe K, Hasebe N, Takamatsu F, Yasuda H, Ikeda T, Inui K, Egashira N, Iwasaki K, Fujiwara M. Cannabidiol prevents infarction via the non-CB<sub>1</sub> cannabinoid receptor mechanism. *Neuroreport.* 2004; 15: 2381–2385.
222. Pazos MR, Mohammed N, Lafuente H, Santos M, Martínez-Pinilla E, Moreno E, Valdizan E, Romero J, Pazos A, Franco R, Hillard CJ, Alvarez FJ, Martínez-Orgado J. Mechanisms of cannabidiol neuroprotection in hypoxic-ischemic newborn pigs. Role of 5HT<sub>(1A)</sub> and CB<sub>2</sub> receptors. *Neuropharmacology.* 2013; 71: 282–291.

223. Perez M, Benitez SU, Cartarozzi LP, Del Bel E, Guimarães FS, Oliveira ALR. Neuroprotection and reduction of glial reaction by cannabidiol treatment after sciatic nerve transection in neonatal rats. *Eur J Neurosci.* 2013; 38: 3424–3434.
224. Gomes FV, Resstel LBM, Guimarães FS. The anxiolytic-like effects of cannabidiol injected into the bed nucleus of the stria terminalis are mediated by 5-HT<sub>1A</sub> receptors. *Psychopharmacology (Berl)*. 2011; 213: 465–473.
225. Valdeolivas S, Satta V, Pertwee RG, Fernández-Ruiz J, Sagredo O. Sativex-like combination of phytocannabinoids is neuroprotective in malonate-lesioned rats, an inflammatory model of Huntington's disease. Role of CB<sub>1</sub> and CB<sub>2</sub> receptors. *ACS Chem Neurosci.* 2012; 3: 400–406.
226. López-Sendón Moreno JL, García Caldentey J, Trigo Cubillo P, Ruiz Romero C, García Ribas G, Alonso Arias MAA, García de Yébenes MJ, Tolón RM, Galve-Roperh I, Sagredo O, Valdeolivas S, Resel E, Ortega-Gutierrez S et al. A double-blind, randomized, cross-over, placebo-controlled, pilot trial with Sativex in Huntington's disease. *J Neurol.* 2016; 263: 1390–1400.
227. Valdeolivas S, Sagredo O, Delgado M, Pozo MA, Fernández-Ruiz J. Effects of a Sativex-like combination of phytocannabinoids on disease progression in R6/2 mice, an experimental model of Huntington's disease. *Int J Mol Sci.* 2017; 18: pii: E684.
228. Schmuhl E, Ramer R, Salamon A, Peters K, Hinz B. Increase of mesenchymal stem cell migration by cannabidiol via activation of p42/44 MAPK. *Biochem Pharmacol.* 2014; 87: 489–501.
229. Ruiz-Valdepeñas L, Martínez-Orgado JA, Benito C, Millán A, Tolón RM, Romero J. Cannabidiol reduces lipopolysaccharide-induced vascular changes and inflammation in the mouse brain: an intravital microscopy study. *J Neuroinflammation.* 2011; 8: 5.
230. Mukhopadhyay P, Rajesh M, Horváth B, Bátakai S, Park O, Tanchian G, Gao RY, Patel V, Wink DA, Liaudet L, Haskó G, Mechoulam R, Pacher P. Cannabidiol protects against hepatic ischemia/reperfusion injury by attenuating inflammatory signaling and response, oxidative/nitrative stress, and cell death. *Free Radic Biol Med.* 2011; 50: 1368–1381.
231. Yang L, Rozenfeld R, Wu D, Devi LA, Zhang Z, Cederbaum A. Cannabidiol protects liver from binge alcohol-induced steatosis by mechanisms including inhibition of oxidative stress and increase in autophagy. *Free Radic Biol Med.* 2014; 68: 260–267.
232. Mecha M, Torrao AS, Mestre L, Carrillo-Salinas FJ, Mechoulam R, Guaza C. Cannabidiol protects oligodendrocyte progenitor cells from inflammation-induced apoptosis by attenuating endoplasmic reticulum stress. *Cell Death Dis.* 2012; 3: e331.
233. Ramer R, Hinz B. Inhibition of cancer cell invasion by cannabinoids via increased expression of tissue inhibitor of matrix metalloproteinases-1. *J Natl Cancer Inst.* 2008; 100: 59–69.

234. Ramer R, Merkord J, Rohde H, Hinz B. Cannabidiol inhibits cancer cell invasion via upregulation of tissue inhibitor of matrix metalloproteinases-1. *Biochem Pharmacol.* 2010; 79: 955–966.
235. Ramer R, Rohde A, Merkord J, Rohde H, Hinz B. Decrease of plasminogen activator inhibitor-1 may contribute to the anti-invasive action of cannabidiol on human lung cancer cells. *Pharm Res.* 2010; 27: 2162–2174.
236. Ramer R, Bublitz K, Freimuth N, Merkord J, Rohde H, Haustein M, Borchert P, Schmuhl E, Linnebacher M, Hinz B. Cannabidiol inhibits lung cancer cell invasion and metastasis via intercellular adhesion molecule-1. *FASEB J.* 2012; 26: 1535–1548.
237. Ramer R, Fischer S, Haustein M, Manda K, Hinz B. Cannabinoids inhibit angiogenic capacities of endothelial cells via release of tissue inhibitor of matrix metalloproteinases-1 from lung cancer cells. *Biochem Pharmacol.* 2014; 91: 202–216.
238. Ramer R, Heinemann K, Merkord J, Rohde H, Salamon A, Linnebacher M, Hinz B. COX-2 and PPAR- $\gamma$  confer cannabidiol-induced apoptosis of human lung cancer cells. *Mol Cancer Ther.* 2013; 12: 69–82.
239. Haustein M, Ramer R, Linnebacher M, Manda K, Hinz B. Cannabinoids increase lung cancer cell lysis by lymphokine-activated killer cells via upregulation of ICAM-1. *Biochem Pharmacol.* 2014; 92: 312–325.
240. Hinz B, Ramer R. Anti-tumour actions of cannabinoids. *Br J Pharmacol.* 2018: [Epub ahead of print]. doi: 10.1111/bph.14426.
241. Stanley CP, Hind WH, O'Sullivan SE. Is the cardiovascular system a therapeutic target for cannabidiol? *Br J Clin Pharmacol.* 2013; 75: 313–322.
242. Rajesh M, Mukhopadhyay P, Bátkaí S, Haskó G, Liaudet L, Drel VR, Obrosova IG, Pacher P. Cannabidiol attenuates high glucose-induced endothelial cell inflammatory response and barrier disruption. *Am J Physiol Heart Circ Physiol.* 2007; 293: H610-9.
243. Durst R, Danenberg H, Gallily R, Mechoulam R, Meir K, Grad E, Beerli R, Pugatsch T, Tarsish E, Lotan C. Cannabidiol, a nonpsychoactive *Cannabis* constituent, protects against myocardial ischemic reperfusion injury. *Am J Physiol Heart Circ Physiol.* 2007; 293: H3602-H3607.
244. Sardana MK, Kappas A. Dual control mechanism for heme oxygenase: tin(IV)-protoporphyrin potently inhibits enzyme activity while markedly increasing content of enzyme protein in liver. *Proc Natl Acad Sci U S A.* 1987; 84: 2464–2468.
245. Xia Z-W, Zhong W-W, Xu L-Q, Sun J-L, Shen Q-X, Wang J-G, Shao J, Li Y-Z, Yu S-C. Heme oxygenase-1-mediated CD4<sup>+</sup>CD25<sup>high</sup> regulatory T cells suppress allergic airway inflammation. *J Immunol.* 2006; 177: 5936–5945.
246. Chang T, Wu L, Wang R. Inhibition of vascular smooth muscle cell proliferation by chronic hemin treatment. *Am J Physiol Heart Circ Physiol.* 2008; 295: H999-H1007.

247. Johns DG, Behm DJ, Walker DJ, Ao Z, Shapland EM, Daniels DA, Riddick M, Dowell S, Staton PC, Green P, Shabon U, Bao W, Aiyar N et al. The novel endocannabinoid receptor GPR55 is activated by atypical cannabinoids but does not mediate their vasodilator effects. *Br J Pharmacol*. 2007; 152: 825–831.
248. Agrawal N, Dasaradhi, P. V. N., Mohmmmed A, Malhotra P, Bhatnagar RK, Mukherjee SK. RNA interference: Biology, mechanism, and applications. *Microbiol Mol Biol Rev*. 2003; 67: 657–685.
249. Mullis K, Faloona F, Scharf S, Saiki R, Horn G, Erlich H. Specific enzymatic amplification of DNA *in vitro*. The polymerase chain reaction. *Cold Spring Harb Symp Quant Biol*. 1986; 51 Pt 1: 263–273.
250. Mullis KB, Faloona FA. Specific synthesis of DNA *in vitro* via a polymerase-catalyzed chain reaction. *Meth Enzymol*. 1987; 155: 335–350.
251. Spiegelman S, Watson KF, Kacian DL. Synthesis of DNA complements of natural RNAs. A general approach. *Proc Natl Acad Sci U S A*. 1971; 68: 2843–2845.
252. Shaffer AL, Wojnar W, Nelson W. Amplification, detection, and automated sequencing of gibbon interleukin-2 mRNA by *Thermus aquaticus* DNA polymerase reverse transcription and polymerase chain reaction. *Anal Biochem*. 1990; 190: 292–296.
253. Beisker W, Hittelman WN. Measurement of the kinetics of DNA repair synthesis after UV irradiation using immunochemical staining of incorporated 5-bromo-2'-deoxyuridine and flow cytometry. *Exp Cell Res*. 1988; 174: 156–167.
254. Smith PK, Krohn RI, Hermanson GT, Mallia AK, Gartner FH, Provenzano MD, Fujimoto EK, Goeke NM, Olson BJ, Klenk DC. Measurement of protein using bicinchoninic acid. *Anal Biochem*. 1985; 150: 76–85.
255. Laemmli UK. Cleavage of structural proteins during the assembly of the head of bacteriophage T4. *Nature*. 1970; 227: 680–685.
256. Reynolds JA, Tanford C. Binding of dodecyl sulfate to proteins at high binding ratios. Possible implications for the state of proteins in biological membranes. *Proc Natl Acad Sci U S A*. 1970; 66: 1002–1007.
257. Orr AW, Hastings NE, Blackman BR, Wamhoff BR. Complex regulation and function of the inflammatory smooth muscle cell phenotype in atherosclerosis. *J Vasc Res*. 2010; 47: 168–180.
258. Lusis AJ. Atherosclerosis. *Nature*. 2000; 407: 233–241.
259. Hao H, Gabbiani G, Bochaton-Piallat M-L. Arterial smooth muscle cell heterogeneity: implications for atherosclerosis and restenosis development. *Arterioscler Thromb Vasc Biol*. 2003; 23: 1510–1520.
260. Chistiakov DA, Orekhov AN, Bobryshev YV. Vascular smooth muscle cell in atherosclerosis. *Acta Physiol (Oxf)*. 2015; 214: 33–50.
261. Carmeliet P. Mechanisms of angiogenesis and arteriogenesis. *Nat Med*. 2000; 6: 389–395.

262. Takeuchi H, Hashimoto N, Kitai R, Kubota T, Kikuta K. Proliferation of vascular smooth muscle cells in glioblastoma multiforme. *J Neurosurg.* 2010; 113: 218–224.
263. Louvet A, Teixeira-Clerc F, Chobert M-N, Deveau V, Pavoine C, Zimmer A, Pecker F, Mallat A, Lotersztajn S. Cannabinoid CB<sub>2</sub> receptors protect against alcoholic liver disease by regulating Kupffer cell polarization in mice. *Hepatology.* 2011; 54: 1217–1226.
264. Steib CJ, Gmelin L, Pfeiler S, Schewe J, Brand S, Göke B, Gerbes AL. Functional relevance of the cannabinoid receptor 2 - heme oxygenase pathway. A novel target for the attenuation of portal hypertension. *Life Sci.* 2013; 93: 543–551.
265. Li H, Wood JT, Whitten KM, Vadivel SK, Seng S, Makriyannis A, Avraham HK. Inhibition of fatty acid amide hydrolase activates Nrf2 signalling and induces heme oxygenase 1 transcription in breast cancer cells. *Br J Pharmacol.* 2013; 170: 489–505.
266. Mishima K, Hayakawa K, Abe K, Ikeda T, Egashira N, Iwasaki K, Fujiwara M. Cannabidiol prevents cerebral infarction via a serotonergic 5-hydroxytryptamine<sub>1A</sub> receptor-dependent mechanism. *Stroke.* 2005; 36: 1071–1076.
267. Ward SJ, McAllister SD, Kawamura R, Murase R, Neelakantan H, Walker EA. Cannabidiol inhibits paclitaxel-induced neuropathic pain through 5-HT<sub>1A</sub> receptors without diminishing nervous system function or chemotherapy efficacy. *Br J Pharmacol.* 2014; 171: 636–645.
268. Vaccani A, Massi P, Colombo A, Rubino T, Parolaro D. Cannabidiol inhibits human glioma cell migration through a cannabinoid receptor-independent mechanism. *Br J Pharmacol.* 2005; 144: 1032–1036.
269. Massi P, Vaccani A, Ceruti S, Colombo A, Abbracchio MP, Parolaro D. Antitumor effects of cannabidiol, a nonpsychoactive cannabinoid, on human glioma cell lines. *J Pharmacol Exp Ther.* 2004; 308: 838–845.
270. MacLennan SJ, Reynen PH, Kwan J, Bonhaus DW, Martin GR. [<sup>35</sup>S]GTPγS binding to assess inverse agonist actions of ligands at human recombinant CB<sub>1</sub> and CB<sub>2</sub> receptors. In: *Symposium on the cannabinoids*, p. 7. Burlington. 1998.
271. Sacerdote P, Martucci C, Vaccani A, Bariselli F, Panerai AE, Colombo A, Parolaro D, Massi P. The nonpsychoactive component of marijuana cannabidiol modulates chemotaxis and IL-10 and IL-12 production of murine macrophages both *in vivo* and *in vitro*. *J Neuroimmunol.* 2005; 159: 97–105.
272. Stanley CP, Hind WH, Tufarelli C, O'Sullivan SE. Cannabidiol causes endothelium-dependent vasorelaxation of human mesenteric arteries via CB<sub>1</sub> activation. *Cardiovasc Res.* 2015; 107: 568–578.
273. Thomas A, Baillie GL, Am Phillips, Razdan RK, Ross RA, Pertwee RG. Cannabidiol displays unexpectedly high potency as an antagonist of CB<sub>1</sub> and CB<sub>2</sub> receptor agonists *in vitro*. *Br J Pharmacol.* 2007: 613–623.

274. Laprairie RB, Bagher AM, Kelly MEM, Denovan-Wright EM. Cannabidiol is a negative allosteric modulator of the cannabinoid CB<sub>1</sub> receptor. *Br J Pharmacol*. 2015; 172: 4790–4805.
275. Usami N, Yamamoto I, Watanabe K. Generation of reactive oxygen species during mouse hepatic microsomal metabolism of cannabidiol and cannabidiol hydroxy-quinone. *Life Sci*. 2008; 83: 717–724.
276. Lim MP, Devi LA, Rozenfeld R. Cannabidiol causes activated hepatic stellate cell death through a mechanism of endoplasmic reticulum stress-induced apoptosis. *Cell Death Dis*. 2011; 2: e170.
277. Pan H, Mukhopadhyay P, Rajesh M, Patel V, Mukhopadhyay B, Gao B, Haskó G, Pacher P. Cannabidiol attenuates cisplatin-induced nephrotoxicity by decreasing oxidative/nitrosative stress, inflammation, and cell death. *J Pharmacol Exp Ther*. 2009; 328: 708–714.
278. Rajesh M, Mukhopadhyay P, Bátkai S, Patel V, Saito K, Matsumoto S, Kashiwaya Y, Horváth B, Mukhopadhyay B, Becker L, Haskó G, Liaudet L, Wink DA et al. Cannabidiol attenuates cardiac dysfunction, oxidative stress, fibrosis, and inflammatory and cell death signaling pathways in diabetic cardiomyopathy. *J Am Coll Cardiol*. 2010; 56: 2115–2125.
279. Proudfoot D, Shanahan C. Human vascular smooth muscle cell culture. *Methods Mol Biol*. 2012; 806: 251–263.
280. Ross R. The pathogenesis of atherosclerosis: a perspective for the 1990s. *Nature*. 1993; 362: 801.
281. Bauters C, Six I, Meurice T, van Belle E. Growth factors and endothelial dysfunction. *Drugs*. 1999; 58 Spec No 1: 11–15.
282. Yang X, Liaw L, Prudovsky I, Brooks PC, Vary C, Oxburgh L, Friesel R. Fibroblast growth factor signaling in the vasculature. *Curr Atheroscler Rep*. 2015; 17: 509.
283. Brenninkmeijer L, Kuehl C, Geldart AM, Arons E, Christou H. Heme oxygenase-1 does not mediate the effects of extracellular acidosis on vascular smooth muscle cell proliferation, migration, and susceptibility to apoptosis. *J Vasc Res*. 2011; 48: 285–296.
284. Duckles H, Boycott HE, Al-Owais MM, Elies J, Johnson E, Dallas ML, Porter KE, Giuntini F, Boyle JP, Scragg JL, Peers C. Heme oxygenase-1 regulates cell proliferation via carbon monoxide-mediated inhibition of T-type Ca<sup>2+</sup> channels. *Pflugers Arch*. 2015; 467: 415–427.
285. Moraes JA, Barcellos-de-Souza P, Rodrigues G, Nascimento-Silva V, Silva SV, Assreuy J, Arruda MA, Barja-Fidalgo C. Heme modulates smooth muscle cell proliferation and migration via NADPH oxidase: A counter-regulatory role for heme oxygenase system. *Atherosclerosis*. 2012; 224: 394–400.

286. Li Y, Wang H, Yang B, Yang J, Ruan X, Yang Y, Wakeland EK, Li Q, Fang X. Influence of carbon monoxide on growth and apoptosis of human umbilical artery smooth muscle cells and vein endothelial cells. *Int J Biol Sci.* 2012; 8: 1431–1446.
287. Loboda A, Jazwa A, Wegiel B, Jozkowicz A, Dulak J. Heme oxygenase-1-dependent and -independent regulation of angiogenic genes expression. Effect of cobalt protoporphyrin and cobalt chloride on VEGF and IL-8 synthesis in human microvascular endothelial cells. *Cell Mol Biol (Noisy-le-grand).* 2005; 51: 347–355.
288. Dulak J, Jozkowicz A, Foresti R, Kasza A, Frick M, Huk I, Green CJ, Pachinger O, Weidinger F, Motterlini R. Heme oxygenase activity modulates vascular endothelial growth factor synthesis in vascular smooth muscle cells. *Antioxid Redox Signal.* 2002; 4: 229–240.
289. Drummond GS, Kappas A. Prevention of neonatal hyperbilirubinemia by tin protoporphyrin IX, a potent competitive inhibitor of heme oxidation. *Proc Natl Acad Sci U S A.* 1981; 78: 6466–6470.
290. Yoshinaga T, Sassa S, Kappas A. Purification and properties of bovine spleen heme oxygenase. Amino acid composition and sites of action of inhibitors of heme oxidation. *J Biol Chem.* 1982; 257: 7778–7785.
291. Wong RJ, Vreman HJ, Schulz S, Kalish FS, Pierce NW, Stevenson DK. *In vitro* inhibition of heme oxygenase isoenzymes by metalloporphyrins. *J Perinatol.* 2011; 31 Suppl 1: S35-41.
292. He JZ, Ho JJD, Gingerich S, Courtman DW, Marsden PA, Ward ME. Enhanced translation of heme oxygenase-2 preserves human endothelial cell viability during hypoxia. *J Biol Chem.* 2010; 285: 9452–9461.
293. Chen D, Jin Z, Zhang J, Jiang L, Chen K, He X, Song Y, Ke J, Wang Y. HO-1 protects against hypoxia/reoxygenation-induced mitochondrial dysfunction in H9C2 cardiomyocytes. *PLOS ONE.* 2016; 11: e0153587.
294. Scott KA, Dennis JL, Dalglish AG, Liu WM. Inhibiting heat shock proteins can potentiate the cytotoxic effect of cannabidiol in human glioma cells. *Anticancer Res.* 2015; 35: 5827–5837.
295. Athanasiou A, Clarke AB, Turner AE, Kumaran NM, Vakilpour S, Smith PA, Bagiokou D, Bradshaw TD, Westwell AD, Fang L, Lobo DN, Constantinescu CS, Calabrese V et al. Cannabinoid receptor agonists are mitochondrial inhibitors. A unified hypothesis of how cannabinoids modulate mitochondrial function and induce cell death. *Biochem Biophys Res Commun.* 2007; 364: 131–137.
296. Hao E, Mukhopadhyay P, Cao Z, Erdélyi K, Holovac E, Liaudet L, Lee W-S, Haskó G, Mechoulam R, Pacher P. Cannabidiol protects against doxorubicin-induced cardiomyopathy by modulating mitochondrial function and biogenesis. *Mol Med.* 2015; 21: 38–45.

297. Sun S, Hu F, Wu J, Zhang S. Cannabidiol attenuates OGD/R-induced damage by enhancing mitochondrial bioenergetics and modulating glucose metabolism via pentose-phosphate pathway in hippocampal neurons. *Redox Biol.* 2017; 11: 577–585.
298. Fiedler J, Stöhr A, Gupta SK, Hartmann D, Holzmann A, Just A, Hansen A, Hilfiker-Kleiner D, Eschenhagen T, Thum T. Functional microRNA library screening identifies the hypoxamir miR-24 as a potent regulator of smooth muscle cell proliferation and vascularization. *Antioxid Redox Signal.* 2014; 21: 1167–1176.
299. Wu H-Y, Chu R-M, Wang C-C, Lee C-Y, Lin S-H, Jan T-R. Cannabidiol-induced apoptosis in primary lymphocytes is associated with oxidative stress-dependent activation of caspase-8. *Toxicol Appl Pharmacol.* 2008; 226: 260–270.
300. Wu H-Y, Chang A-C, Wang C-C, Kuo F-H, Lee C-Y, Liu D-Z, Jan T-R. Cannabidiol induced a contrasting pro-apoptotic effect between freshly isolated and precultured human monocytes. *Toxicol Appl Pharmacol.* 2010; 246: 141–147.
301. Furfaro AL, Traverso N, Domenicotti C, Piras S, Moretta L, Marinari UM, Pronzato MA, Nitti M. The Nrf2/HO-1 axis in cancer cell growth and chemoresistance. *Oxid Med Cell Longev.* 2016; 2016: 1958174.
302. Nitti M, Piras S, Marinari UM, Moretta L, Pronzato MA, Furfaro AL. HO-1 induction in cancer progression. A matter of cell adaptation. *Antioxidants (Basel).* 2017; 6: pii: E29.
303. Saahene RO, Wang J, Wang M-L, Agbo E, Pang D. The antitumor mechanism of paeonol on CXCL4/CXCR3-B signals in breast cancer through induction of tumor cell apoptosis. *Cancer Biother Radiopharm.* 2018; 33: 233–240.
304. Lee H-N, Jin H-O, Park J-A, Kim J-H, Kim J-Y, Kim B, Kim W, Hong S-E, Lee Y-H, Chang YH, Hong S-I, Hong YJ, Park I-C et al. Heme oxygenase-1 determines the differential response of breast cancer and normal cells to piperlongumine. *Mol Cells.* 2015; 38: 327–335.
305. Tsai C-F, Chen J-H, Chang C-N, Lu D-Y, Chang P-C, Wang S-L, Yeh W-L. Fisetin inhibits cell migration via inducing HO-1 and reducing MMPs expression in breast cancer cell lines. *Food Chem Toxicol.* 2018; 120: 528–535.
306. Consroe P, Kennedy K, Schram K. Assay of plasma cannabidiol by capillary gas chromatography/ion trap mass spectroscopy following high-dose repeated daily oral administration in humans. *Pharmacol Biochem Behav.* 1991; 40: 517–522.
307. Manini AF, Yiannoulos G, Bergamaschi MM, Hernandez S, Olmedo R, Barnes AJ, Winkel G, Sinha R, Jutras-Aswad D, Huestis MA, Hurd YL. Safety and pharmacokinetics of oral cannabidiol when administered concomitantly with intravenous fentanyl in humans. *J Addict Med.* 2015; 9: 204–210.
308. Matés JM, Pérez-Gómez C, Núñez de Castro I. Antioxidant enzymes and human diseases. *Clin Biochem.* 1999; 32: 595–603.



- 
309. Dröge W. Free radicals in the physiological control of cell function. *Physiol Rev.* 2002; 82: 47–95.
  310. Casanova T, Garigliany M. *N*-acetylcysteine. An old drug with variable anti-influenza properties. *JCBMR.* 2016; 2: 1.



## 9 List of Figures

Figure 1-1:	Schematic cross-section of an arterial blood vessel structure.....	3
Figure 1-2:	Phenotype-dependent characteristics and marker proteins of VSMC.....	4
Figure 1-3:	Reaction of the enzyme-coupled heme degradation.....	8
Figure 1-4:	Nrf2-dependent mechanism of <i>HMOX1</i> transcription under normal and stress conditions. ....	10
Figure 1-5:	Chemical structures of endocannabinoids. ....	14
Figure 1-6:	Chemical structures of endocannabinoid-like compounds.....	15
Figure 1-7:	Chemical structures of synthetic cannabinoid receptor agonists. ....	15
Figure 1-8:	Chemical structures of synthetic cannabinoid receptor antagonists. ....	16
Figure 1-9:	Chemical structures of CBD and THC. ....	17
Figure 3-1:	Scheme of RNA interference.....	26
Figure 3-2:	Schematic representation of the qRT-PCR process. ....	27
Figure 3-3:	Scheme of the qRT-PCR temperature profile. ....	29
Figure 3-4:	Chemical reaction of the BCA protein assay. ....	32
Figure 4-1:	Effects of cannabinoids on HO-1 and HO-2 protein expression in HUASMC.....	37
Figure 4-2:	Effect of CBD on HO-1 and HO-2 mRNA and protein expression in HUASMC. ....	39
Figure 4-3:	Presence of potential target receptors of CBD in HUASMC and investigation of their involvement in CBD-mediated induction of HO-1 protein.....	40
Figure 4-4:	Effect of NAC on CBD-mediated induction of HO-1 protein and ROS generation in HUASMC. ....	42
Figure 4-5:	Effect of CBD on viability and proliferation of HUASMC. ....	45
Figure 4-6:	Involvement of receptor-signaling in CBD-mediated anti-proliferative effects in HUASMC.....	46
Figure 4-7:	Effect of HO-1 activity inhibitor SnPPiX on CBD-mediated anti-proliferative effects and viability of HUASMC. ....	48
Figure 4-8:	Effect of HO-1 siRNA on CBD-mediated anti-proliferative effects and viability of HUASMC. ....	50
Figure 4-9:	Role of HO-1 in CBD-mediated anti-migratory effects in HUASMC. ....	52
Figure 4-10:	Impact of N-acetylcysteine (NAC) on CBD-mediated anti-proliferative effects and viability of HUASMC. ....	54
Figure 5-1:	Schematic representation of the experimental outcomes of this thesis.....	55
Figure 11-1:	Sequence alignment of HO-1 and HO-2. ....	111
Figure 11-2:	NAC and the antioxidant-scavenging glutathione system. ....	112
Figure 11-3:	Principle of immunologic protein detection and horseradish peroxidase reaction.....	113
Figure 11-4:	Scheme of the construction and function of a flow cytometer.....	114
Figure 11-5:	Effect of CBD on HO-2 mRNA and protein expression in HUASMC. ....	115



## 10 List of Tables

Table 3-1:	Composition of qRT-PCR master mix.....	28
Table 3-2:	Antibody dilutions used for immunologic detection. ....	34
Table 4-1:	Effect of media composition on proliferation of HUASMC .....	43
Table 4-2:	Effect of PDGF on proliferation of HUASMC .....	44
Table 11-1:	Cells, cell culture media and supplements.....	103
Table 11-2:	Chemicals and reagents.....	103
Table 11-3:	Assay kits .....	104
Table 11-4:	Antibodies for Western blot analysis .....	105
Table 11-5:	Non-antibody products for Western blot analysis.....	105
Table 11-6:	Gene expression assays and consumables for mRNA analysis .....	106
Table 11-7:	Reagents for RNA interference experiments.....	106
Table 11-8:	Technical equipment.....	106
Table 11-9:	Software .....	107
Table 11-10:	Consumables .....	108
Table 11-11:	Composition of buffers and other solutions .....	108
Table 11-12:	Composition of stacking and separation gel for SDS-PAGE .....	110



## 11 List of Abbreviations

$\mu\text{l}$ .....	microlitre(s)
$\mu\text{m}$ .....	micrometre(s)
$\mu\text{M}$ .....	micromol per liter
5-HT .....	5-hydroxytryptamine/serotonin
AEA .....	<i>N</i> -arachidonoyl-ethanolamide / anandamide
AM251 .....	1-(2,4-dichlorophenyl)-5-(4-iodophenyl)-4-methyl- <i>N</i> -piperidin-1-ylpyrazole-3-carboxamide
AM630 .....	[6-iodo-2-methyl-1-(2-morpholin-4-ylethyl)indol-3-yl]-(4-methoxyphenyl)methanone / 6-iodopravadoline
APS .....	ammonium persulphate
AV .....	Annexin V
BACH1 .....	BTB Domain And CNC Homolog 1
BCA .....	bicinchoninic acid
bFGF .....	basic fibroblast growth factor
BrdU .....	bromodeoxyuridine
BS .....	blocking solution
CBD .....	cannabidiol
CBR.....	cannabinoid receptor(s)
cDNA .....	complementary DNA
chap.....	<i>chapter</i>
$\text{cm}^2$ .....	square centimetre
CNS.....	central nervous system
CO .....	carbon monoxide
$\text{CO}_2$ .....	carbon dioxide
$\text{CoCl}_2$ .....	cobalt(II) chloride
CoPPIX .....	cobalt protoporphyrin IX
CP55,940 .....	(-)-cis-3-[2-hydroxy-4-(1,1-dimethylheptyl)-phenyl]-trans-4-(3-hydroxypropyl)cyclohexanol
cSMCGM .....	complete SMCGM
$C_t$ .....	threshold cycle
CYP450 .....	cytochrome P450
DMEM .....	Dulbecco's modified Eagle's medium

---

DNA.....	desoxyribonucleic acid
DPBS.....	Dulbecco's phosphate buffered saline
e.g.....	exempli gratia [lat.: for example]
ECL .....	enhanced chemiluminescence
ECS.....	endocannabinoid system
EDTA .....	ethylenediamine-tetraacetic acid
EGF.....	epidermal growth factor
ER.....	endoplasmic reticulum
ERK.....	extracellular signal-regulated kinase
FCS .....	fetal calf serum
Fe .....	chemical element: iron
Fe <sup>2+</sup> .....	divalent iron ion
FePPIX .....	iron protoporphyrin IX / heme
g.....	gram
h .....	hour(s)
H <sub>2</sub> O <sub>2</sub> .....	hydrogen peroxide
HCl .....	hydrochloric acid
HO.....	heme oxygenase
hPDGF-BB .....	human PDGF-BB [dimer]
HRP .....	horseradish peroxidase
HUASMC .....	human umbilical artery smooth muscle cells
HUVEC .....	human umbilical vein endothelial cells
i. e.....	id est [lat.: that means]
I/R.....	ischemia/reperfusion
IC <sub>50</sub> .....	mean inhibitory concentration
INN .....	international nonproprietary name
JWH-133 .....	1-deoxy-3-(1',1'-dimethylbutyl)- $\Delta^8$ -THC
kDa .....	kilodalton
Keap1 .....	Kelch-like ECH-associated protein 1
K <sub>i</sub> .....	dissociation constant
LDL.....	low-density lipoprotein
mA .....	milliampere



MA .....	R(+)-methanandamide
MAPK .....	mitogen-activated protein kinase(s)
MFI .....	mean fluorescence intensity
Mg <sup>2+</sup> .....	divalent magnesium ion
min .....	minute(s)
ml.....	millilitre(s)
mRNA .....	messenger RNA(s)
mW.....	milliwatt
NAC.....	<i>N</i> -acetylcysteine
NaCl.....	sodium chloride
NADPH .....	phosphorylated form of reduced nicotinamide adenine dinucleotide
NaOH.....	sodium hydroxide
ng/ml.....	nanogram per millilitre
nm .....	nanometre
NON.....	non-targeting siRNA
Nrf2.....	nuclear factor (erythroid-derived 2)-like 2
O-1602.....	5-methyl-4-[(1R,6R)-3-methyl-6-prop-1-en-2-ylcyclohex-2-en-1-yl]benzene-1,3-diol
O-1918.....	1,3-dimethoxy-5-methyl-2-[(1R,6R)-3-methyl-6-prop-1-en-2-ylcyclohex-2-en-1-yl]benzene
PCR.....	polymerase chain reaction
PDGF .....	platelet-derived growth factor
PI .....	propidium iodide
pmol.....	picomol
PTX.....	pertussis toxin
RNA.....	ribonucleic acid(s)
ROS.....	reactive oxygen species
rSMCGM.....	reduced SMCGM
RT.....	reverse transcriptase
RTASMC.....	rat thoracic aorta smooth muscle cells
SDS-PAGE.....	sodium dodecyl sulfate-polyacrylamide gel electrophoresis
SEM .....	standard error of the mean
siRNA .....	small interfering RNA(s)
SMC .....	smooth muscle cells
SMCGM.....	smooth muscle cell growth medium

---

SnPPIX .....	tin protoporphyrin IX
SSC.....	side scatter
TBHP .....	tert-butyl hydroperoxide
TBS-T.....	TRIS-buffered saline/Tween®20
TC75-flask .....	tissue culture flasks with a growth area of 75 cm <sup>2</sup>
TE .....	Trypsin-EDTA
TEMED.....	tetramethylethylenediamine
TF .....	transcription factor
THC.....	$\Delta^9$ -tetrahydrocannabinol ( $\Delta^9$ -THC)
TRIS .....	tris(hydroxymethyl)aminomethane
TRPV1 .....	transient receptor potential vanilloid 1
V.....	volt
v/v .....	volume per volume
VEGF.....	vascular endothelial growth factor
VSMC.....	vascular smooth muscle cells
w/v .....	weight per volume
x g.....	multiplied by the mean acceleration due to gravity

## 12 Attachment

### 12.1 Materials

Unless otherwise stated, all materials listed have been purchased from German suppliers.

**Table 12-1: Cells, cell culture media and supplements**

Product	Supplier
HUASMC	PromoCell, Heidelberg
DMEM	Lonza, Cologne
- with 4.5 g/L glucose and L-glutamine	
FCS	PAN Biotech, Aidenach
SMCGM	PromoCell, Heidelberg
- with FCS (5 % [v/v])	PromoCell, Heidelberg
EGF (0.5 ng/ml)	PromoCell, Heidelberg
bFGF (2 ng/ml)	PromoCell, Heidelberg
Insulin (5 ng/ml)	PromoCell, Heidelberg

**Table 12-2: Chemicals and reagents**

Product	Supplier
AM251	Biomol, Hamburg
AM630	Biomol, Hamburg
APS	Carl Roth®, Karlsruhe
Aqua ad iniectabilia	Braun Melsungen AG, Melsungen
Blotting grade blocker	Bio-Rad, Munich
Bromophenol blue	Sigma-Aldrich, Taufkirchen
Capsazepine	Sigma-Aldrich, Taufkirchen
CBD	Biotrend AG, Cologne
DMSO	AppliChem, Darmstadt
DPBS (without Ca <sup>2+</sup> and Mg <sup>2+</sup> )	PAN Biotech, Aidenach
Ethanol	Central pharmacy, Rostock
Glycerine (water-free)	AppliChem, Darmstadt
Glycine	AppliChem, Darmstadt
H <sub>2</sub> O <sub>2</sub>	Sigma-Aldrich, Taufkirchen
HCl	Merck, Darmstadt

Product	Supplier
hPDGF-BB	Thermo Fisher Scientific Inc., Waltham (MA, USA)
Isopropanol	J. T. Baker, Griesheim
JWH133	Tocris Bioscience, Wiesbaden-Nordenstadt
Luminol	Sigma-Aldrich, Taufkirchen
Methanol	J. T. Baker, Griesheim
NAC	Sigma-Aldrich, Taufkirchen
NaCl	AppliChem, Darmstadt
NaOH	AppliChem, Darmstadt
O-1602	Tocris Bioscience, Bristol (UK)
O-1918	Tocris Bioscience, Bristol (UK)
p-Coumaric acid	Sigma-Aldrich, Taufkirchen
R-(+)-Methanandamid	Tocris Bioscience, Wiesbaden-Nordenstadt
Rotiphorese® Gel 30	Carl Roth®, Karlsruhe
SDS ultrapure	AppliChem, Darmstadt
SnPPIX (chloride)	Enzo Life Sciences GmbH, Lörrach
TEMED	Carl Roth®, Karlsruhe
THC	Lipomed GmbH, Weil am Rhein
TRIS (ultrapure)	AppliChem, Darmstadt
TRIS/HCl	AppliChem, Darmstadt
Trypan blue solution (0.4 %)	ThermoFisher Scientific Inc., Waltham (MA, USA)
Trypsin-EDTA (10X)	ThermoFisher Scientific Inc., Waltham (MA, USA)
Tween® 20	Carl Roth®, Karlsruhe
β-Mercaptoethanol	Ferak®, Berlin

**Table 12-3: Assay kits**

Product	Supplier
BrdU cell proliferation ELISA	Abcam, Cambridge (UK)
CellROX™ green flow cytometry assay kit	Thermo Fisher Scientific Inc., Waltham (MA, USA)
Diff Quick staining	Labor + Technik Eberhard Lehmann GmbH, Berlin

Product	Supplier
FTTC-Annexin V apoptosis detection kit I	BD Biosciences, Heidelberg
Pierce™ BCA protein assay kit	Pierce, Rockford (IL, USA)
RNeasy Mini kit	Qiagen, Hilden
TaqMan® RNA-to-CT™ 1-Step kit	Thermo Fisher Scientific Inc.

**Table 12-4: Antibodies for Western blot analysis**

Primary antibody	Supplier
CB <sub>1</sub> R antibody (#sc-293419)	Santa Cruz Biotechnology, Inc., Heidelberg
CB <sub>2</sub> R antibody (#sc-293188)	Santa Cruz Biotechnology, Inc., Heidelberg
GPR55 antibody (#720285)	Thermo Fisher Scientific Inc., Waltham (MA, USA)
HO-1 polyclonal antibody (#ADI-SPA-895)	Enzo Life Sciences GmbH, Lörrach
HO-2 polyclonal antibody (ADI-SPA-897)	Enzo Life Sciences GmbH, Lörrach
TRPV1 antibody (#PA5-34498)	Thermo Fisher Scientific Inc., Waltham (MA, USA)
β-actin monoclonal antibody (#A5316)	Sigma-Aldrich, Taufkirchen
Secondary antibodies	Supplier
anti-mouse IgG, HRP-linked antibody (#7076S)	Cell Signaling Technology Europe, Leiden (The Netherlands)
anti-rabbit IgG, HRP-linked antibody (#7074S)	Cell Signaling Technology Europe, Leiden (The Netherlands)

**Table 12-5: Non-antibody products for Western blot analysis**

Product	Supplier
Prestained SDS-PAGE standard (broad range; #161-0318)	Bio-Rad, Munich
Amersham™ Protran™ 0.2 μM NC nitrocellulose membrane	Carl Roth®, Karlsruhe

**Table 12-6: Gene expression assays and consumables for mRNA analysis**

Gene expression assays	Supplier
HO-1 (Hs01110251_m1; FAM™ dye/MGB probe)	Thermo Fisher Scientific Inc., Waltham (MA, USA)
HO-2 (Hs00157969_m1; FAM™ dye/MGB probe)	Thermo Fisher Scientific Inc., Waltham (MA, USA)
β-Actin (#4352935E; human ACTB endogenous control (FAM™ dye/ MGB probe, non-primer limited)	Thermo Fisher Scientific Inc., Waltham (MA, USA)
Consumables	Supplier
Amersham™ Protran™ 0.2 μM NC nitrocellulose membrane	Carl Roth®, Karlsruhe
MicroAmp™ fast optical 96-well reaction plate, 0.1 mL	Thermo Fisher Scientific Inc., Waltham (MA, USA)
MicroAmp™ optical adhesive film	Thermo Fisher Scientific Inc., Waltham (MA, USA)

**Table 12-7: Reagents for RNA interference experiments**

siRNAs	Supplier
HO-1 siRNA (sc-35554)	Santa Cruz Biotechnology, Inc., Heidelberg
Negative control siRNA (#1022076)	Qiagen, Hilden
Transfection reagents	Supplier
Lipofectamine® RNAiMAX reagent	Thermo Fisher Scientific Inc., Waltham (MA, USA)
Opti-MEM I reduced serum medium	Thermo Fisher Scientific Inc., Waltham (MA, USA)

**Table 12-8: Technical equipment**

Equipment	Supplier
7500 Fast Real-Time PCR System	Thermo Fisher Scientific Inc., Waltham (MA, USA)
AccuriC6™ flow cytometer	BD Biosciences, Heidelberg
Anthos HT II plate reader	Anthos Labtec Instruments GmbH, Wals-Siezenheim (Austria)

Equipment	Supplier
AxioCam ERc 5s digital microscope camera	Carl Zeiss AG, Oberkochen
Bio-Rad Mini-PROTEAN® Tetra Cell System	Bio-Rad, Munich
CB 201 CO <sub>2</sub> incubator	Binder GmbH, Tuttlingen
Centrifuges (5417R / 5810R)	Eppendorf AG, Hamburg
ChemiDoc™ XRS System	Bio-Rad, Munich
Herasafe™ (KS18) biological safe cabinet	Thermo Fisher Scientific Inc., Waltham (MA, USA)
LaminAir HB2448	Heraeus Holding GmbH, Hanau
Luna-II™ automated cell counter	Biozym Scientific GmbH, Hessisch Oldendorf
Megafuge 1.0R	Heraeus Holding GmbH, Hanau
Mr. Frosty™ freezing container	Thermo Fisher Scientific Inc., Waltham (MA, USA)
Multi axle rotating mixer RM5-30V	CAT Ingenieurbüro, M. Zipperer GmbH, Staufen
Pipettes (variable volumes)	Eppendorf AG, Hamburg
PowerPac (300 / universal)	Bio-Rad, Munich
PrimoVert inverted microscope	Carl Zeiss AG, Oberkochen
SE 250 Mini-Vertical Unit	GE Healthcare Europe GmbH, Freiburg
Sonopuls HD	Bandelin electronic GmbH & Co KG, Berlin
Thermomixer comfort	Eppendorf AG, Hamburg
Touchmixer VortexGenie1	Scientific Industries, Inc., Bohemia, USA
Trans-Blot SD semi-dry transfer cell	Bio-Rad, Munich

**Table 12-9: Software**

Software	Supplier
ACD/ChemSketch	Advanced Chemistry Development, Inc. (ACD/Labs), Toronto (Canada)
BD Accuri™ C6 software	BD Biosciences, Heidelberg
GraphPad Prism 6.01	GraphPad Software, Inc, LaJolla (CA, USA)

Software	Supplier
Microsoft® Office	Microsoft Corporation, Redmond (WA, USA)
Quantity One 1-D analysis software	Bio-Rad, Munich

**Table 12-10: Consumables**

Product	Supplier
Cell culture well plates (6-, 12-, 24-, 96-well; sterile)	BD Biosciences, Heidelberg
Centrifuge tubes (15 ml, 50 ml)	Sarstedt, Nümbrecht
Combitips for Eppendorf Multipette®)	Eppendorf AG, Hamburg
Cryopreservation vials (2 ml)	Greiner Bio-One GmbH, Frickenhausen
Falcon® cell culture inserts (pore size: 8 µM)	Corning, Wiesbaden, Germany
Microtest plate (96-well)	Sarstedt, Nümbrecht
Pipette tips	Sarstedt, Nümbrecht
Reaction vials (1.5 ml, 0.5 ml; clear)	Sarstedt, Nümbrecht
Reaction vials (2 ml; clear)	Greiner Bio-One GmbH, Frickenhausen
Safe-Lock tubes, amber (0.5 ml, 2 ml)	Carl Roth®, Karlsruhe
Serological pipettes (5 ml, 10 ml, 25 ml)	Sarstedt, Nümbrecht
Tissue culture flask (75 cm <sup>2</sup> ) Cell <sup>+</sup> (vented cap)	Sarstedt, Nümbrecht

**Table 12-11: Composition of buffers and other solutions**

Buffer/Solution	Component
10X TRIS-buffered saline (TBS)	1,000 mM TRIS (ultrapure) 2,500 mM NaCl pH 7.5
1X TRIS-buffered saline/Tween®20 (TBS-T)	100 ml 10X TBS 900 ml deionized water 1 ml Tween®20
10X electrophoresis buffer	250 mM TRIS (ultrapure) 1,920 mM Glycine 0.1% (m/v) SDS



Buffer/Solution	Component
1X electrophoresis buffer	100 ml 10X electrophoresis buffer 900 ml deionized water
5X Stripping-buffer	1,000 mM Glycine 2500 mM NaCl pH 2.5 (adjusted with HCl)
1X Stripping buffer	50 ml 5X Stripping buffer 200 ml deionized water
10% SDS [w/v]	10 g SDS 100 ml deionized water
Enhanced chemiluminescence solution I (ECL I)	2.5 mM Luminol 400 $\mu$ M p-Coumaric acid 100 mM TRIS/HCl (pH 8.5)
Enhanced chemiluminescence solution II (ECL II)	76 mM H <sub>2</sub> O <sub>2</sub> 100 mM TRIS/HCl (pH 8.5)
ECL detection solution	1 volume ECL I 1 volume ECL II
1X Trypsin/EDTA (TE)	5 ml 10X Trypsin/EDTA 45 ml DPBS
Sample buffer (for protein isolation)	62.5 mM TRIS/HCl 2% [v/v] SDS 10% [v/v] Glycerol
Blocking solution	5 g Blotting grade blocker 100 ml deionized water
Semi-dry transfer buffer	190 mM Glycine 25 mM TRIS (ultrapure) 20% (v/v) Methanol

**Table 12-12: Composition of stacking and separation gel for SDS-PAGE**

Stacking gel; 4% acrylamide concentration	Volume
Aqua ad injectabilia	11.5 ml
0.5 M TRIS (ultrapure)	4.7 ml
SDS (10% [w/v])	188 µl
Rotiphorese® gel 30 (acrylamide donor)	2.5 ml
TEMED	19 µl
APS	95 µl
Separation gel, 12% acrylamide concentration	Volume
Aqua ad injectabilia	12.7 ml
1.5 M TRIS (ultrapure)	9.5 ml
SDS (10% [w/v])	380 µl
Rotiphorese® gel 30 (acrylamide donor)	15.2 ml
TEMED	19 µl
APS	190 µl

Note: These values serve to produce four gels with a thickness of 1.5 mm each. First, the components for the separating gel are mixed and the liquid is filled into the prepared gel chamber. The liquid gel is carefully coated with approx. 3 ml of isopropanol. For polymerization (solidification), the gel is incubated for 30 min at room temperature, protected from light. After preparation of the stacking gel, the isopropanol is removed with filter paper. The separating gel is then coated with the stacking gel. After positioning of the pocket comb, the gel is incubated again at room temperature for 30 min, protected from light. The prepared gels are individually wrapped in wet paper towels and stored at 4 °C until use (for a maximum of seven days).

## 12.2 Supplementary information

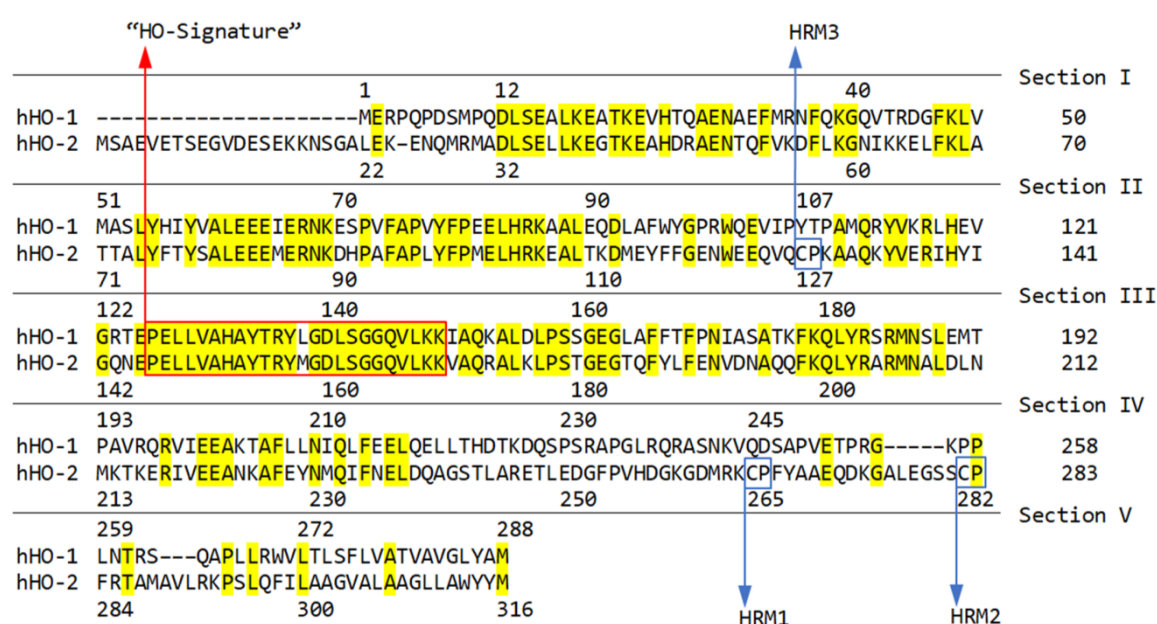


**Figure 12-1: Sequence alignment of HO-1 and HO-2.** Alignment was performed using protein-protein BLAST. Protein sequences used were NP\_002124 (Homo sapiens) for HO-1 and P30519 (Homo sapiens) for HO-2 according to the NCBI reference sequences. Compliant amino acids are marked in yellow. Heme regulatory motifs (HRM) 1–3 of HO-2 are indicated in the blue boxes. The specific amino acid sequence of the “HO-signature” is indicated in the red box.

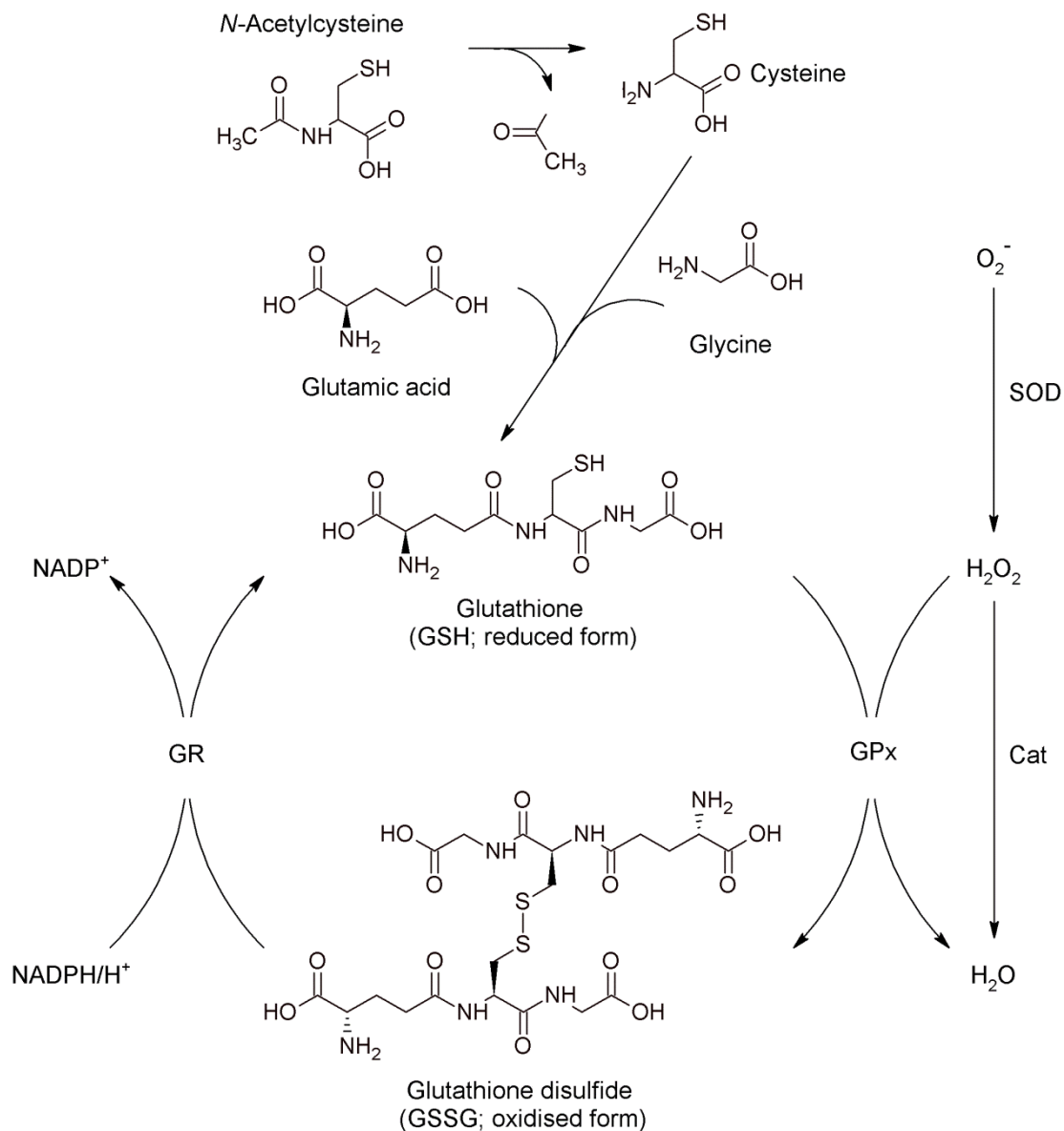


**Figure 12-2: NAC and the antioxidant-scavenging glutathione system.** *N*-Acetylcysteine is hydrolyzed to the amino acid cysteine and an acetyl group. Cysteine, together with glutamic acid and glycine is converted to glutathione in its reduced form (GSH). Superoxide anions ( $O_2^-$ ) are generated by several oxidases and by mitochondrial respiration under hypoxic conditions (not shown here). Superoxide dismutase (SOD) converts  $O_2^-$  to hydrogen peroxide. The reactive oxygen species hydrogen peroxide may be converted into water by the enzymes catalase (Cat) or glutathione peroxidase (GPx). The latter oxidizes GSH to glutathione disulfide (GSSG), which can be converted back to GSH by glutathione reductase (GR) in an NADPH-consuming process. (Illustration created according to [308–310])

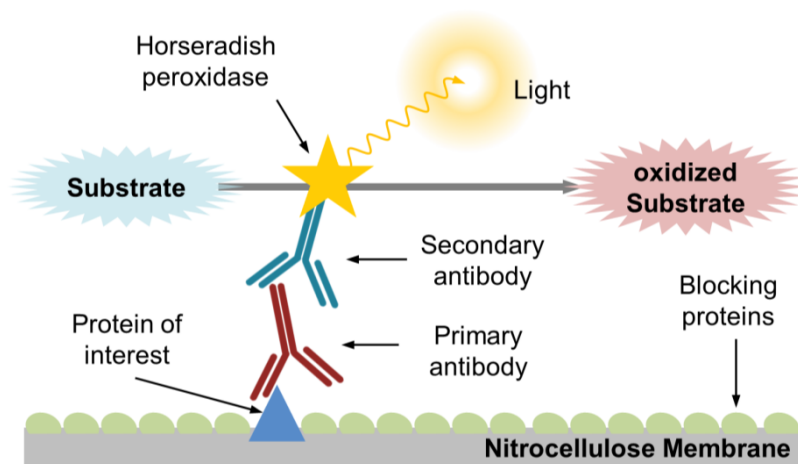


**Figure 12-3: Principle of immunologic protein detection and horseradish peroxidase reaction.** Bound to the nitrocellulose membrane, the protein of interest is recognized by the corresponding primary antibody. The secondary antibody is directed against the immunoglobulins of the species from which the primary antibody originates. A horseradish peroxidase (HRP) is linked to the secondary antibody. The ECL solution contains luminol and  $\text{H}_2\text{O}_2$ , the latter being the substrate of the HRP. The  $\text{H}_2\text{O}_2$  is reduced to water ( $\text{H}_2\text{O}$ ) by the HRP. Light is emitted by simultaneous oxidation of the luminol.

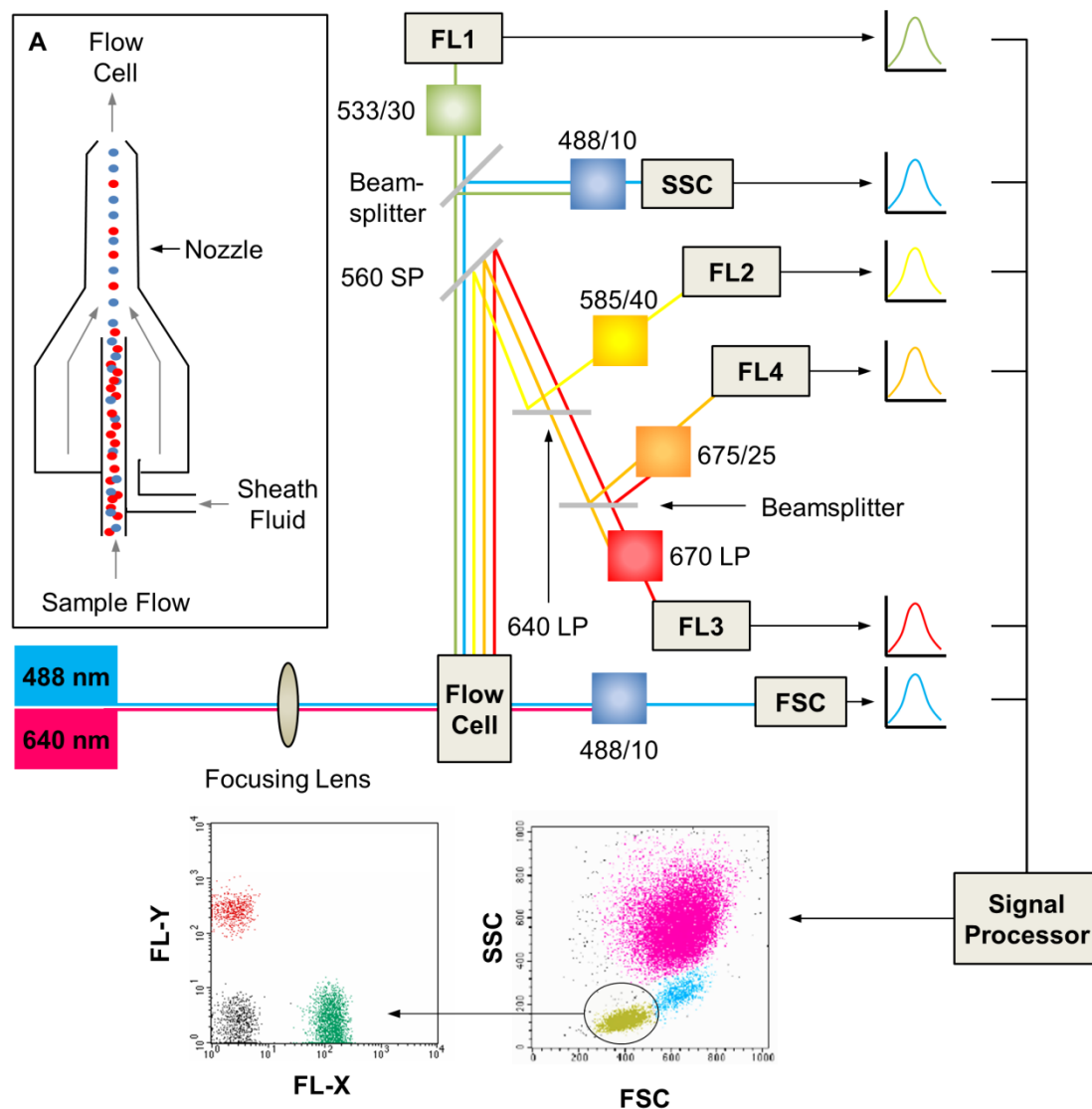


**Figure 12-4: Scheme of the construction and function of a flow cytometer.** Representation of the hydrodynamic focusing of the cells (A). The sample is aspirated by the needle. The sheath fluid surrounds the sample flow whereby the cells are separated and focused in the middle of the sample stream. The sample is transferred to the flow cell where the single cells pass the laser beams. The scattered light is filtered by diverse bandpass filters (e.g. 488/10, light with 478–498 nm can pass the filter) and directed towards the detectors (FSC, SSC, FL1–4). The signals are processed and plotted as dot plots (e.g. FSC vs. SSC). Fluorescently-labelled cells can be analyzed and plotted as FL-X vs. FL-Y. FL-X: fluorescence 1 (e.g. for FITC-Annexin V); FL-Y: fluorescence 2 (e.g. for propidium iodide); LP: longpass filter (light with higher wavelength passes, light with lower wavelength is reflected); SP: shortpass filter (light with lower wavelength passes, light with higher wavelength is reflected); FSC: forward scatter; SSC: side scatter

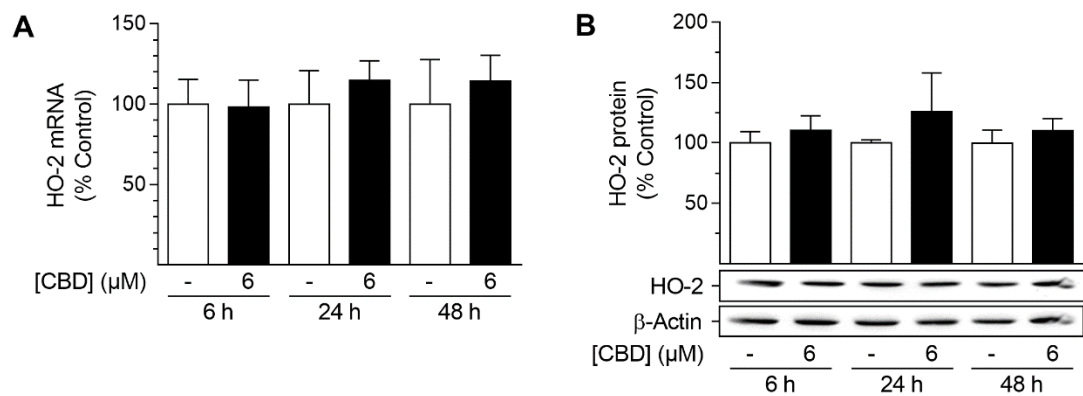


**Figure 12-5: Effect of CBD on HO-2 mRNA and protein expression in HUASMC.** Cells were incubated with CBD at 6  $\mu$ M for the indicated times (A, B). After incubation, cells were analyzed for mRNA expression (A) or protein expression (B) of HO-2. Expression values were normalized to  $\beta$ -actin. Percent control represents comparison with the corresponding vehicle-treated, time-matched group (set as 100%). Values are means  $\pm$  SEM of  $n = 4-5$  (A) or  $n = 3$  (B) experiments. \* $P < 0.05$  vs. time-matched vehicle control; Student's two-tailed  $t$  test (A, B).





## 13 Statutory Declaration

I hereby declare that I have written this thesis independently. Any help and support I have received during the preparation of this thesis is fully acknowledged and disclosed in the acknowledgements. Furthermore, I confirm that I have referenced all publications and sources from which I have taken information, ideas or words completely and at the appropriate place. All sources are cited and listed according to accepted standards for professional publications.

Furthermore, I confirm that my work has been carried out in accordance with the "Rules to ensure good scientific practice and to avoid scientific misconduct" of University of Rostock.

---

Rostock, 06.11.2018

Margit Schwartz



## 14 Acknowledgements / Danksagungen



## 15 Curriculum Vitae

